Irrigation Makes It Rain? Climate Spillovers and Adaptation in India

Mathilde Degois*

November 10, 2026

The most recent version is available **here**.

Abstract

One-fifth of the world's cropland is equipped for irrigation. This paper documents a previously overlooked climate externality of India's $100 billion investment in surface irrigation, combining five decades of administrative, climatic, and agricultural data with wind-driven variation in exposure to distant canal irrigation. Over the period, increased evapotranspiration from irrigated land raised downwind rainfall volume and frequency by 20%, primarily during the dry season. These persistent climatic changes pushed farmers to invest further in private irrigation downwind in order to cultivate the second cropping season, revealing complementarities between rainfall and irrigation. In the long run, these investments helped smallholders to survive and reduced exits from agriculture. Overall, this climate externality accounts for 7 percent of India's agricultural production growth, equivalent to an additional $1 billion annually.

Keywords: Irrigation, Climate Spillovers, Adaptation, Climate Change, India

JEL codes: O13, 053, Q15, Q54, Q56, Q58.

*Email: mathilde.degois@ens-paris-saclay.fr. ENS Paris-Saclay, CEPS & AgroParisTech, PSAE.

I thank Tamma Carleton, Kelsey Jack, William Boos, Sandy Sum, Anna Papp, Ram Fishman, Simon Greenhill, Marco Gonzalez-Navarro, Ted Miguel, Michael Anderson, Ellen Bruno, Eugenie Dugoua, Florian Grosset-Touba, Pierre Mérel, Hugo Molina, Yannick Guyonvarch, Julien Wolfersberger, and Thomas Vendryes for their insights and helpful comments. I thank Tamma Carleton's team for excellent feedback. I thank seminar and conference participants from Development and Environment PhD Workshop at OsloMet, PSAE Internal Seminar, IPWSD Workshop, Climate Economic Lunch ARE at UC Berkeley, Agricultural Econ. PhD Workshop ARE at UC Davis, Big Sky Workshop, AMIE Workshop, WCERE, FAERE, Land-Use Policies & Climate Change Adaptation Workshop and BioEcon. Any remaining errors are my own.

1 Introduction

Irrigation is a cornerstone of agricultural development, covering one-fifth of the world's cropland (FAO, 2023), but its net returns are debated (Dillon and Fishman, 2019). It raises productivity, reduces poverty (Dillon and Fishman, 2019; Giordano et al., 2019), and helps farmers adapt to climate risk (Taylor, 2026). Yet irrigation also generates environmental externalities. Intensive use drives rapid groundwater depletion (Wada et al., 2010), which in turn constrains development (Sekhri, 2014; Blakeslee et al., 2020). Beyond resource depletion, the climate science literature documents that irrigation affects the climate above and beyond irrigated areas (Puma and Cook, 2010; Alter et al., 2015; Nocco et al., 2019; Greve et al., 2025). By increasing evapotranspiration, irrigation modifies land–atmosphere interactions, affecting cloud formation and precipitation downwind.

This paper documents the positive climatic externality of irrigation on rainfall and its economic benefits. To do so, I combine historical administrative records on irrigation infrastructure over the period 1960–2010 with high-resolution climate data and administrative agricultural data. Causal identification exploits exogenous variation in exposure to distant upwind irrigation projects generated by wind flows, while absorbing local, seasonal, and state-year shocks. I trace the resulting climatic and economic responses at short, medium, and long horizons using annual panels, five- and ten-year averages, and long differences.

I focus on India, the country with the largest irrigated area in the world. Over the past five decades, India has invested over $100 billion to build an extensive network of dams and canals that now irrigates nearly one-third of its cropped area (Planning Commission, 2011; Ministry of Water Resources, 2011). These investments were rolled out in a staggered fashion across space, generating substantial spatial and temporal variation. During the same period, the country has experienced a delayed structural transformation, with a large share of the population remaining in agriculture and a slow transition toward more efficient farm structures.

I first show that irrigation has substantially altered India's precipitation over the past fifty years. A 10-percentage-point increase in upwind irrigation exposure, about half of India's Green Revolution expansion, raises rainfall by 5–6 mm per month, a magnitude equivalent to roughly

20% of average monthly precipitation. The effect is concentrated during the winter months, India's dry season, consistent with both peak irrigation application and the high reliance on land-sourced atmospheric moisture during this season (Koppa et al., 2026). This increase in rainfall volume is also accompanied by an 11% increase in the frequency of rainy days and a reduction in temperature of about half a degree, with persistent effects over five- and ten-year horizons.

These seasonal changes have a counterintuitive implication: additional rainfall can increase, rather than reduce, farmers' investment in irrigation downwind. While higher annual rainfall would typically raise yields and reduce irrigation incentives, its seasonal distribution matters. In India, where limited rainfall constrains cultivation during the dry season, additional precipitation can make a second harvest profitable without providing enough water to sustain it on its own. By increasing the returns to dry-season cultivation, rainfall can therefore increase the returns to investing in irrigation, making irrigation and precipitation complements rather than substitutes.

Consistent with this prediction, I find that farmers invest in private irrigation downwind, increasing irrigation intensity by 1.3 percentage points, equivalent to 5% of India's aggregate increase between 1960 and 2010. This allows farmers to cultivate land during the winter months, increasing cropping intensity by 1.2 percentage points, roughly 4% of India's increase over the period. Cultivating a second season represents an important income-generating margin for Indian farmers (Blakeslee et al., 2023; Jain et al., 2021). I show that the expansion increases the production of wheat, India's major winter crop, by 5%. In contrast to findings in developed-country contexts such as the United States (Grosset-Touba et al., 2024), I find no improvement in yields, nor investment in other adaptation strategies such as mechanization, fertilizer use, or changes in crop composition. This suggests that improved climatic conditions encourage farmers to bring more marginal land into cultivation without corresponding yield gains or investment in yield-enhancing technologies.

In the long run, these changes in the returns to cultivation reshape India's farm structure, as the opportunity to cultivate an additional season can affect farms differently across the size distribution. For smallholders, higher returns from existing land can make otherwise marginal

holdings economically viable, reducing incentives to exit farming. For larger farms, the same increase in the profitability of cultivation can encourage expansion of the area they operate. Consistent with these mechanisms, I find that small farms are more likely to survive, slowing their transition toward medium-sized holdings, while large farms expand their operated area without a corresponding increase in their number. The resulting pattern is one of agricultural polarization: irrigation-induced climate change sustains small-scale farming while promoting land consolidation among larger producers, ultimately slowing agricultural structural transformation.

To quantify the economic value of these climatic externalities, I perform a counterfactual exercise comparing India's agricultural trajectory with and without canal irrigation expansion. I find that these spillovers account for 7% of wheat production growth between 1967 and 2010, worth an additional $1 billion annually. I then project the effects of canal-irrigated areas currently under construction. These projects would increase dry-season rainfall by 8.4% and wheat production by 3.6 million tonnes, equivalent to 4.6% of current production, with 30% of the rainfall gains occurring over rainfed land.

Related literature. Focusing on irrigation, this paper improves our understanding of the feedbacks between development and climate (Jack and Ryan, 2026). It contributes to three strands of the literature.

First, I provide new causal evidence on how irrigation infrastructure affects development by documenting a previously overlooked externality. There is a long-standing debate on the returns to irrigation (Dillon and Fishman, 2019). A large body of work has studied irrigation's economic benefits since the seminal work of Duflo and Pande (2007), with subsequent studies documenting gains in farm income, productivity, and broader development outcomes (Hansen et al., 2011; Strobl and Strobl, 2011; Blanc and Strobl, 2014; Olmstead and Sigman, 2015; Dillon and Fishman, 2019; Zaveri et al., 2020; Jones et al., 2022).[1] More recent work emphasizes surface irrigation's consequences for India's structural transformation (Asher et al., 2022; Blakeslee et al.,

[1]Other studies document similar effects for groundwater irrigation (Fishman et al., 2013; Sekhri, 2014; Hornbeck and Keskin, 2014, 2015; Ryan and Sudarshan, 2020; Blakeslee et al., 2020; Butler and Boudot Reddy, 2023).

2023).[2] This paper estimates the spatial redistribution of rainfall volume and frequency induced by irrigation, and quantifies the consequences for agricultural production, farmers' adaptation strategies, and long-run agricultural structure over five decades.

The second contribution bridges climatic and economic evidence by showing that climate is partly endogenous to human activity. Natural science evidence shows that land-use changes – deforestation, irrigation, crop choice, urbanization – alter land–atmosphere interactions, with documented effects on temperature and precipitation (Puma and Cook, 2010; Alter et al., 2015; Greve et al., 2025; Butt et al., 2011; Leite-Filho et al., 2021; Loarie et al., 2011; Manoli et al., 2019).[3] A nascent literature in economics has begun to examine these effects. Focusing on forest cover change, it documents the downwind consequences of deforestation for hydropower in the Amazon (Araujo, 2024) and for conflict in West Africa (Degois et al., 2026), and of U.S. afforestation programs for agriculture (Li, 2021; Grosset-Touba et al., 2024). Closely related to this paper, Braun and Schlenker (2023) document that irrigation in the United States lowers temperatures, increasing agricultural productivity and reducing mortality. This paper focuses on the effect of irrigation on rainfall and shows that the climatic effects of irrigation depend on the underlying climate regime. In contrast to existing evidence from temperate regions, I find that irrigation reshapes the seasonal distribution of rainfall in monsoon systems, which sustain nearly two-thirds of the world's population. Climate models have predicted such responses (Saeed et al., 2009; Guimberteau et al., 2012a; Chou et al., 2018; Devanand et al., 2019); this paper provides, to my knowledge, the first empirical evidence. I then trace the economic consequences of this climate feedback over the short, medium, and long run.

Third, this paper contributes to the literature on climate change, adaptation, and development. I document a feedback loop between adaptation and climate focusing on irrigation, and introduce a new source of quasi-experimental variation to study the effects of persistent climatic change. Existing work typically relies either on short-run weather shocks (Schlenker and Roberts, 2009;

[2] More broadly, this paper also relates to the literature on the spatial allocation of infrastructure and place-based policies (Donaldson and Hornbeck, 2016; Donaldson, 2018; Asher and Novosad, 2020; Bustos et al., 2016, 2020).

[3] See te Wierik et al. (2021) for a review of the literature.

Lobell et al., 2011; Dell et al., 2012, 2014; Carleton and Hsiang, 2016) or long-run differences in climate trends across locations (Henderson et al., 2017; Kala, 2017; Taraz, 2017, 2018; Emerick, 2018; Liu et al., 2023) to study the impact of climate change on the economy. Both approaches treat climate variation as external to local adaptation decisions (Dell et al., 2014). Yet, farmers are known to adapt to weather shocks and monsoon shifts through irrigation investment (Burlig et al., 2025; Taraz, 2017; Kala, 2017). If irrigation also affects rainfall and temperature, observed climate variation may partly embed past adaptation responses. This paper provides empirical evidence of this feedback: irrigation is both a driver of persistent climatic change and an adaptation to it.[4] I address this challenge by exploiting irrigation-induced climatic spillovers documented in this paper, which generate climate variation that is persistent yet orthogonal to local adaptation decisions. Finally, the paper shows that understanding adaptation requires looking beyond annual climate averages to the seasonal distribution of rainfall.

The remainder of the paper is organized as follows. Section 2 presents the climatic and agricultural context. Section 3 presents a simple model of irrigation adoption under seasonal rainfall reallocation, to build intuition for the results that follow. Section 4 describes the data sources and variables. Section 5 outlines the empirical strategy. Section 6 presents the main results, Section 7 discusses robustness, Section 8 runs a counterfactual exercise and projection, and Section 9 concludes.

2 Climatic and Agricultural Context

This section describes the climatic and agricultural context of the study, characterized by the Indian monsoon system, India's agricultural calendar and irrigation use.

[4]This has methodological implications: if adaptation has moderated climatic extremes, estimates based on observed long-run climate variation may understate true damages, generating attenuation bias. This concern relates to the interpretation of long-run climate estimates as evidence of adaptation (Burke and Emerick, 2016; Liu et al., 2023) and aligns with recent macro-climate models that endogenize adaptation in spatial equilibrium dynamics (Krusell and Smith, 2022; Cruz and Rossi-Hansberg, 2024; Fillon, 2025).

The Indian Monsoon India's climate is dominated by the monsoon system, characterized by heavy rain over the months of June to September delivering 70% of the country's annual rainfall. The rest of the year is particularly dry, with the median district receiving 10mm in January against 288mm in July (Appendix Figure A6). Precipitation patterns are also spatially heterogeneous (Appendix Figure A7), with the north-west and the south-eastern coast receiving the retreating monsoon. Temperature follows the same calendar, with a median district-month of 21.4°C in the dry season against 27.2°C during the monsoon (Appendix Figure A8). Over the past two decades, monsoon onset and progression have grown increasingly erratic, with the underlying causes still debated in the literature (Kapa et al., 2025).

The Agricultural Calendar: Kharif and Rabi India's agricultural calendar follows this seasonal rhythm and is organized into two main cropping seasons. The *Kharif* season runs from June to September, coinciding with the monsoon: rain-fed crops such as rice, cotton, and pulses are sown at the onset of the rains and harvested in autumn. The *Rabi* season runs from roughly November to March, during the dry winter months, and is dominated by wheat. Rabi is the main irrigation season: wheat alone accounts for over a third of India's irrigated crop area. Because little rain falls during this period, Rabi cultivation depends almost entirely on irrigation. Access to irrigation therefore determines whether farmers can grow a second crop each year, a key margin for raising agricultural income (Duflo and Pande, 2007).

Sources and Cost of Irrigation Irrigation in India is delivered through two main channels: canal networks fed by dams and reservoirs, and groundwater extracted through privately owned tubewells. Canals were the principal source for most of the period studied here, before tubewells overtook them as the dominant source from the 1990s onward (Singh et al., 2022). The two technologies differ in cost structure: canal construction requires large, long-term public investment, while a tubewell requires a smaller, sunk drilling cost, after which pumping is cheap due to subsidized agricultural electricity.

3 Irrigation Adoption under Seasonal Rainfall Reallocation

If irrigation is not only a productive input but also reshapes the seasonal distribution of rainfall downwind, an important question arises: how do such climatic spillovers affect other farmers' incentives to invest in irrigation, potentially creating feedback effects across space and time?

In standard theoretical models, irrigation and rainfall are technological substitutes. When rainfall is abundant, the marginal return to irrigation declines as water inputs exhibit diminishing returns (Feder et al., 1985). In such frameworks rainfall enters production as a single aggregate input, and irrigation augments total water availability. However, in many agricultural systems irrigation does more than increase productivity within a growing season. In environments with a distinct monsoon and dry season, irrigation may enable cultivation during the dry season and increase cropping intensity (Jones et al., 2022; Hussain and Hanjra, 2004; Foster and Rosenzweig, 1995; Duflo and Pande, 2007). In these contexts irrigation affects production along two margins: it increases water availability within a season and expands the feasible production calendar by activating an additional cropping season. This distinction implies that the relationship between rainfall and irrigation adoption depends not only on total annual rainfall but also on its seasonal distribution.

This section develops a simple model of irrigation adoption under seasonal rainfall variation. The model highlights how changes in seasonal rainfall distribution can generate different adoption responses than an analysis based on aggregated annual totals would suggest.

3.1 Baseline model: Single-Season Agriculture

I begin with a standard one-season model to establish the benchmark prediction. A farmer cultivates one crop during the monsoon season. Land and other inputs are fixed. The farmer is risk neutral and chooses whether to invest in irrigation. Installing irrigation requires a fixed cost $F > 0$ and provides an additional water input $\alpha > 0$.

Let rainfall be denoted by r. Effective water is given by total water availability $w = r + \alpha I$,

where $I \in \{0, 1\}$ denotes irrigation adoption. Output per hectare is $f(w)$, where $f'(w) > 0$ and $f''(w) < 0$, implying diminishing returns to water.

Profits are given by $\Pi(I; r) = f(r+\alpha I) - FI$. The gain from adopting irrigation is therefore

$$\Delta(r) = f(r + \alpha) - f(r) - F. \tag{1}$$

Because production is concave in water, the marginal product of water declines as rainfall increases.

Proposition 1 (Substitution)**.** *Higher rainfall reduces the profitability of irrigation:*

$$\frac{\partial \Delta}{\partial r} < 0.$$

Thus in the standard single-season environment rainfall and irrigation are technological substitutes, and rainfall availability reduces incentives to adopt irrigation.

3.2 Two-Season Agriculture

Now consider an agricultural year composed of two seasons: the monsoon season (Kharif), indexed K, and the dry season (Rabi), indexed R. Seasonal rainfall is denoted by (r_K, r_R), with total annual rainfall $r = r_K + r_R$.

A key feature of the environment is that dry-season cultivation requires irrigation.[5] This assumption captures environments where residual soil moisture is insufficient to sustain the entire Rabi production. Irrigation therefore does not merely increase productivity; it activates production in an additional season.

Output without irrigation is $\Pi^0(r_K) = f_K(r_K)$. When irrigation is adopted, both seasons are cultivated and total output is

$$\Pi^1(r_K, r_R) = f_K(r_K + \alpha_K) + f_R(r_R + \alpha_R) - F,$$

where $f_s(\cdot)$ is increasing and concave in effective water and α_s denotes irrigation water in season s. Irrigation is adopted whenever the gain $\Delta(r_K, r_R) = \Pi^1 - \Pi^0$ is non-negative. Rewriting the

[5] More generally, irrigation may increase the share of land that can be cultivated during the dry season.

gain yields

$$\Delta(r_K, r_R) = \underbrace{[f_K(r_K + \alpha_K) - f_K(r_K)]}_{\text{Substitution}} + \underbrace{f_R(r_R + \alpha_R)}_{\text{Activation}} - F. \tag{2}$$

Two distinct channels determine irrigation profitability. The first term captures the *substitution effect*: irrigation increases water availability during the monsoon season when rainfall is scarce. The second term captures the *activation effect*: irrigation enables cultivation during the dry season. Seasonal rainfall affects irrigation adoption through these two margins.

Following Proposition 1, higher rainfall during the monsoon season reduces irrigation profitability ($\frac{\partial \Delta}{\partial r_K} < 0$) as it lowers the marginal value of irrigation. I focus on the second activation term, which leads to a positive effect of higher Rabi rainfall on irrigation adoption.

Proposition 2 (Activation)**.** *Higher rainfall during the dry season increases irrigation profitability:*

$$\frac{\partial \Delta}{\partial r_R} > 0.$$

Higher rainfall during the dry season (r_R) raises the productivity of Rabi cultivation, which is activated only when irrigation is installed.

The overall effect of rainfall shocks therefore depends on how rainfall is distributed across seasons. Consider a change in rainfall allocation such that total rainfall changes by $\Delta r = \Delta r_K + \Delta r_R$. Irrigation adoption increases whenever

$$f'_R(r_R + \alpha_R)\Delta r_R > [f'_K(r_K) - f'_K(r_K + \alpha_K)]\,|\Delta r_K|. \tag{3}$$

Climatic shocks that reallocate rainfall across seasons may therefore either increase or decrease irrigation incentives depending on their direction, the degree of substitution between rainfall and irrigation during the monsoon season, and the profitability of dry-season production.

The comparative statics above can be summarized by an adoption frontier that separates rainfall states in which irrigation is profitable from those in which it is not. Figure A12 in Appendix B illustrates the irrigation adoption frontier implied by the model. Irrigation is adopted whenever the pair (r_K, r_R) lies above the frontier. Panels (b)–(d) illustrate how the adoption frontier shifts. Higher Rabi productivity lowers the threshold as irrigation becomes more valuable through the

activation of dry-season production. Higher Kharif scarcity value increases the marginal benefit of irrigation when monsoon rainfall is low. Finally, higher fixed costs shift the entire frontier upward, reducing irrigation adoption in all rainfall states.

In contrast to the single-season benchmark where higher total rainfall would unambiguously reduce irrigation incentives, the two-season environment highlights that the effect depends on how rainfall is distributed across seasons.

4 Data

This paper combines spatial and temporal variation in irrigation coverage across India with remote satellite measures of climate and district-level agricultural panel data. I first estimate the effects of irrigation on downwind climate using district-month observations from 1966 to 2020, allowing me to account for the seasonal dynamics of atmospheric moisture transport. Because the agricultural data are available only at the annual level, I then aggregate the irrigation exposure measure accordingly to examine how irrigation-induced precipitation shapes downstream agricultural productivity and farmers' adaptation. Appendix Table A6 reports descriptive statistics for the estimation sample.

Climate Data. To characterize atmospheric dynamics, this paper uses the ERA5 reanalysis dataset developed by the European Centre for Medium-Range Weather Forecasts (ECMWF).[6] ERA5 provides pressure fields together with the horizontal wind components (u and v), which jointly describe wind speed and direction. These data are available globally at a spatial resolution of 0.25 degree (approximately 24 km at the equator) at monthly frequency. The analysis focuses on the 1960–2020 period, during which wind trajectories are reconstructed by tracing air mass movements backward in time in order to connect pixels, following the approach of Araujo (2024) for each pixel-month. Rainfall data come from gridded precipitation data produced by the India Meteorological Department (IMD), which reports daily rainfall at a resolution of 0.25 degree for

[6]Downloaded from ERA5 on the 17/06/2025.

the period 1960–2024 (Pai et al., 2014).[7] This dataset combines in-situ measurement with satellite re-analysis and is considered the most reliable source for India (Burgess et al., 2017).[8] Temperature data come from ERA5-Land, available at a finer resolution of 0.1 degree (about 9 km at the equator). To characterize specifically the onset and length of the monsoon, I use the pentad (5-day period) rainy/dry season detection algorithm of Bombardi et al. (2019), applied to CHIRPS precipitation data.

Irrigation Data. Information on irrigation infrastructure is obtained from the India Water Resources Information System (WRIS), which provides geolocalized geometries of canals, irrigated areas by canals, aquifers, and rivers.[9] An irrigation project typically consists of a reservoir (or a river diversion) that supplies a network of canals distributing water to the surrounding area. The command area of a project is defined as the land that can be reached by these canals and is therefore eligible for irrigation. The size of the command area is determined by the storage capacity of water (often a dammed reservoir, though sometimes a direct river diversion) and the terrain's topography. In addition to spatial coverage, I retrieve information on the start and end years of canal construction as well as project status (ongoing vs. completed) using the Central Water Commission's Management Information System of Water Resources Projects and the India WRIS Wiki. As documented by Asher et al. (2022), reported canal start dates sometimes refer to rehabilitation rather than initial construction. To address this issue, open-access construction dates compiled by Asher et al. (2022) are used and supplemented with manual validation based on government documents, news articles, and academic reports.[10] Appendix Figure A10 maps the spatial and temporal coverage of canal irrigation projects (i.e., command areas) since 1960.[11] Pixel-level irrigation is defined as the proportion of each pixel's area irrigated by canals

[7] Dataset available at IMD Gridded Rainfall Data.

[8] As a robustness check, rainfall estimates from ERA5-Land are also used. Results are consistent across both data sources.

[9] Canal shapefiles and identifiers were originally available at NWIC Canal Dataset, accessed on 28/05/2025. The dataset was last updated on May 5, 2025 (10:46 AM, UTC+02:00), but the link is no longer accessible.

[10] I acknowledge the use of ChatGPT's deep search to support this validation, with all findings cross-checked against primary sources.

[11] Table A7 shows that canals with an unknown completion year represent 3.5% of all completed canals in the sample, and that approximately 18% of India's total area is currently irrigated by canals. An additional 8% of the

in a given year. This measure, which ranges from 0 to 1, captures the cumulative expansion of irrigated command areas over time.

Agricultural Data. Agricultural outcomes are measured using the District-Level Data (DLD) from ICRISAT, which provides a comprehensive yearly panel of agricultural statistics for Indian districts from 1966 to 2009. District boundaries correspond to those of India in 1966, including 311 districts at the time.[12] Appendix Figure A11 maps the explanatory variable used in the analysis, i.e. Upwind Irrigation Exposure, on the 1966 boundary districts. The dataset covers a wide range of agricultural indicators, including cropped area, production and yields[13] disaggregated by major crop types. In addition, it includes information on agricultural practices such as irrigation by type, fertilizer use, double cropping, and land allocation. Data on farm size distribution are available only at five-year intervals, corresponding to the Agricultural Census of India for census years from 1970 to 2005. These data report the number and total area of farms disaggregated into five size categories: *marginal* (< 1 ha), *small* (1–2 ha), *semi-medium* (2–4 ha), *medium* (4–10 ha), and *large* (> 10 ha).

Additional Controls. The robustness analysis in Section 7 draws on a broad set of geographic, agricultural, and environmental covariates. Geographic controls include elevation and its within-district dispersion, slope, terrain ruggedness, distance to the coast, latitude, longitude, and aquifer composition. I construct the topographic measures from WorldClim's 30 arc-second SRTM-derived elevation data (Fick and Hijmans, 2017), using the terrain ruggedness index of Riley et al. (1999), and derive aquifer shares from the Central Ground Water Board's principal aquifer map. Agricultural controls are available in the ICRISAT dataset and include baseline forest cover, population, and the area planted with high-yielding varieties (HYV). Finally, I measure air pollution using the monthly satellite-derived surface $PM_{2.5}$ product of van Donkelaar et al. (2021), available from 1998 at a $0.01°$ resolution and aggregated to the $0.25°$ analysis grid.

country's surface area is under ongoing construction.

[12] ICRISAT consolidated data on Indian districts from multiple sources, see ICRISAT Data and Shapefile.

[13] Calculated as production over area.

5 Empirical Strategy

The empirical strategy exploits variation in prevailing wind trajectories and the timing of irrigation expansion to construct quasi-experimental exposure to upwind irrigation. The underlying idea is that air masses passing over irrigated land acquire additional moisture, thereby affecting rainfall and temperature downwind and, ultimately, agricultural outcomes. Identification relies on the exogeneity of wind paths, rich spatial and temporal fixed effects, and the substantial distance between focal cells and their upwind counterparts, which limits the scope for reverse causality. I first describe the construction of the exposure measure in Section 5.1. I then present the empirical framework used to estimate its relationship with rainfall and temperature in Section 5.2, before extending the analysis to agricultural outcomes in Section 5.3. Finally, Section 5.4 outlines the empirical approach used to study the medium- and long-run effects.

5.1 Methodology

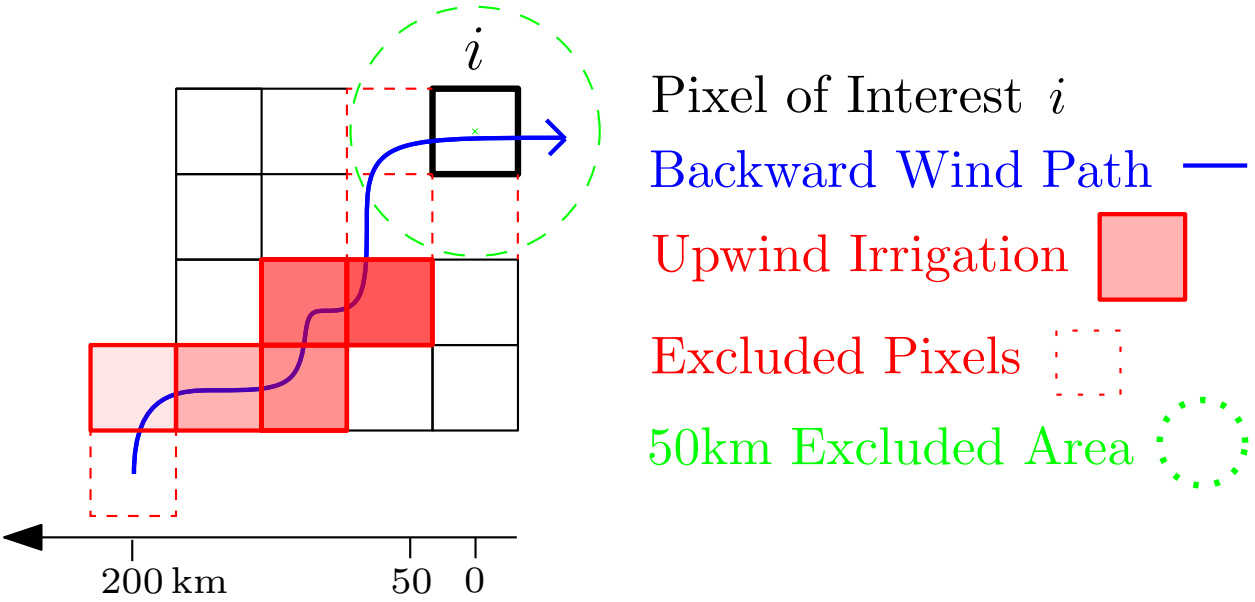
The key explanatory variable, *Upwind Irrigation*, is constructed by combining wind-trajectory with the spatial irrigation dataset described in Section 4. The following wind connectivity matrix is defined at a 0.25° spatial resolution (approximately 24 km at the equator). For each pixel of interest i, I (i) trace its monthly backward wind path at the 800 hPa level,[14] and (ii) retain only the segments of this trajectory that lie between 50 and 150km from i, following Araujo (2024) and Degois et al. (2026). Pixels within 50 km are excluded to minimize potential reverse causality (e.g., irrigation decisions in neighboring areas could be correlated with local climate conditions), while segments beyond 150km are discarded because the influence of irrigation on moisture transport is expected to dissipate at larger distances (Spracklen et al., 2012; Degois et al., 2026).[15] For each pixel i, year t, and month m, *Upwind Irrigation* is defined as the average share of irrigated land across

[14] This choice ensures that wind paths are determined at an altitude largely unaffected by local surface conditions such as vegetation or irrigation, and can therefore be considered exogenous to pixel-level agricultural activities. In addition, this is the atmospheric level at which most clouds form, strengthening the ability to capture the effects of rainfall rather than other wind-borne confounders.

[15] Robustness checks using alternative exclusion buffers and outer radii do not change the results (Appendix D.2, Figure A17).

cells lying along i's backward wind trajectory within the 50–150 km window. By construction, this variable takes values in $[0, 1]$ and varies over time due to year-to-year changes in irrigated area and monthly fluctuations in wind direction.

Figure 1: Upwind Irrigation



Notes: The **upwind neighbors** (in red) are linked to the **pixel of interest *i*** (in bold black) through its backward wind path, represented in blue. To mitigate concerns about reverse causality, pixels located within a 50 km buffer around the centroid of the pixel of interest (in green) are excluded, as are pixels located more than 150km away. The explanatory variable *Upwind Irrigation* is constructed by identifying all pixels lying along the backward wind path and located between 50 and 150km from each pixel of interest (highlighted in red). *Upwind Irrigation* is then defined as the average proportion of irrigated area across these upwind neighbors, weighted inversely by their distance to *i* (darker red: larger weight). The figure is not drawn to scale and is intended for illustrative purposes only.

Figure 1 illustrates this construction. The pixel of interest i (in black) is connected to its upwind neighbors (in red) through its backward wind path (in blue). Neighbors along the wind path falling within the 50–150km window are retained, while those too close (in green) or too distant are excluded. The resulting measure thus captures the intensity of irrigation in the relevant upwind zone. Figure 2 illustrates the independent variable *Upwind Irrigation* across India, averaged over the period 1966–2020. To implement placebo tests, I reverse the connection matrix and repeat the same procedure, defining exposure to downwind rather than upwind irrigation.

District-Level Exposure. Because agricultural outcomes are observed at the district level, I construct a district-level measure of *Upwind Irrigation* by spatially aggregating pixel-level exposure. For each district, year, and month, I average exposure across all pixels intersecting the district, using the area of overlap between each pixel and the district as spatial weights. Formally,

$$E^{\uparrow}_{d,t,m} = \frac{\sum_{i \in d} e^{\uparrow}_{i,t,m}\, a_{i \cap d}}{\sum_{i \in d} a_{i \cap d}},$$

where $e^{\uparrow}_{i,t,m}$ is the monthly grid-cell-level *Upwind Irrigation* exposure of pixel i in year t and month m, and $a_{i \cap d}$ represents the area of overlap between pixel i and district d. This procedure yields a continuous monthly district-level exposure measure bounded between 0 and 1, which is comparable across districts and independent of district size. To avoid mechanical endogeneity, irrigation located within the district itself is excluded from the calculation, such that exposure captures only irrigation occurring in upwind districts. The resulting district-level measure is plotted in Appendix Figure A11 for each of the 311 districts defined under the 1966 administrative boundaries included in the sample.

5.2 Irrigation and Climate

I first estimate the effect of upwind irrigation on downwind climate, providing the empirical first stage for testing whether irrigation expansion alters atmospheric moisture transport. Given the strong seasonality of both irrigation and climate in India, the atmospheric impacts of irrigation are expected to vary over the agricultural calendar. To capture this seasonal heterogeneity, I estimate the following district-month specification:

$$y_{d,t,m} = \beta_{Jul} E^{\uparrow}_{d,t,m} + \sum_{m \neq \text{Jul}} \beta_m \, \mathbf{1}\{M_{d,t,m} = m\} \cdot E^{\uparrow}_{d,t,m} + \mu_d + \delta_m + \lambda_{s,t} + \varepsilon_{d,t,m} \tag{4}$$

where $y_{d,t,m}$ is the outcome of interest, i.e., total precipitation (in mm) or mean temperature (in °C), for district d, year t, and month m. The key explanatory variable, *Upwind Irrigation* $E^{\uparrow}_{d,t,m}$, measures the share of irrigated land located upwind of district d at time (t, m). The specification

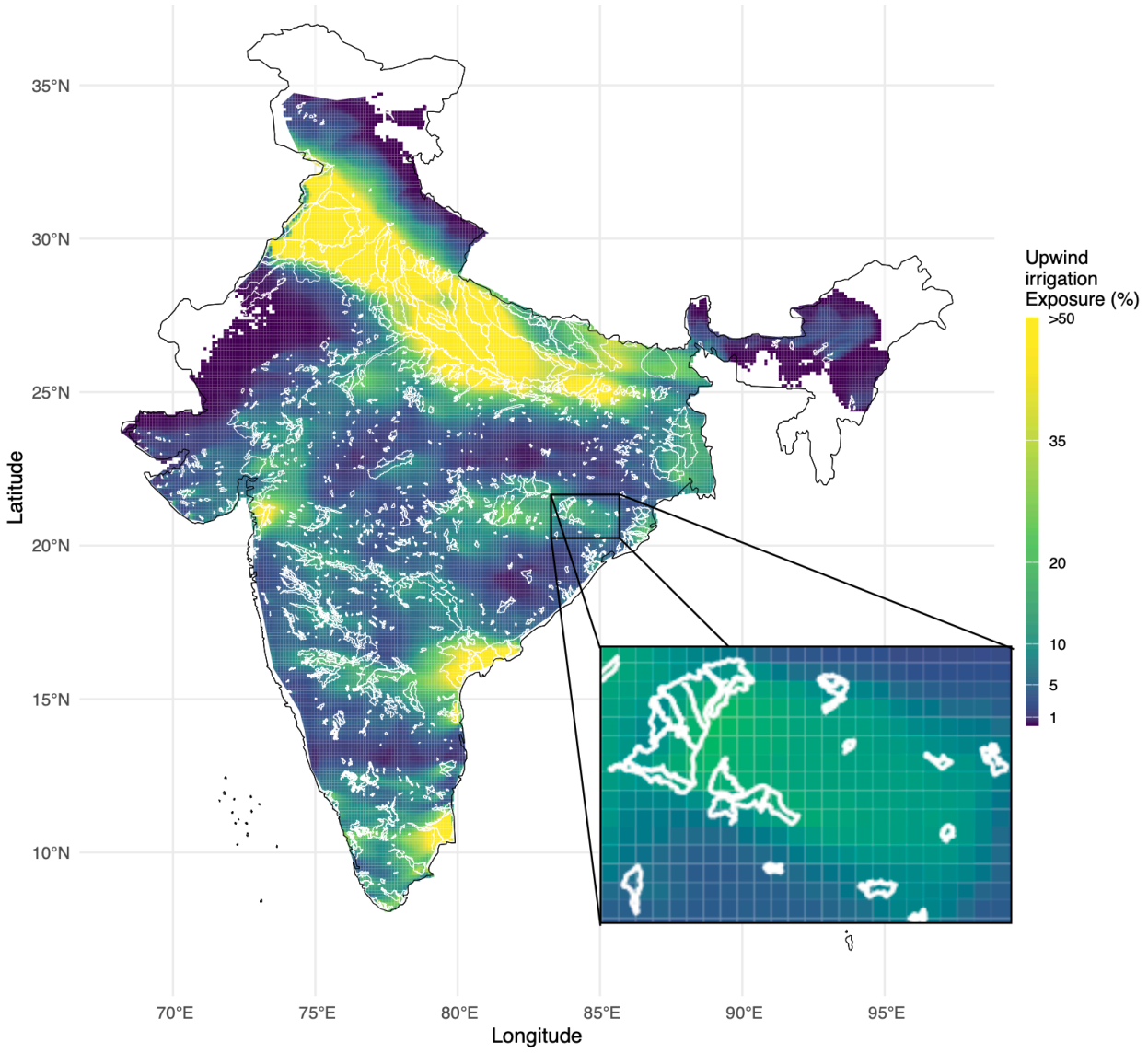


Figure 2: Average Upwind Irrigation Exposure Across India (1966-2020)

Notes: The figure maps the spatial distribution of the key explanatory variable, *Upwind Irrigation*, at a 0.1 degree resolution. It captures the average share of irrigated land across upwind pixels located along the seven-day backward wind trajectory, restricted to a 50–150km upstream range of each pixel of interest i. Areas irrigated by canals, i.e. command areas, are outlined in white. Exposure variable is averaged over the full study period, spanning 1966–2020.

introduces $\mathbf{1}\{M_{d,t,m} = m\}$, an indicator variable for each month m, with July as the reference category. District fixed effects, μ_d, absorb time-invariant location characteristics, month fixed effects δ_m account for seasonality, and state-by-year fixed effects $\lambda_{s,t}$ capture local shocks and regional climate trends. Standard errors are clustered at the district level. β therefore captures

the total effect of upwind irrigation exposure on climate variables in July. For any other month m, the total effect is given by $\beta + \beta_m$. To ease interpretation, I scale the estimates to a 10 percentage point increase in upwind irrigation exposure, roughly half of India's irrigation expansion during the Green Revolution. The resulting month-specific coefficients provide a dynamic perspective on how both the direction and magnitude of irrigation-induced climate effects evolve throughout the year.

5.3 Climatic Spillovers, Agriculture and Adaptation

Having established that upwind irrigation alters downwind weather, I next examine whether such irrigation-induced climatic changes translate into measurable agricultural performance.

Annual Aggregation. Because agricultural outcomes are observed annually, I aggregate monthly district-level exposure to the yearly level. I compute a time-weighted average using the number of days in each month as weights, which accounts for unequal month lengths:

$$E^{\uparrow}_{d,t} = \frac{\sum_{m=1}^{12} E^{\uparrow}_{d,t,m}\, w_{t,m}}{\sum_{m=1}^{12} w_{t,m}},$$

where $w_{t,m}$ denotes the number of days in month m of year t. In robustness checks, I apply the same aggregation procedure separately between wet- and dry-season months to construct season-specific annual exposure measures.

Effects on Agricultural Production. I then estimate the effect of upwind irrigation exposure on agricultural outcomes using the following district-year panel specification:

$$Y_{d,s,t} = \beta\, E^{\uparrow}_{d,t} + \mu_d + \lambda_{s,t} + \varepsilon_{d,s,t}, \tag{5}$$

where $Y_{d,s,t}$ denotes agricultural outcomes (e.g., total production, cultivated area, yields, etc.) in district d and year t. The variable $E^{\uparrow}_{d,t}$ is the yearly district-level exposure to upwind irrigation. District fixed effects μ_d absorb time-invariant district characteristics, including soil quality, to-

pography, and baseline agro-climatic conditions, while state-by-year fixed effects $\lambda_{s,t}$ capture policy, market, and climatic shocks common to districts within the same state and year. Standard errors are clustered at the district level.

5.4 Medium- and Long-Run Effects

Finally, I examine whether irrigation spillovers persist over longer horizons. This exercise is motivated by two considerations. First, I test whether irrigation generates persistent changes in downwind weather conditions, rather than only transitory year-to-year fluctuations. Second, agricultural responses may take time to materialize, as farmers gradually adjust input use, crop choices, irrigation adoption and production practices. I therefore complement the annual panel estimates with moving-average and long-difference specifications.

I first estimate medium-run specifications using five- and ten-year moving averages. For each district d and anchor year τ, I average outcomes, upwind irrigation exposure, and potential controls over windows centered around τ. Let $L \in \{5, 10\}$ denote the window length. For any district-year variable $Z_{d,t}$ entering the specification, I define

$$\overline{Z}_{d,\tau}^{(L)} = \frac{1}{L} \sum_{k \in \mathcal{W}_L(\tau)} Z_{d,k},$$

where $\mathcal{W}_5(\tau) = \{\tau - 2, \ldots, \tau + 2\}$ and $\mathcal{W}_{10}(\tau) = \{\tau - 4, \ldots, \tau + 5\}$. I estimate the five-year specification for census anchor years $\tau \in \{1970, \ldots, 2000\}$,[16] and the ten-year specification for $\tau \in \{1970, 1980, 1990, 2000\}$. I then estimate

$$\overline{y}_{d,\tau}^{(L)} = \beta_1 \overline{E}_{d,\tau}^{\uparrow,(L)} + \mu_d + \lambda_{s,\tau} + \varepsilon_{d,\tau}. \tag{6}$$

The specification includes district fixed effects μ_d and state-by-anchor-year fixed effects $\lambda_{s,\tau}$. Identification comes from changes in medium-run upwind irrigation exposure within districts, relative to other districts in the same state and anchor year.

[16] These anchor years correspond to the availability of India's agricultural census, which allows me to estimate the same specification for farm-structure outcomes.

I further estimate a long-difference specification comparing the beginning and end of the sample. I define changes as the difference between five-year averages centered on 2000 and 1970: $\Delta Z_d = \overline{Z}^{(2)}_{d,2000} - \overline{Z}^{(2)}_{d,1970}$. I then estimate

$$\Delta y_d = \beta_1 \Delta E_d^{\uparrow} + \lambda_s + \varepsilon_d. \tag{7}$$

By differencing outcomes and exposures between the initial and final periods, this specification removes all time-invariant district characteristics by construction. State fixed effects λ_s absorb state-level differences in long-run trends, policies, and institutional changes. Standard errors are clustered at the district level throughout.

6 Results

Section 6.1 first quantifies the seasonal heterogeneity of climatic responses to upwind irrigation exposure; Section 6.2 then examines their implications for agricultural development.

6.1 The Climate Externality of Irrigation

A Wetter Dry-Season. Rainfall, temperature, and irrigation exhibit strong seasonal variations in India, shaped by the monsoon cycle, with a wet *Kharif* season (June–September) and a dry *Rabi* season (October–March), as explained in Section 2. The effect of irrigation on the climate is therefore expected to vary across the year. Figure 3 reports the monthly effects of upwind irrigation on precipitation and the frequency of rainy days.

The results reveal a substantial increase in precipitation during the dry *Rabi* season. A 10-percentage-point increase in upwind irrigation exposure raises monthly rainfall by 5–6 mm, equivalent to approximately 17–21 percent of the dry-season monthly mean of 29 mm. This increase in volume is accompanied by more frequent precipitation, with the number of rainy days rising by 11 percent. This distinction is relevant for agriculture, as higher total rainfall does not necessarily improve crop production if it is concentrated in a few intense events rather than distributed across the growing season (Fishman, 2016). The precipitation response is accompa-

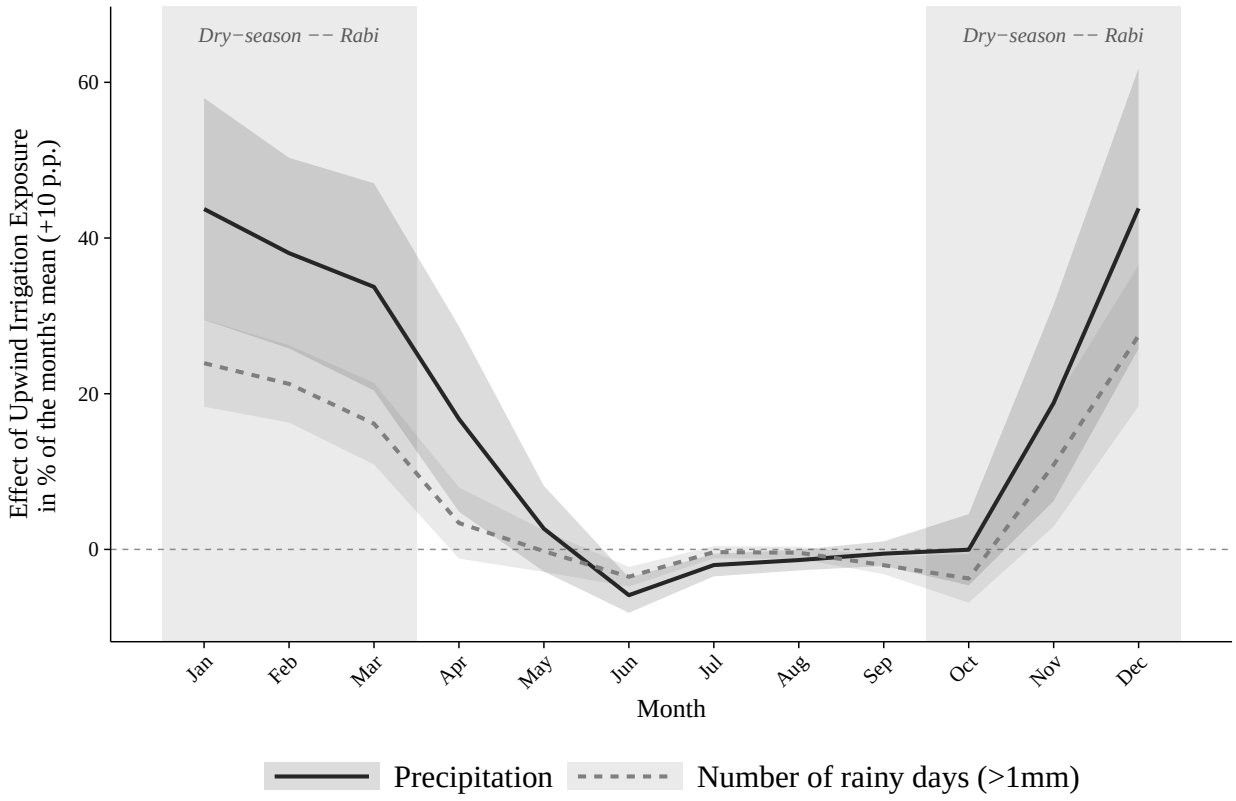


Figure 3: Seasonal Effect of Upwind Irrigation on Rainfall

Notes: Figure 3 reports the estimated coefficients from specification (4) on (i) monthly precipitation (solid line) and (ii) the number of rainy days ($>$ 1mm, dashed line), both expressed in percent of the monthly mean. The monthly mean is computed over the exposed districts, those with average upwind exposure of at least 10 percentage points. Each estimated coefficient β_m measures the *total* marginal effect of a 10 percentage point increase in upwind irrigation exposure in month m. Upwind irrigation is defined as the mean share of irrigated area in pixels located 50–150 km upwind of the focal pixel, weighted inversely by distance, averaged over the district. All regressions are estimated at the district level (corresponding to 311 districts) and include district fixed effects, month fixed effects and state-by-year fixed effects. Standard errors are clustered at the district level. Shaded areas represent 90% confidence intervals.

nied by lower temperatures, with an average cooling of 0.3°C and a peak of 0.5°C in January (Figure A13).

In contrast, upwind irrigation also reduces rainfall in June, around the onset of the summer monsoon. The estimated decline is approximately 6 mm, comparable in absolute magnitude to the dry-season increase but smaller relative to typical monsoon rainfall.

Matching Theory. These seasonal effects of irrigation on climate are consistent with predictions from climate modeling studies (Guimberteau et al., 2012b; Agrawal et al., 2019; Mathur and AchutaRao, 2020). During the dry *Rabi* season, increased irrigation enhances evapotranspiration, promoting cloud formation, increasing precipitation, and lowering surface temperatures. The concentration of the rainfall response during these months is consistent with both peak irrigation and the greater importance of terrestrial moisture recycling, compared with the predominantly oceanic moisture supply during *Kharif* (Koppa et al., 2026). However, irrigation-induced cooling can also affect the subsequent monsoon. By reducing land-surface temperatures in the months preceding the monsoon, irrigation weakens the land–sea thermal contrast that drives monsoon circulation, potentially delaying its onset and reducing rainfall in June. The empirical evidence presented in this paper closely matches these predictions and, to the best of my knowledge, provides the first empirical evidence of this mechanism.

Given the magnitude of the dry-season response relative to prevailing rainfall levels, the remainder of the analysis focuses on the agricultural implications of this positive externality.[17]

6.2 Downwind Development and Adaptation

Agricultural Outputs. I first examine whether the climatic spillovers documented above translate into greater agricultural production. Table 1 reports the estimated effects of upwind irrigation exposure on wheat, India's major winter cereal crop, considering total production, cultivated area, and yields.[18]

A 10 percentage point increase in upwind irrigation exposure raises wheat production by 3.3%, driven almost entirely by a 3.1% expansion in cultivated area, with no impact on yields. At first glance, these results are puzzling as more favorable climatic conditions are expected to improve crop productivity. Here, the gains from upwind irrigation appear to operate primarily through the

[17] A more in depth analysis of the reverse monsoon impact is discussed in Appendix C.1.
[18] Yields are constructed as total production divided by cultivated area.

extensive margin of dry-season cultivation rather than improvements in land productivity. Wheat production increases without detectable yield gains, consistent with cultivation expanding onto more marginal land. These patterns suggest that more favorable climatic conditions are mediated by farmers' adaptation decisions, rather than reflecting only the direct effect of weather on crop productivity.

Adaptation. The expansion of wheat cultivation raises the question of how farmers adjust their production decisions in response to the more favorable climate. In particular, the implications for irrigation are not straightforward. While rainfall and irrigation are considered substitutes in meeting crop water requirements, the model developed in Section 3 predicts that additional dry-season rainfall can instead increase the returns to irrigation by making a second cropping season more profitable. I examine this prediction by investigating farmers' adjustments in irrigation, cropping intensity, crop choices, mechanization and agricultural inputs.

Table 2 shows that farmers primarily respond by expanding both irrigation and cropping intensity. A 10-percentage-point increase in upwind irrigation exposure raises irrigation intensity by 4.9% and cropping intensity by 1.2% relative to their respective sample means.[19] These joint increases are consistent with the complementarity between rainfall and irrigation at the margin of dry-season cultivation highlighted by the model. Rather than simply reducing irrigation needs, more favorable climatic conditions may encourage farmers to expand cultivation while continuing to rely on irrigation to sustain production during the dry season.

The expansion in irrigation intensity is accompanied by changes in the composition of irrigation sources. Table 3 shows that the share of net irrigated area supplied by sources other than canals, tanks, and wells rises by 0.9 percentage points, while the canal share declines by 1.2 percentage points. The tubewell share moves in the expected direction, but is not significant. The negative coefficient on canal irrigation is reassuring, as it suggests that the results are not mechanically driven by spatial correlation with the upwind canal irrigation exposure vari-

[19] Irrigation intensity is defined as the ratio of net irrigated to net cropped area, while cropping intensity is defined as the ratio of gross to net cropped area.

able. Instead, farmers appear to rely increasingly on diversified and privately controlled water sources.

Beyond irrigation and cropping intensity, farmers may adjust their production through changes in crop choices. Figure 5 reports effects for rice and three different major cereal crops in India: pearl millet, maize, and sorghum. There is little evidence of systematic switching across cereal types, particularly from less water-intensive to more water-intensive crops. Instead, farmers continue to cultivate a diversified cereal portfolio.

Similarly, there is limited evidence of increased fertilizer use or mechanization. Table 4 reports an estimated increase in fertilizer application of 3 kg per hectare of net cropped area, approximately 3.6 percent of the sample mean of 82 kg, but the coefficient is not statistically significant. Table 4 also shows no detectable effects on the number of tractors or power tillers, while the number of electric pumps declines by approximately 870. This decline may reflect substitution toward other irrigation technologies or constraints on electric pump adoption, such as limited electrification or unreliable power supply. In either case, mechanization does not appear to be a primary channel of adjustment.

Taken together, these findings suggest that farmers respond to better climate conditions mainly by expanding irrigation in order to increase cropping intensity. Interestingly, and in contrast to evidence from developed country contexts such as the United States (Braun and Schlenker, 2023; Grosset-Touba et al., 2024), there is no evidence of investment into yield-enhancing technologies. Combined with the expansion in wheat cultivation, these responses are consistent with rainfall and irrigation acting as complements at the margin of dry-season agricultural production.

Farm Structure. While the previous results document how farmers are affected by and adapt to upwind irrigation exposure, they do not reveal who benefits from these adjustments. Adaptation may differ substantially across farms if investment capacity varies with farm size. To investigate this margin, I examine how upwind irrigation exposure affects the farm size distribution, using five-year moving averages as in specification (6).

Table 5 shows that in more exposed districts, the share of cultivated area operated by large farms ($\geq$10 ha) rises by 0.75 percentage points, a 4.5% relative increase, largely at the expense of small (1–2 ha) and medium (4–10 ha) farms, whose operated-area shares decline by 1.9% and 1.5%, respectively. Importantly, the number of large farms does not increase significantly, indicating that the rise in their share of cultivated area reflects within-farm growth among existing large operations rather than the entry of new large farms.

At the other end of the distribution, greater exposure is associated with approximately 6,080 additional marginal farms ($<$ 1 ha), an increase of 3.5%, yet without corresponding growth in their operated area. This greater concentration of marginal holdings comes at the expense of medium-sized farms (4–10 ha), whose number declines by 361, or 1.5% relative to the sample mean.

These patterns point to a polarization of the agrarian structure in more exposed districts. Large farms expand their operated area, whereas smallholders–who constitute the vast majority of farms in India–remain trapped at the bottom of the farm-size distribution. As a result, the "missing middle" of medium-sized farms erodes, consistent with a slower structural transformation in which better climatic conditions foster consolidation at the top and stagnation at the bottom.

7 Robustness

The identification strategy is subject to several potential threats, which I address in this section. Corresponding robustness checks are reported in Appendix D.

7.1 Placebo Specifications

Placebo Specifications. The identifying restriction is directional: irrigation should affect a district only when it lies on the air mass's upwind path. Irrigation measured along the reversed,

downwind path should therefore have no effect. I test this implication by estimating

$$y_{d,t} = \beta_1 E^{\uparrow}_{d,t} + \beta_2 E^{\downarrow}_{d,t} + \mu_d + \lambda_{s,t} + \varepsilon_{d,t}, \tag{8}$$

where $E^{\downarrow}_{d,t}$ is exposure to irrigation located downwind of district d. Under the proposed mechanism, the upwind coefficient should remain stable while β_2 should be close to zero and statistically insignificant. The rest of the parameters are defined as in equation (6). Appendix E reports the robust placebo specification for all major results at different time horizon.

Geographic Confounders. The identifying assumption is that, conditional on the fixed effects, changes in upwind irrigation exposure are unrelated to other changes that affect outcomes. A concern is that districts more exposed to upwind irrigation may also have distinct geographic characteristics that generate different climate or agricultural trajectories. For example, if more exposed districts are flatter or more alluvial and those features shape their evolution over time, the estimates could attribute these differential trends to irrigation exposure. This concern is empirically relevant: highly exposed districts are flatter, lower, more alluvial, and more irrigated at baseline (Appendix Table A13). District and pixel fixed effects absorb such time-invariant differences, but not geography-specific trends. I therefore allow the eight principal geographic characteristics to have separate year effects, individually and jointly. The full set changes monthly climate coefficients by at most 0.80 mm and 0.005°C, and leaves agricultural estimates within the baseline confidence intervals (Appendix Figures A18–A19).

Part of the identifying variation is concentrated in the Gangetic plain (Panel B of Figure A11, Appendix A). If the results were driven by an unobserved shock or a feature unique to this region, the full-sample estimates could reflect that local factor rather than the proposed mechanism. I therefore re-estimate the model excluding each state, including Uttar Pradesh, and each of the 311 districts in turn. No estimate falls outside the full-sample confidence band. These exercises cannot rule out every unobserved geographic trend, but they show that neither observed geography nor a single location drives the results.

Wind-Borne Confounders. Wind is the source of identifying variation, but it can transport more than moisture. This creates a confounding risk when irrigated source regions covary with other wind-borne atmospheric inputs that affect climate or agriculture downwind. Crop-residue burning is the leading concern in India: irrigation is correlated with cropped area, crop burning releases aerosols, and those aerosols are carried downwind. Aerosols can cool the surface while altering the monsoon and precipitation (Bollasina et al., 2011; Rosenfeld et al., 2008; Ramanathan et al., 2005); rainfall also scavenges particulate matter, so the relationship between pollution and precipitation is bidirectional. Consistent with this mechanism, upwind exposure raises winter $PM_{2.5}$ (Figure A24), showing that the identifying wind corridor carries particulate pollution alongside moisture, making air pollution a potential confounder.

No single pollution control can resolve this issue. Contemporaneous $PM_{2.5}$ begins only in 1998 and is partly affected by rainfall, so conditioning on it may introduce post-treatment bias. I therefore combine three tests. First, on the common post-2000 sample, controlling for $PM_{2.5}$ barely changes the January temperature coefficient; a predetermined pollution measure interacted with year produces the same conclusion in the full panel (Appendix Figure A25). Second, I exclude the burning regions and the burning months: the climate profile is unchanged throughout (Figure A26), and rebuilding annual exposure with the residue-burning months taken out of the treatment leaves wheat production at 0.033 to 0.034 against 0.033 in the baseline (Appendix Table A15). Finally, I control for forest cover and fertiliser use. These variables capture other source-region changes correlated with initial irrigation expansion, including fertiliser-related emissions and afforestation, that may also affect the atmosphere. They leave the estimates qualitatively unchanged. Taken together, the tests make pollution and related land-use changes unlikely explanations for the findings.

The Green Revolution. The expansion of irrigation projects overlapped with the Green Revolution. If districts most exposed to upwind irrigation were also those where high-yielding varieties, fertiliser, or other agricultural inputs expanded most rapidly, the estimates could capture

differential agricultural modernization rather than irrigation-induced climate effects. State-by-year fixed effects absorb policies and input diffusion common to a state in a given year; the remaining concern is therefore differential adoption within a state and year.I first test this implication directly. Table A14 regresses each candidate confounder on exposure under the paper's own fixed effects, in percent of the confounder's residual standard deviation: none moves, the largest estimate being high-yielding varieties at 14.5%. I then add contemporaneous adoption measures and, separately, predetermined baseline measures interacted with year. The wheat production result is robust (Figure A23). These controls are imperfect, since contemporaneous adoption may itself respond to treatment and some series are incomplete, but the two exercises together weigh against differential Green Revolution trends as a confounder.

Spatial Dependence and Functional Form. Weather observations are not independent draws. Rainfall and temperature are serially correlated in space.I therefore report Conley standard errors that allow correlation to decay with distance over cutoffs from 100 to 1,000 km. Most estimates are robust to these specifications (Figures A27–A28). I also estimate agricultural outcomes by PPML to retain zero observations, which account for 15% of district-years for wheat. The crop results strengthen and no longer depend on Uttar Pradesh (Figure A21). A last concern is with inference itself rather than with the estimate: upwind exposure is smooth in space, smooth in time and almost monotonically increasing, and regressing such a variable on outcomes that are themselves smooth, trending and spatially correlated can produce apparently significant coefficients under the null. Reassigning each district's entire exposure series to another district 500 times and re-estimating equation (4) on each draw, no permutation reaches the seasonal climate coefficients or the two intensity margins (Appendix D.8).

Canal Construction Dates and Strategic Placement. Canal completion dates are sometimes measured imprecisely, and irrigation may become operational gradually rather than in the recorded year. Such timing error could mechanically attenuate annual estimates or make them sensitive to short-run noise around construction. Re-estimating the model on five- and ten-year

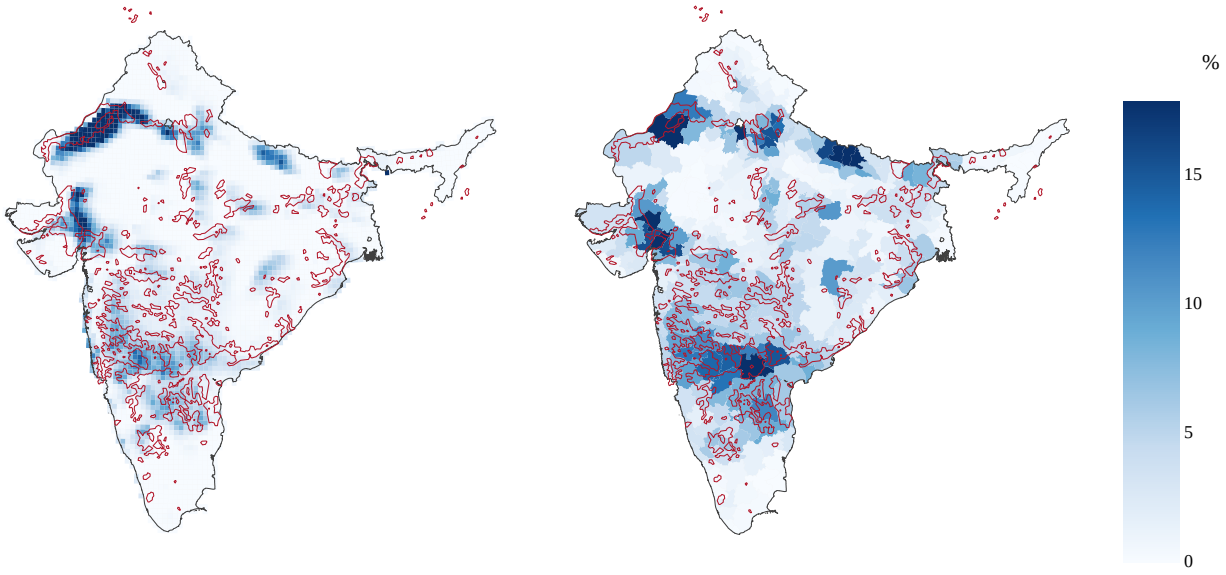
moving averages smooths both concerns. The dry-season effects remain, while the temperature effects persist and strengthen over longer horizons (Figure A14).

A related concern is that canals are not placed randomly. Where a command area is built is set by the storage capacity of the reservoir and by the gradient of the land it can command. Qualitative record describes siting in those engineering terms — river flow, dam capacity, topography — and never with reference to the districts lying downwind. It is therefore unlikely that canal irrigation schemes were placed to benefit downwind districts through the climatic spillovers documented in this paper. However, exposed districts do differ in geography (Table A13) and corresponding estimates could therefore capture differential trends associated with those. Allowing each characteristic its own year effects leaves the estimates unchanged (Figures A18–A19).

8 Policy Implications and Discussion

I use a stylized accounting exercise to quantify the effects of upwind irrigation on India's dry-season climate and wheat sector. I first remove its estimated historical contribution, then project the effects of command areas under construction. This is not an equilibrium prediction: it holds prices, land, labour and capital fixed, and the identifying assumption is within-state-year, aggregated here as if it measured a level.

Historical importance of spillovers. I construct district-year counterfactuals by netting out the estimated effects of upwind irrigation. Between 1967 and 2020, dry-season rainfall declined by 10.9 mm; without upwind irrigation, the estimated decline would have been 27.0 mm. Temperature rose by 0.39°C over the same period, compared with a counterfactual increase of 0.76°C (Appendix Figure A32). Upwind irrigation therefore offset a substantial share of the drying and warming that would otherwise have occurred, with substantial geographical heterogeneity (see Appendix F, Figure A35). The same exercise shows that these climatic spillovers account for 7% of the 1967–2010 increase in wheat production and 14% of the increase in wheat area. By 2006–2010, they generated 4.9 million tonnes of annual wheat production, worth 1.0 billion USD a year (19



(a) Dry-season Rainfall (b) Wheat production

Figure 4: Projected effects of canal irrigation schemes under construction

Notes: Both panels report the increment from the command areas recorded as ongoing or completed after 2010, a further 10.2 percentage points of area-weighted exposure. Panel (a) is the dry-season rainfall it would deliver, $\sum_m \hat{\beta}_m E_{i,m}$ summed over the Rabi months on the 0.25° grid and divided by the pixel's mean annual rainfall; Panel (b) is the share of district wheat production attributable to the same increment, on the 311 ICRISAT districts. The pixel grid is clipped to those districts, so the two panels cover the same territory and share one colour scale, trimmed at the 98th percentile of the two series pooled. Every command area under construction is outlined in red, at its actual size. Exposure is a leave-own-district-out average, so no unit is credited with a canal of its own; both panels show rainfall imported from elsewhere.

USD per hectare of command area), and increased both irrigation and cropping intensity by 1.7 percentage points (Table A16, Panel A).

Future irrigation expansion. Canal command areas currently under construction would add 32.3 million hectares of large-scale irrigation and raise irrigation exposure by 10 percentage points. Applying my estimates implies 48 km³ of additional dry-season rainfall per year, equivalent to 8.4% of India's observed dry-season rainfall, and 3.6 million additional tonnes of wheat, or 4.6% of today's India production. Figure 4 maps the geographical distribution of these externalities with 30% of the benefits falling outside any command area (Table A16, Panel B).

Discussion The accounting exercise highlights a productive climate externality of canal irrigation, but it is not a full welfare evaluation of large-scale irrigation infrastructure. The policy interpretation depends on margins that remain outside the analysis. Existing evidence on large dams in India shows that agricultural gains and poverty reductions downstream can coexist with higher poverty where dams are built (Duflo and Pande, 2007). The atmospheric spillovers documented here add a further channel of redistribution, as irrigation infrastructure can reallocate water and agricultural opportunities through the climate system itself. These gains must also be weighed against social, environmental, and health costs. Large reservoirs and canal systems can require land acquisition, displacement, and resettlement; they can also alter downstream environments by changing river flows, water quality, sediment transport, wetlands, and fisheries (WCD, 2000; Dougherty and Hall, 1995). Within command areas, canal systems can raise water tables, increase seepage, and generate waterlogging and soil salinization when drainage is weak (Dougherty and Hall, 1995). They may also alter disease environments by changing humidity, standing water, and cropping systems. Such effects can occur directly within irrigated areas, as documented for malaria in canal-irrigated regions, but the mechanism in this paper suggests that they may also propagate downwind through rainfall, humidity, and temperature spillovers (Tyagi, 2004; Keiser et al., 2005). The wet-season effects documented in this paper may also matter for urban health: in exposed cities such as Delhi, heavy monsoon moisture coincides with higher temperatures, leading to increased moist heat stress, with consequences for mortality (Mishra et al., 2020; Choudhary et al., 2024). Finally, the long-run value of these investments depends on maintenance and governance; the World Bank's dam rehabilitation work in India emphasizes the need to break the costly "build-neglect-rebuild" cycle in dam management (World Bank, 2020). These considerations do not overturn the productive effects estimated above. Rather, they qualify their policy interpretation: large-scale irrigation can raise output by reshaping climate, but its welfare consequences depend on distribution, resettlement, drainage, health, ecological impacts, and long-run asset management.

9 Conclusion

This paper provides new causal evidence that large-scale irrigation infrastructure can generate climatic spillovers by altering atmospheric dynamics and redistributing rainfall and temperature downwind. Leveraging exogenous variation in wind trajectories and five decades of high-resolution data on irrigation, wind, and rainfall, the empirical strategy isolates irrigation-induced climatic feedbacks from local agricultural decisions. It shows that irrigation redistributes water across space and time, with persistent consequences for downwind development trajectories.

The climatic effects are strongly seasonal: upwind irrigation increases rainfall during the dry Rabi season but reduces precipitation during the monsoon Kharif season and delays monsoon onset. A simple model shows how this seasonal rainfall reallocation can raise incentives to invest in downwind irrigation by increasing the value of dry-season cultivation while raising the marginal value of irrigation during the monsoon.

Consistent with this mechanism, irrigation-induced rainfall increases agricultural output primarily along the extensive margin through double cropping rather than yield gains. Farmers invest in private irrigation, generating a feedback loop whereby irrigation alters the climate and further encourages irrigation adoption. By contrast, farmers do not adapt through greater mechanization, crop switching, or increased use of yield-enhancing inputs. The benefits of these climatic spillovers are unevenly distributed: larger farms expand while smallholders remain stagnant, leading to increasing polarization in the farm size distribution.

Whether these agricultural responses translate into broader structural transformation remains an important question for future research. Suggestive evidence in Tables A11 and A12 points to early signs of reallocation outside agriculture: net cropped area declines, non-agricultural land use rises, and female field wages fall weakly with upwind exposure. More broadly, the welfare consequences of land-use climate spillovers may extend beyond agricultural production. Changes in rainfall timing, humidity, and standing water could affect health, including exposure to mosquito-borne diseases. A related open question is whether groundwater irrigation generates similar feedbacks as aquifer depletion intensifies, in which case the estimates in this paper

would capture only part of irrigation's climate effects.

The estimated rainfall response is physically plausible given the scale of the canal network. The regression estimates imply 37 km^3 [$\pm$18] of additional dry-season rainfall per year, or 9 percent [$\pm$4.2] of observed rainfall in the region. Because the coefficient is identified from relative differences in exposure across districts, this figure is best interpreted as an order-of-magnitude benchmark rather than the canal network's aggregate precipitation effect. The network irrigates about sixteen million hectares net, including roughly ten million hectares in the dry season, implying approximately 30 km^3 of additional Rabi evapotranspiration relative to unirrigated land. Moisture-recycling rates typical of South Asia imply that this additional water vapour could return as anything from a few cubic kilometres to about 35 km^3 of local rainfall. The regression estimate therefore lies within the range implied by a simple water-balance calculation. Consistent with this magnitude, Koppa et al. (2026) estimate, using Lagrangian atmospheric moisture tracking, that upwind irrigation contributes 7 percent [$\pm$5.2] of rainfall over India's rainfed cropland nationally, with contributions exceeding 20% in the Indo-Gangetic Plain.

Taken together, the findings highlight an overlooked externality of development infrastructure: its ability to generate climatic spillovers that reshape economic incentives and adaptation strategies. More broadly, the results underscore the importance of accounting for intra-annual climate distribution and raise methodological challenges for causal identification when economic activity feeds back into the climate system.

Table 1: Effect of Upwind Irrigation on Wheat Outputs

	(1)	(2)	(3)
	Wheat – in log()		
	Production	Area	Yield
Upwind Irrigation (10 pp.)	0.033**	0.031**	0.002
	(0.014)	(0.013)	(0.006)
Mean	3.731	3.368	0.332
Std. Dev.	2.295	2.072	0.575
Obs.	11,582	11,637	11,572
Nb. District	281	283	281
Within R^2	0.0021	0.0023	0.0001
Fixed Effects	District and State×Year		

Notes: Each coefficient corresponds to the parameter β in equation (5), which captures the estimated effect of a 10 percentage point increase in upwind irrigation exposure. Production, cultivated area, and yields are expressed in logs. Regressions include district fixed effects and state-by-year fixed effects, and no baseline controls: neither log population nor crop-specific log high-yielding variety area enters any column. Standard errors are clustered at the district level. Significance levels are denoted as follows: * $p < 0.10$, ** $p < 0.05$, *** $p < 0.01$.

Table 2: Effect of Upwind Irrigation on Cropping and Irrigation Intensities

	(1) Irrigation Intensity	(2) Cropping Intensity
Upwind Irrigation (10 pp.)	0.017***	0.016***
	(0.005)	(0.005)
Mean	0.351	1.314
Std. Dev.	0.273	0.243
Obs.	12,472	13,300
Nb. District	311	311
Within R^2	0.0221	0.0099
Fixed Effects	District and State×Year	

Notes: Each coefficient corresponds to the parameter β in equation (5), which captures the estimated effect of a 10 percentage point increase in upwind irrigation exposure. Upwind irrigation is defined as the average share of irrigated land in pixels located 50–150 km upwind of the focal pixel, weighted inversely by distance. Irrigation intensity is measured as the ratio of net irrigated area (NIA) to net cropped area (NCA). Cropping intensity is measured as the ratio of gross cropped area (GCA) to net cropped area, and serves as a proxy for double cropping. Means and standard deviations are computed over the estimation sample. All regressions are estimated at the district level (corresponding to 311 districts based on 1966 administrative boundaries) and include district fixed effects as well as state-by-year fixed effects, without baseline controls. Standard errors, clustered at the district level, are reported in parentheses. Significance levels are denoted as follows: * $p < 0.10$, ** $p < 0.05$, *** $p < 0.01$.

Table 3: Effect of Upwind Irrigation on Irrigation Composition

	(1)	(2)	(3)	(4)	(5)
	Dep. Var.: Share of Net Irrigated Area Attributed to ...				
	Canals	Wells	Tubewells	Other Wells	Other Sources
Upwind Irrigation (10 pp.)	-0.012*	0.005	0.006	-0.001	0.009***
	(0.007)	(0.007)	(0.005)	(0.007)	(0.003)
Mean	0.273	0.506	0.210	0.297	0.114
Std. Dev.	0.293	0.341	0.288	0.320	0.235
Obs.	12,380	12,360	12,380	12,362	12,349
Nb. District	311	310	311	310	310
Within R^2	0.0033	0.0005	0.0012	0.0000	0.0026
Fixed Effects	District and State×Year				

Notes: Each coefficient corresponds to the parameter β in equation (5), which captures the estimated effect of a 10 percentage point increase in upwind irrigation exposure. Upwind irrigation is defined as the average share of irrigated land in pixels located 50–150 km upwind of the focal pixel, weighted inversely by distance. Results are reported for the shares of net irrigated area allocated to different irrigation practices. The sum of all shares in the sample equals one. Means and standard deviations are computed over the estimation sample. All regressions are estimated at the district level (corresponding to 311 districts based on 1966 administrative boundaries) and include district fixed effects as well as state-by-year fixed effects, without baseline controls. Standard errors, clustered at the district level, are reported in parentheses. Significance levels are denoted as follows: * $p < 0.10$, ** $p < 0.05$, *** $p < 0.01$.

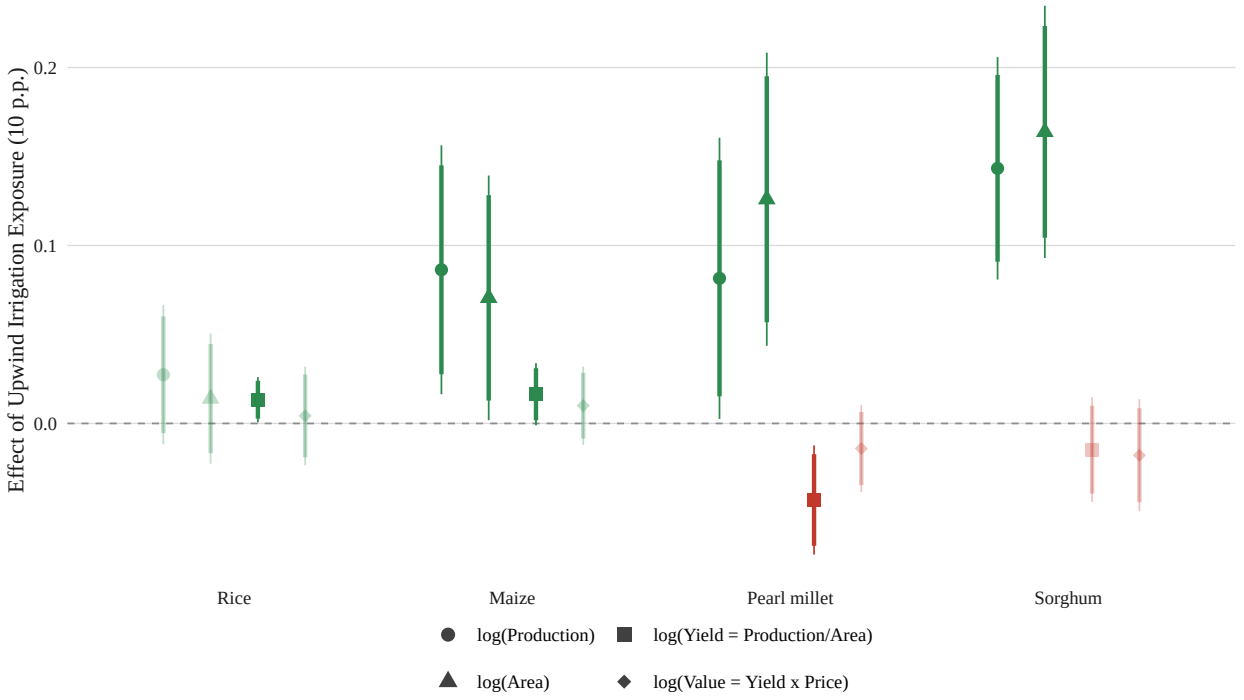


Figure 5: Effect of Upwind Irrigation by Crop

Notes: Figure 5 reports the estimated coefficients from specification (5), the effect of a 10 percentage point increase in upwind irrigation exposure, for rice and for three other major cereals: maize, pearl millet and sorghum. Rice is the crop of the main text and is drawn here for comparison. Upwind irrigation is the mean share of irrigated land in pixels located 50–150 km upwind of the focal pixel, weighted inversely by distance. Area is in thousand hectares, production in tonnes, yield is production over area, and value is yield times the district's annual crop price from ICRISAT. All four dependent variables are in logs, as marked, and estimated on the positive observations. Regressions include district and state-by-year fixed effects and *no baseline controls*: neither log population nor log high-yielding-variety area enters. Standard errors are clustered at the district level. Thick bars are 90 percent intervals, thin bars 95 percent; estimates not significant at 10 percent are drawn at reduced opacity.

Table 4: Effect of Upwind Irrigation on Mechanisation and Fertiliser Use

	(1)	(2)	(3)	(4)	(5)
	Number of … ('000)				t/ha of NCA
	Diesel Pump	Electric Pump	Power Tiller	Tractors	NPK
Upwind Irrigation (10 pp.)	0.057	-0.867*	-0.075	-0.002	2.988
	(0.735)	(0.451)	(0.090)	(0.251)	(2.290)
Mean	14.673	16.179	0.490	4.425	81.932
Std. Dev.	21.078	25.705	1.583	8.533	94.269
Obs.	1,903	1,913	1,511	2,013	13,070
Nb. District	311	311	311	311	311
Within R^2	0.0000	0.0018	0.0012	0.0000	0.0029
Specification	5-yr mean exposure, anchor years				Annual
Fixed Effects	District and State×Year				

Notes: Columns (1)–(4) report the parameter β of equation (6): upwind exposure averaged over the five years preceding the anchor year, the anchor year itself excluded, on the Livestock Census anchor years 1966, 1972, 1977, 1982, 1987, 1992, 1997, 2003 and 2007. Column (5) reports total NPK fertiliser per hectare of net cropped area on the annual panel under equation (5). This table is estimated without the baseline controls: neither log population nor log high-yielding-variety area enters any column. The HYV control is a sample restriction rather than a control — its coverage ends in 1989 in Uttar Pradesh and in 1987 in West Bengal, so including it deletes the two largest eastern rice states over the last two decades of the panel. Upwind irrigation is defined as the average share of irrigated land in pixels located 50–150 km upwind of the focal pixel, weighted inversely by distance. All regressions are estimated at the district level (311 districts on 1966 administrative boundaries) and include district and state-by-year fixed effects. Standard errors, clustered at the district level, are in parentheses. Significance: * $p < 0.10$, ** $p < 0.05$, *** $p < 0.01$.

Table 5: Effect of Upwind Irrigation on Farm Size

	(1) Marginal (<1 ha)	(2) Small (1–2 ha)	(3) Semi-medium (2–4 ha)	(4) Medium (4–10 ha)	(5) Large (≥ 10 ha)	(6) Total
	Dep. Var.: Share of Total Area					Area ('000 ha)
Upwind Irrigation (10 pp.)	0.003	-0.003**	-0.002	-0.004*	0.007**	3.977
	(0.003)	(0.001)	(0.003)	(0.002)	(0.003)	(3.042)
Mean	0.167	0.180	0.229	0.259	0.165	535.047
Std. Dev.	0.152	0.084	0.068	0.112	0.161	333.874
Obs.	2,014	2,014	2,014	2,014	2,014	2,043
Nb. District	311	311	311	311	311	311
Within R^2	0.0024	0.0043	0.0011	0.0034	0.0075	0.0013
	Dep. Var.: Number of Farms ('000)					
Upwind Irrigation (10 pp.)	6.080*	-0.535	-0.368	-0.361*	0.118	4.901
	(3.131)	(0.730)	(0.464)	(0.213)	(0.131)	(3.400)
Mean	171.926	58.045	41.375	24.562	6.296	304.031
Std. Dev.	184.954	40.515	26.894	21.128	9.625	214.213
Obs.	2,181	2,181	2,181	2,181	2,181	2,206
Nb. District	311	311	311	311	311	311
Within R^2	0.0040	0.0003	0.0003	0.0003	0.0006	0.0020
Fixed Effects	District and State×Year					

Notes: Each coefficient is the parameter β of equation (6): upwind exposure averaged over the five years *preceding* the anchor year, the anchor year itself excluded, with the dependent variable measured at the anchor year. Anchor years are those of the Agricultural Census: 1970, 1976, 1980, 1985, 1990, 1995, 2000 and 2005. Panel A reports shares of total farm area, built on the reported total and truncated to $[0, 1]$, and total area in column (6); Panel B reports the number of farms in each class. Regressions include district and state-by-anchor-year fixed effects and no baseline controls; this table carried none in the earlier draft either, so its estimates are unchanged by the removal of log population and log high-yielding-variety area. Upwind irrigation is the average share of irrigated land in pixels located 50–150 km upwind of the focal pixel, weighted inversely by distance. Standard errors, clustered at the district level, are in parentheses. Significance: * $p < 0.10$, ** $p < 0.05$, *** $p < 0.01$.

References

Agrawal, S., A. Chakraborty, N. Karmakar, et al. (2019): "Effects of winter and summer-time irrigation over Gangetic Plain on the mean and intra-seasonal variability of Indian summer monsoon," *Climate Dynamics*, 53, 3147–3166.

Alter, R. E., E.-S. Im, and E. A. B. Eltahir (2015): "Rainfall Consistently Enhanced around the Gezira Scheme in East Africa Due to Irrigation," *Nature Geoscience*, 8, 763–767.

Araujo, R. (2024): "When Clouds Go Dry: An Integrated Model of Deforestation, Rainfall, and Agriculture," *Working Paper*.

Asher, S., A. Campion, D. Gollin, and P. Novosad (2022): "The Long-Run Development Impacts of Agricultural Productivity Gains: Evidence from Irrigation Canals in India," CEPR Discussion Paper No. 17414.

Asher, S. and P. Novosad (2020): "Rural Roads and Local Economic Development," *American Economic Review*, 110, 797–823.

Blakeslee, D., A. Dar, R. Fishman, S. Malik, H. S. Pellegrina, and K. S. Bagavathinathan (2023): "Irrigation and the Spatial Pattern of Local Economic Development in India," *Journal of Development Economics*, 161, 102997.

Blakeslee, D., R. Fishman, and V. Srinivasan (2020): "Way Down in the Hole: Adaptation to Long-Term Water Loss in Rural India," *American Economic Review*, 110, 200–224.

Blanc, E. and E. Strobl (2014): "Is Small Better? A Comparison of the Effect of Large and Small Dams on Cropland Productivity in South Africa," *The World Bank Economic Review*, 28, 545–576.

Bollasina, M. A., Y. Ming, and V. Ramaswamy (2011): "Anthropogenic Aerosols and the Weakening of the South Asian Summer Monsoon," *Science*, 334, 502–505.

Bombardi, R. J., J. L. Kinter, and O. W. Frauenfeld (2019): "A Global Gridded Dataset of the Characteristics of the Rainy and Dry Seasons," *Bulletin of the American Meteorological Society*, 100, 1315–1328.

Braun, T. and W. Schlenker (2023): "Cooling Externality of Large-Scale Irrigation," NBER Working Paper No. 30966.

Burgess, R., O. Deschênes, D. Donaldson, and M. Greenstone (2017): "Weather, Climate Change and Death in India," London School of Economics Working Paper.

Burke, M. and K. Emerick (2016): "Adaptation to Climate Change: Evidence from US Agriculture," *American Economic Journal: Economic Policy*, 8, 106–140.

Burlig, F., R. A. Hrozencik, L. Preonas, and M. Woerman (2025): "Evidence of Climate Adaptation: Temperature and Groundwater Extraction in California Agriculture," *Working Paper*.

Bustos, P., B. Caprettini, and J. Ponticelli (2016): "Agricultural Productivity and Structural Transformation: Evidence from Brazil," *American Economic Review*, 106, 1320–1365.

Bustos, P., G. Garber, and J. Ponticelli (2020): "Capital Accumulation and Structural Transformation*," *The Quarterly Journal of Economics*, 135, 1037–1094.

Butler, A. and C. Boudot Reddy (2023): "Watering the Seeds of the Rural Economy: Evidence from Groundwater Irrigation in India," *Available at SSRN 4575998*.

Butt, N., P. A. de Oliveira, and M. H. Costa (2011): "Evidence That Deforestation Affects the Onset of the Rainy Season in Rondonia, Brazil," *Journal of Geophysical Research: Atmospheres*, 116.

Carleton, T. A. and S. M. Hsiang (2016): "Social and Economic Impacts of Climate," *Science*, 353, aad9837.

Chou, C., D. Ryu, M.-H. Lo, H.-W. Wey, and H. M. Malano (2018): "Irrigation-Induced Land–Atmosphere Feedbacks and Their Impacts on Indian Summer Monsoon," *Journal of Climate*, 31, 8785–8801.

Choudhary, A., N. Joshi, S. Ghosh, A. R. Ganguly, K. Balakrishnan, D. Singh, R. Mall, R. Kumar, and S. Dey (2024): "Excess Mortality Risk Due to Heat Stress in Different Climatic Zones of India," *Environmental Science & Technology*, 58, 342–351.

Conley, T. G. (1999): "GMM Estimation with Cross Sectional Dependence," *Journal of Econometrics*, 92, 1–45.

Cruz, J.-L. and E. Rossi-Hansberg (2024): "The Economic Geography of Global Warming," *Review of Economic Studies*, 91, 899–939.

Degois, M., T. Vendryes, and J. Wolfersberger (2026): "Clearing the Way to Conflict: Deforestation and Downwind Rainfall," *Working Paper*.

Dell, M., B. F. Jones, and B. A. Olken (2012): "Temperature Shocks and Economic Growth: Evidence from the Last Half Century," *American Economic Journal: Macroeconomics*, 4, 66–95.

——— (2014): "What Do We Learn from the Weather? The New Climate-Economy Literature," *Journal of Economic Literature*, 52, 740–98.

Devanand, A., M. Huang, M. Ashfaq, B. Barik, and S. Ghosh (2019): "Choice of Irrigation Water Management Practice Affects Indian Summer Monsoon Rainfall and Its Extremes," *Geophysical Research Letters*, 46, 9126–9135.

Dillon, A. and R. Fishman (2019): "Dams: Effects of Hydrological Infrastructure on Development," *Annual Review of Resource Economics*, 11, 125–148.

Donaldson, D. (2018): "Railroads of the Raj: Estimating the Impact of Transportation Infrastructure," *American Economic Review*, 108, 899–934.

Donaldson, D. and R. Hornbeck (2016): "Railroads and American Economic Growth: A "Market Access" Approach," *The Quarterly Journal of Economics*, 131, 799–858.

Dougherty, T. C. and A. W. Hall (1995): "Environmental Impact Assessment of Irrigation and Drainage Projects," FAO Irrigation and Drainage Paper 53, FAO, Rome.

Duflo, E. and R. Pande (2007): "Dams*," *The Quarterly Journal of Economics*, 122, 601–646.

Emerick, K. (2018): "Agricultural Productivity and the Sectoral Reallocation of Labor in Rural India," *Journal of Development Economics*, 135, 488–503.

FAO (2023): "Land Statistics and Indicators 2000–2021: Global, Regional and Country Trends," FAOSTAT Analytical Briefs Series 71, FAO, Rome.

Feder, G., R. Just, and D. Zilberman (1985): "Adoption of Agricultural Innovations in Developing Countries: A Survey," *Economic Development and Cultural Change*, 33, 255–98.

Fick, S. E. and R. J. Hijmans (2017): "WorldClim 2: New 1-km Spatial Resolution Climate Surfaces for Global Land Areas," *International Journal of Climatology*, 37, 4302–4315.

Fillon, R. (2025): "The Biophysical Channels of Climate Impacts," *Working Paper*.

Fishman, R. (2016): "More uneven distributions overturn benefits of higher precipitation for crop yields," *Environmental Research Letters*, 11, 024004.

Fishman, R., M. Jain, and A. Kishore (2013): "Groundwater Depletion, Adaptation and Migration: Evidence from Gujarat, India," International Growth Centre Working Paper.

Foster, A. D. and M. R. Rosenzweig (1995): "Learning by Doing and Learning from Others: Human Capital and Technical Change in Agriculture," *Journal of Political Economy*, 103, 1176–1209.

Giordano, M. F., R. E. Namara, and E. Bassini (2019): "The Impacts of Irrigation: A Review of Published Evidence," Policy research working paper, World Bank Group, Washington, D.C., english version.

Greve, P., A. U. Schmitt, D. G. Miralles, S. McDermid, K. L. Findell, A. García-García, and J. Peng (2025): "Observational Evidence of Increased Afternoon Rainfall Downwind of Irrigated Areas," *Nature Communications*, 16, 3415.

Grosset-Touba, F., A. Papp, and C. Taylor (2024): "Rain Follows the Forest: Land Use Policy, Climate Change, and Adaptation," Available at SSRN: https://ssrn.com/abstract=4333147.

Guimberteau, M., K. Laval, A. Perrier, and J. Polcher (2012a): "Global Effect of Irrigation and Its Impact on the Onset of the Indian Summer Monsoon," *Climate Dynamics*, 39, 1329–1348.

——— (2012b): "Global effect of irrigation and its impact on the onset of the Indian summer monsoon," *Climate Dynamics*, 39, 1329–1348.

Hansen, Z. K., G. D. Libecap, and S. E. Lowe (2011): "Climate Variability and Water Infrastructure: Historical Experience in the Western United States," in *The Economics of Climate Change: Adaptations Past and Present*, National Bureau of Economic Research, Inc., NBER Chapters, 253–280.

Henderson, J. V., A. Storeygard, and U. Deichmann (2017): "Has Climate Change Driven Urbanization in Africa?" *Journal of Development Economics*, 124, 60–82.

Hornbeck, R. and P. Keskin (2014): "The Historically Evolving Impact of the Ogallala Aquifer: Agricultural Adaptation to Groundwater and Drought," *American Economic Journal: Applied Economics*, 6, 190–219.

——— (2015): "Does Agriculture Generate Local Economic Spillovers? Short-Run and Long-Run Evidence from the Ogallala Aquifer," *American Economic Journal: Economic Policy*, 7, 192–213.

Hussain, I. and M. A. Hanjra (2004): "Irrigation and poverty alleviation: review of the empirical evidence," *Irrigation and Drainage*, 53, 1–15.

Jack, B. K. and N. Ryan (2026): "Economic Development and the Environment," NBER Working Paper number 34735.

Jain, M., R. Fishman, P. Mondal, G. L. Galford, N. Bhattarai, S. Naeem, U. Lall, Balwinder-Singh, and R. S. DeFries (2021): "Groundwater Depletion Will Reduce Cropping Intensity in India," *Science Advances*, 7, eabd2849.

Jones, M., F. Kondylis, J. Loeser, and J. Magruder (2022): "Factor Market Failures and the Adoption of Irrigation in Rwanda," *American Economic Review*, 112, 2316–52.

Kala, N. (2017): "Learning, Adaptation, and Climate Uncertainty: Evidence from Indian Agriculture," MIT CEEPR Working Paper Series 2017-023.

Kapa, H., K. Bharghavi, and T. L. Reddy (2025): "Variability in Indian monsoon onset: Delays, advances, and regional disruptions," *Evolving Earth*, 4, 100103.

Keiser, J., M. F. Maltese, T. E. Erlanger, R. Bos, M. Tanner, B. H. Singer, and J. Utzinger (2005): "Effect of Irrigated Rice Agriculture on Japanese Encephalitis, Including Challenges and Opportunities for Integrated Vector Management," *Acta Tropica*, 95, 40–57.

Koppa, A., F. Bassani, J. Keune, V. Deman, D. Insua-Costa, V. Hari, S. Ghosh, D. G. Miralles, and S. Bonetti (2026): "Irrigated Agriculture Supports Rainfed Crops in India through Atmospheric Moisture Recycling," *Environmental Research Letters*, 21.

Krusell, P. and A. A. J. Smith (2022): "Climate Change Around the World," NBER Working Paper no. 30338.

Leite-Filho, A. T., B. S. Soares-Filho, J. L. Davis, G. M. Abrahão, and J. Börner (2021): "Deforestation Reduces Rainfall and Agricultural Revenues in the Brazilian Amazon," *Nature Communications*, 12, 2591.

Li, T. (2021): "Protecting the Breadbasket with Trees? The Effect of the Great Plains Shelterbelt Project on Agriculture," *Land Economics*, 97, 321–344.

Liu, M., Y. Shamdasani, and V. Taraz (2023): "Climate Change and Labor Reallocation: Evidence from Six Decades of the Indian Census," *American Economic Journal: Economic Policy*, 15, 395–423.

Loarie, S. R., D. B. Lobell, G. P. Asner, Q. Mu, and C. B. Field (2011): "Direct Impacts on Local Climate of Sugar-Cane Expansion in Brazil," *Nature Climate Change*, 1, 105–109.

Lobell, D. B., W. Schlenker, and J. Costa-Roberts (2011): "Climate Trends and Global Crop Production Since 1980," *Science*, 333, 616–620.

Manoli, G., S. Fatichi, M. Schläpfer, K. Yu, T. W. Crowther, N. Meili, P. Burlando, G. G. Katul, and E. Bou-Zeid (2019): "Magnitude of Urban Heat Islands Largely Explained by Climate and Population," *Nature*, 573, 55–60, pMID: 31485056.

Mathur, R. and K. A. AchutaRao (2020): "A modelling exploration of the sensitivity of India's climate to irrigation," *Climate Dynamics*, 54, 1851–1872.

Ministry of Water Resources (2011): "Report of the Working Group on Major & Medium Irrigation and Command Area Development for the XII Five Year Plan (2012–2017)," Tech. rep., Planning Commission, Government of India, New Delhi.

Mishra, V., A. K. Ambika, A. Asoka, S. Aadhar, J. Buzan, R. Kumar, and M. Huber (2020): "Moist Heat Stress Extremes in India Enhanced by Irrigation," *Nature Geoscience*, 13, 722–728.

Nocco, M. A., R. A. Smail, and C. J. Kucharik (2019): "Observation of irrigation-induced climate change in the Midwest United States," *Global Change Biology*, 25, 3472–3484.

Olmstead, S. M. and H. Sigman (2015): "Damming the Commons: An Empirical Analysis of International Cooperation and Conflict in Dam Location," *Journal of the Association of Environmental and Resource Economists*, 2, 497–526.

Pai, D. S., L. Sridhar, M. Rajeevan, O. P. Sreejith, N. S. Satbhai, and B. Mukhopadhyay (2014): "Development of a new high spatial resolution (0.25° × 0.25°) long period (1901–2010) daily gridded rainfall data set over India and its comparison with existing data sets over the region," *MAUSAM*, 65, 1–18, india Meteorological Department, Pune.

Planning Commission (2011): "Report of the Working Group on Minor Irrigation and Watershed Management for the Twelfth Five Year Plan (2012–2017)," Tech. rep., Government of India, New Delhi.

Puma, M. J. and B. I. Cook (2010): "Effects of irrigation on global climate during the 20th century," *Journal of Geophysical Research*, 115, D16120.

Ramanathan, V., C. Chung, D. Kim, T. Bettge, L. Buja, J. T. Kiehl, W. M. Washington, Q. Fu, D. R. Sikka, and M. Wild (2005): "Atmospheric Brown Clouds: Impacts on South Asian Climate and Hydrological Cycle," *Proceedings of the National Academy of Sciences*, 102, 5326–5333.

Riley, S. J., S. D. DeGloria, and R. Elliot (1999): "A Terrain Ruggedness Index That Quantifies Topographic Heterogeneity," *Intermountain Journal of Sciences*, 5, 23–27.

Rosenfeld, D., U. Lohmann, G. B. Raga, C. D. O'Dowd, M. Kulmala, S. Fuzzi, A. Reissell, and M. O. Andreae (2008): "Flood or Drought: How Do Aerosols Affect Precipitation?" *Science*, 321, 1309–1313.

Ryan, N. and A. Sudarshan (2020): "Rationing the Commons," NBER Working Paper no. w27473.

Saeed, F., S. Hagemann, and D. Jacob (2009): "Impact of Irrigation on the South Asian Summer Monsoon," *Geophysical Research Letters*, 36, L20711.

Schlenker, W. and M. J. Roberts (2009): "Nonlinear Temperature Effects Indicate Severe Damages to U.S. Crop Yields under Climate Change," *Proceedings of the National Academy of Sciences*, 106, 15594–15598.

Sekhri, S. (2014): "Wells, Water, and Welfare: The Impact of Access to Groundwater on Rural Poverty and Conflict," *American Economic Journal: Applied Economics*, 6, 76–102.

Singh, O., A. Kasana, and P. Bhardwaj (2022): "Understanding energy and groundwater irrigation nexus for sustainability over a highly irrigated ecosystem of north western India," *Applied Water Science*, 12, 44.

Spracklen, D. V., S. R. Arnold, and C. M. Taylor (2012): "Observations of Increased Tropical Rainfall Preceded by Air Passage over Forests," *Nature*, 489, 282–285.

Strobl, E. and R. O. Strobl (2011): "The Distributional Impact of Large Dams: Evidence from Cropland Productivity in Africa," *Journal of Development Economics*, 96, 432–450.

Taraz, V. (2017): "Adaptation to Climate Change: Historical Evidence from the Indian Monsoon," *Environment and Development Economics*, 22, 517–545.

——— (2018): "Can Farmers Adapt to Higher Temperatures? Evidence from India," *World Development*, 112, 205–219.

Taylor, C. A. (2026): "Irrigation and Climate Change: Long-run Adaptation and Its Externalities," *Journal of the Association of Environmental and Resource Economists*, 13, 935–973.

te Wierik, S. A., E. L. H. Cammeraat, J. Gupta, and Y. A. Artzy-Randrup (2021): "Reviewing the Impact of Land Use and Land-Use Change on Moisture Recycling and Precipitation Patterns," *Water Resources Research*, 57, e2020WR029234, e2020WR029234 2020WR029234.

Tyagi, B. K. (2004): "A Review of the Emergence of Plasmodium falciparum-Dominated Malaria in Irrigated Areas of the Thar Desert, India," *Acta Tropica*, 89, 227–239.

van Donkelaar, A., M. S. Hammer, L. Bindle, M. Brauer, J. R. Brook, M. J. Garay, N. C. Hsu, O. V. Kalashnikova, R. A. Kahn, C. Lee, R. C. Levy, A. Lyapustin, A. M. Sayer, and R. V. Martin (2021): "Monthly Global Estimates of Fine Particulate Matter and Their Uncertainty," *Environmental Science & Technology*, 55, 15287–15300.

Wada, Y., L. P. H. van Beek, C. M. van Kempen, J. W. T. M. Reckman, S. Vasak, and M. F. P. Bierkens (2010): "Global depletion of groundwater resources," *Geophysical Research Letters*, 37.

WCD (2000): "Dams and Development: A New Framework for Decision-Making," Tech. rep., World Commission on Dams, London and Sterling, VA.

World Bank (2020): "World Bank Approves $250 Million Project to Make Existing Dams Safe and Resilient across India," World Bank press release.

Zaveri, E., J. Russ, and R. Damania (2020): "Rainfall anomalies are a significant driver of cropland expansion," *Proceedings of the National Academy of Sciences*, 117, 10225–10233.

Appendix

A. Data and descriptive statistics
- Descriptive statistics — Table A6.
- The seasonal cycle of precipitation and temperature — Figure A6.
- Precipitation and temperature by season — Figure A7.
- Temperature distribution by season across India — Figure A8.
- The prevailing wind in the Rabi season — Figure A9.
- Canal irrigation potential and command area construction years — Table A7, Figure A10.
- Upwind irrigation exposure, the level and the variation — Figure A11.

B. Model
- Reduced-form adoption frontier and comparative statics — Figure A12.

C. Additional climate results
- Monthly climate response, district and pixel level — Figure A13.
- Monthly climate response under three estimation horizons — Figure A14.
- Net annual effect on precipitation — Table A8.
- Monsoon onset and length, state-trend specification — Table A9.
- Non-linear effect across the temperature distribution — Figure A15, Table A10.

D. Robustness
- Sensitivity to the fixed-effect structure and to the definition of exposure — Figures A16 and A17.
- District characteristics regressed on upwind exposure — Table A13.
- Monthly climate coefficients at pixel level — Figure A18.
- Agricultural coefficients under each geographic control — Figure A19.
- Leave-one-state-out, monthly climate and agricultural outcomes — Figures A20 and A21.
- Log, Poisson and levels on the agricultural outcomes — Figure A22.
- Green Revolution: upwind exposure and the candidate confounders — Table A14, Figure A23.
- Air pollution and crop-residue burning, and controlling for $PM_{2.5}$ directly — Figures A24 to A26, Figure A25, Table A15.
- Conley spatial standard errors, 100 to 500 km — Figures A27 and A28.
- Randomisation inference, the treatment reassigned 500 times — Figure A29.

E. Placebo — the wind-connection matrix reversed
- Wheat production, area, yield and irrigated area — Figure A30.
- Cropping and irrigation intensity — Figure A31.

F. Counterfactual exercise
- The counterfactual, standing network and projects under construction — Table A16.
- State by state, the projects under construction and the network standing by 2010 — Figures A33 and A34.
- Where the counterfactual leaves the identifying range — Figure A35.
- Historical trajectories, temperature and wheat area — Figure A32.

A Data and Descriptive Statistics

Table A6: Descriptive statistics of the estimation sample

			Standard deviation					
	Obs.	Mean	Total	Within	p10	Median	p90	% zero
Treatment								
Upwind irrigation exposure (%), district-month	205,161	17.9	26.0	11.7	0.11	5.42	62.5	7.0
Upwind irrigation exposure (%), district-year	13,683	16.6	24.0	7.62	0.41	5.61	56.0	2.5
Climate								
Precipitation (mm/month)	205,161	95.0	147	138	0.00	26.8	288	10.9
Rabi, October–March	102,621	26.1	53.7	48.6	0.00	4.81	76.4	19.1
Kharif, June–September	68,383	226	179	134	47.7	189	440	–
Mean daily temperature (°C)	205,161	24.3	6.53	4.77	16.8	25.4	31.2	–
Rabi, October–March	102,621	20.9	6.23	3.22	15.1	22.2	26.5	–
Kharif, June–September	68,383	26.9	4.10	1.83	23.5	27.1	31.2	–
Number of rainy days (>1mm, days/month)	205,161	6.66	7.45	7.01	0.00	3.40	18.9	13.7
Rabi, October–March	102,621	2.38	3.54	3.11	0.00	0.94	6.86	23.7
Kharif, June–September	68,383	14.4	6.69	4.97	5.46	14.4	23.4	–
Agriculture								
Wheat production (000 t)	13,566	158	305	145	0.00	40.0	445	14.6
Wheat area (000 ha)	13,578	73.7	95.6	29.2	0.00	35.7	199	14.2
Rice production (000 t)	13,613	205	295	138	0.40	89.8	538	6.5
Rice area (000 ha)	13,614	128	159	31.9	0.60	65.1	350	6.2
Cropping intensity (GCA/NCA)	13,300	1.31	0.24	0.13	1.05	1.27	1.64	–
Irrigation intensity (GIA/GCA)	12,355	0.34	0.26	0.10	0.05	0.27	0.76	0.1
Adaptation margins								
Wheat irrigated area (000 ha)	12,420	62.1	93.5	35.5	0.00	19.0	183	15.2
Rice irrigated area (000 ha)	12,413	57.6	94.0	33.7	0.00	12.1	173	13.9
NPK fertiliser per ha of net cropped area	13,070	81.9	94.3	69.2	4.32	49.1	209	0.7
Tractors (000)	2,292	3.97	8.11	5.85	0.03	0.95	10.8	4.1
Electric pumps (000)	2,202	15.2	25.3	15.5	0.03	4.93	42.5	5.7

Notes: Statistics are computed on the estimation sample. The climate rows are district-months over 1966–2020; every other row is district-years over 1966–2009, on the 311 districts of the 1966 boundaries. *Total* is the standard deviation over all observations, *within* the standard deviation once each district mean is removed — the variation the district fixed effects leave to identify β. Climate variables are reported pooled and then by season; *Rabi* is October to March and *Kharif* June to September. The last column is the share of observations equal to zero, a dash meaning fewer than one in two thousand.

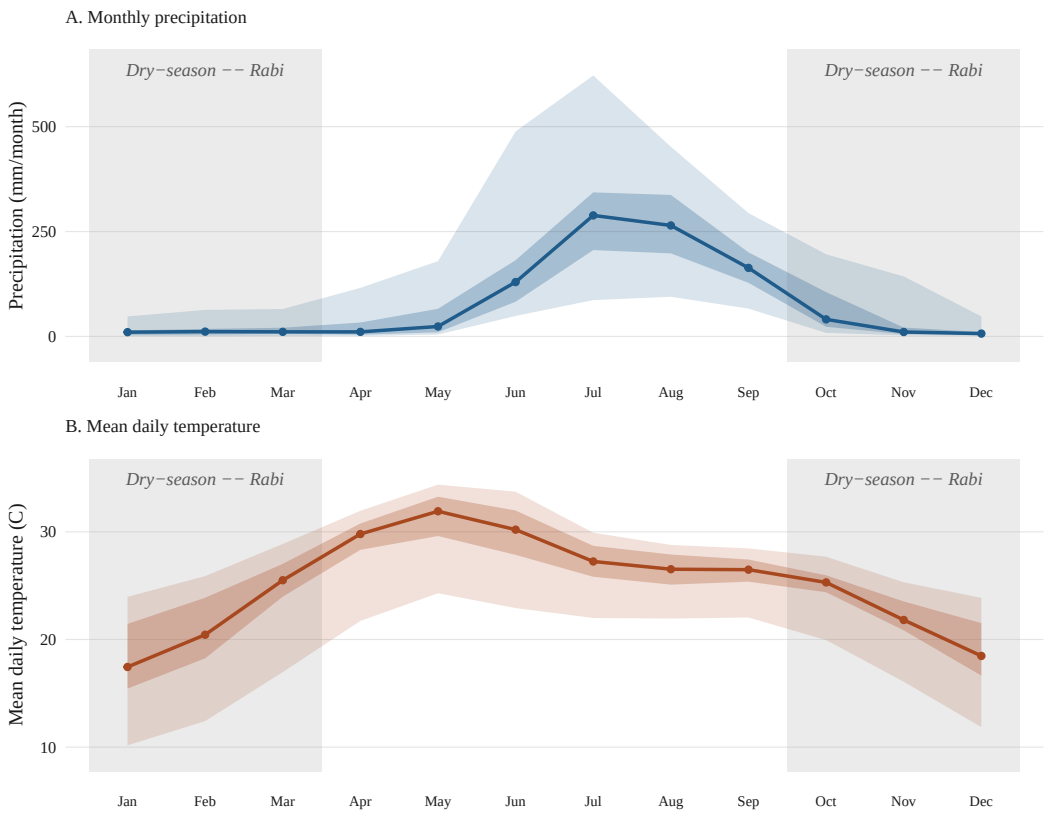


Figure A6: The seasonal cycle of precipitation and temperature

Notes: Figure A6 plots the seasonal cycle of monthly precipitation and mean daily temperature over 1966–2020, on the 311 districts of the estimation sample. Each district's own average for each calendar month is computed first; the line is the median of those normals across districts and the bands are their 25th–75th and 5th–95th percentile ranges. The shaded columns mark the dry Rabi season, October to March.

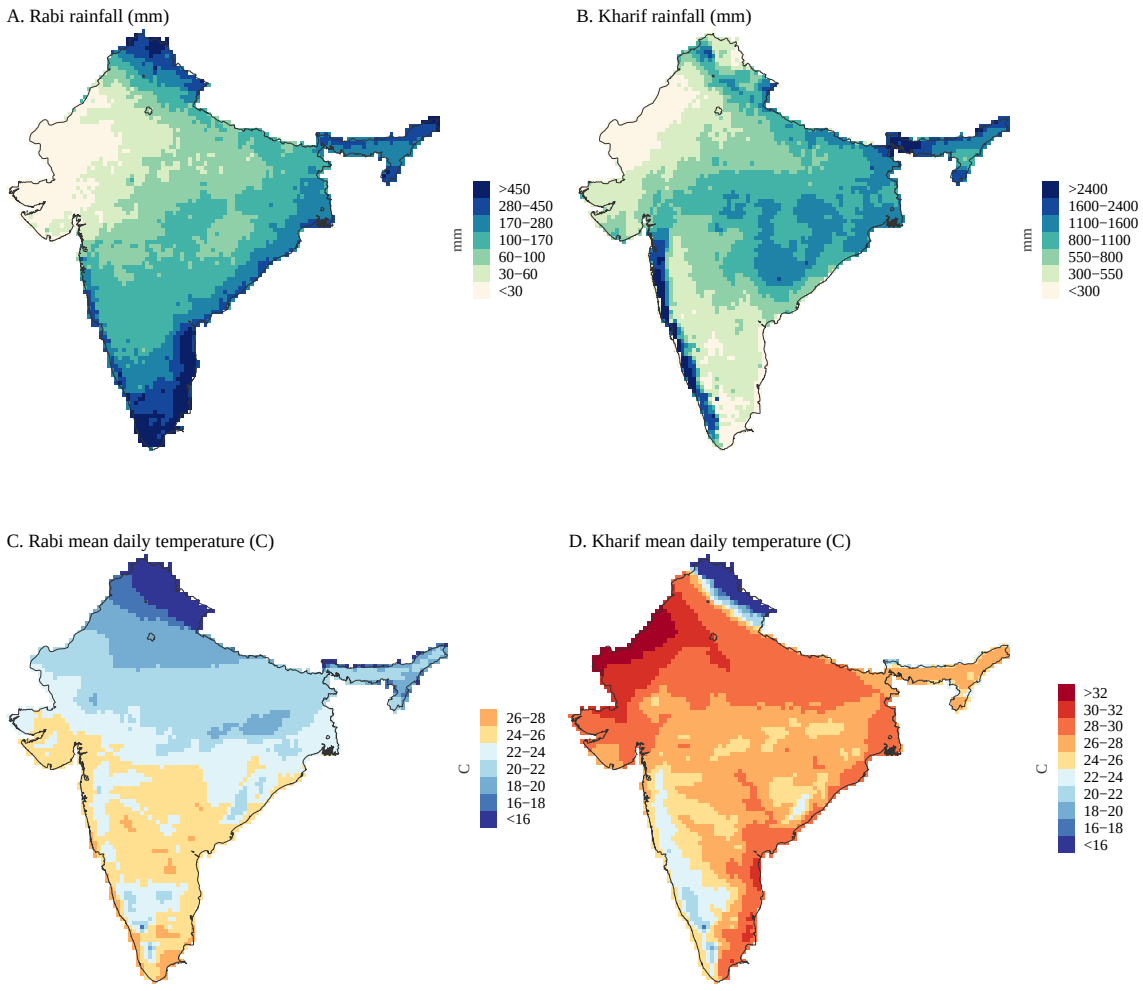


Figure A7: Precipitation and temperature by season

Notes: Figure A7 maps the 1966–2020 normals of rainfall and mean daily temperature by season, on the 4,244 pixels of the 0.25° grid the exposure measure is built on. Rabi is October to March and Kharif June to September. The two rainfall panels carry their own legend, since the monsoon delivers an order of magnitude more water than the dry season; the two temperature panels share one scale in 2°C classes, so a colour denotes the same temperature in both, and classes a season never reaches are dropped from its legend.

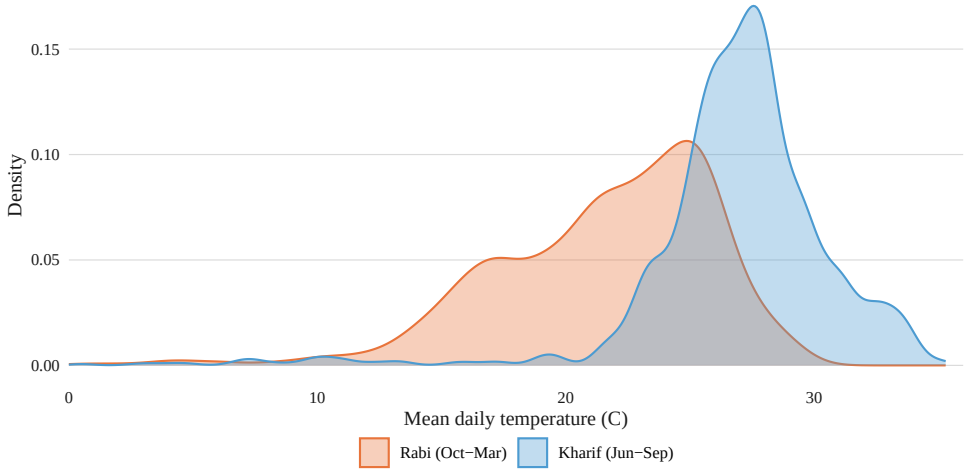


Figure A8: Temperature distribution by season across India

Notes: Figure A8 plots the distribution of mean daily temperature across district-month normals, 1966–2020, one density per cropping season. Each district's own average for each calendar month is computed first, so the unit is a district-month normal. Rabi is October to March and Kharif June to September.

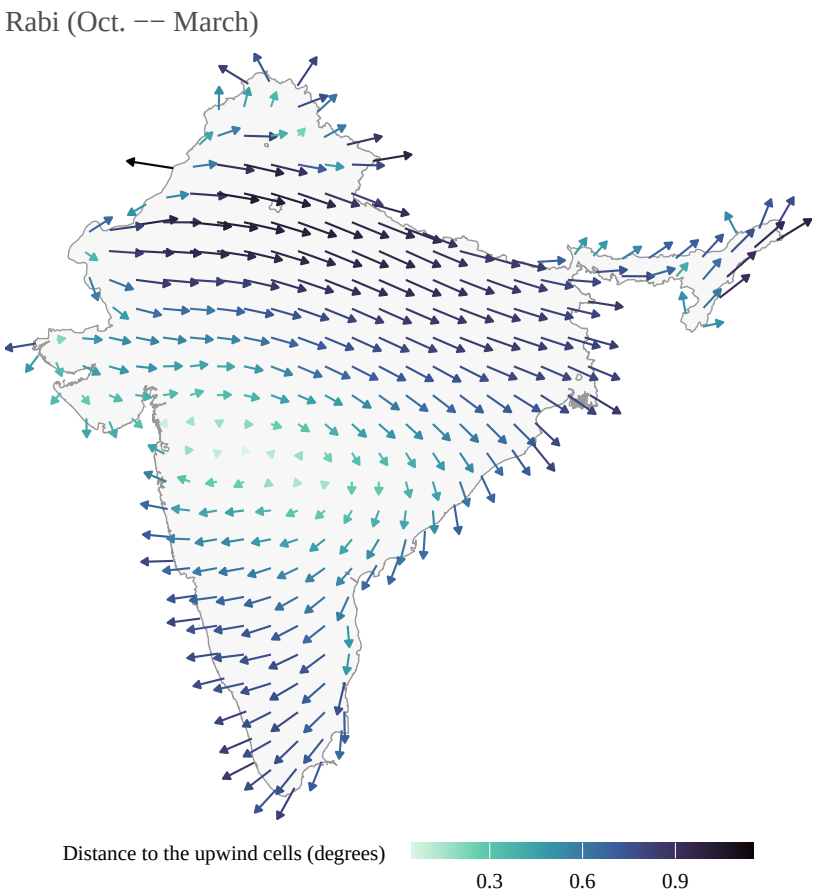


Figure A9: The prevailing wind in the Rabi season

Notes: Figure A9 is drawn from the backward-trajectory matrices at 800 hPa on which the exposure measure of Section 5.1 is built, averaged over 1966–2010. A link joins a pixel to a cell that sends it air; links are kept when their length falls in the 50–150 km window the treatment uses, and each arrow is the mean displacement over the links retained, averaged within one-degree cells and coloured by its length in degrees. Rabi is October to March.

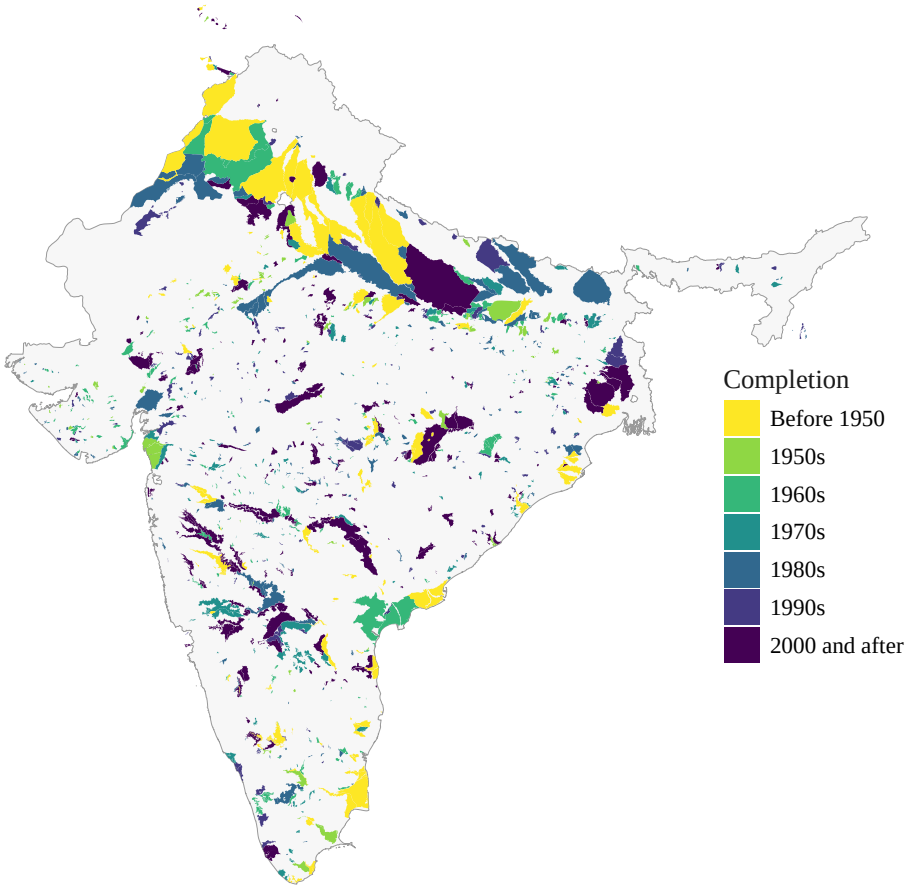


Figure A10: Command Area Construction Years across India

Note: Figure A10 illustrates the canal-irrigated command areas included in the sample, displayed by year of completion, where available.

Table A7: Canal Irrigation Potential of India

	Area (ha)	% of Completed	% of India
Completed (known year)	56,249,134	96.500	17.210
Completed (unknown year)	2,037,783	3.500	0.620
Total Completed	58,286,917	100.000	**17.830**
Ongoing	27,233,781		8.330
Total Potential	85,520,698		**26.160**

Notes: The table reports the total area (in hectares) under canal irrigation in India, according to WRIS. "Completed (known year)" refers to projects with an identified year of completion, while "Completed (unknown year)" includes those for which the completion year is unavailable. "Ongoing" refers to projects under construction during the observation period. % of Completed indicates the share of completed irrigation potential relative to the total completed projects, whereas % of India indicates the share relative to the total surface area of the country.

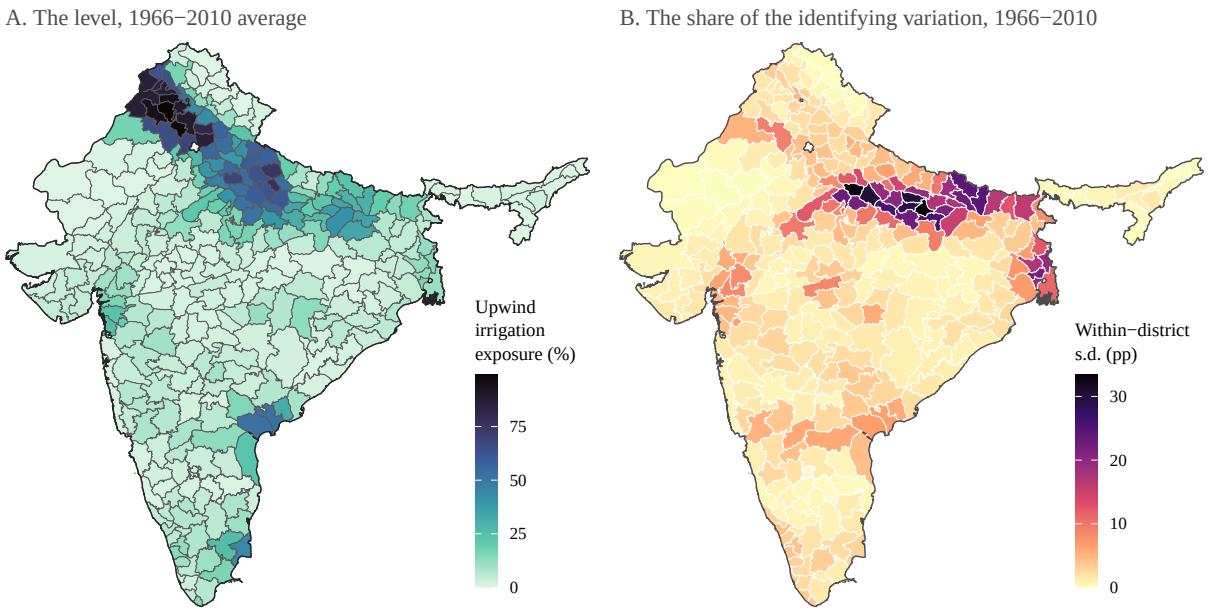


Figure A11: Upwind irrigation exposure: the level and the variation

Notes: Both panels are drawn on the 1966 district boundaries, the 311 districts of the estimation sample, and report upwind irrigation exposure: the share of irrigated area in pixels lying 50–150 km upwind of the district, weighted inversely by distance, with irrigation inside the district itself excluded. Panel A is its 1966–2010 mean, in percent. Panel B is the within-district standard deviation of the same series over the same window, in percentage points — the variation the district and state-by-year fixed effects leave to identify β.

B Reduced-Form Representation and Closed-Form Frontier

To provide additional analytical insight into the comparative statics of the model, I derive a reduced-form representation of the irrigation adoption frontier. The objective is not to impose additional structure on the production functions but rather to approximate the two margins identified in the main text while preserving their theoretical properties.

Recall that the gain from irrigation adoption can be decomposed into two components: a substitution effect in the monsoon season and an activation effect in the dry season. To obtain a tractable expression, I approximate each component with reduced-form functions that capture the qualitative restrictions implied by the model.

First, I represent the activation margin as linear in effective water availability during the Rabi season:

$$A(r_R) = ar_R, \qquad a > 0,$$

where r_R denotes water availability during the dry season and a captures the productivity of activated Rabi cultivation.

Second, the substitution gain in the Kharif season is represented as decreasing in monsoon rainfall:

$$S_K(r_K) = \frac{b}{r_K + \varepsilon}, \qquad b > 0.$$

This functional form captures the idea that irrigation is most valuable when monsoon rainfall is scarce. As rainfall increases, the buffering value of irrigation declines. The expression can be interpreted as a reduced-form approximation of the difference $f_K(r_K + \alpha_K) - f_K(r_K)$ under concavity of the production function. Under these approximations, the adoption gain can be written as

$$\Delta(r_K, r_R) = ar_R + \frac{b}{r_K + \varepsilon} - \bar{F}, \tag{A9}$$

where $\bar{F}$ denotes the fixed cost of installing irrigation.

Closed-Form Adoption Frontier The irrigation adoption frontier is defined by the set of rainfall realizations for which the farmer is indifferent between adopting irrigation and not adopting

it: $\Delta(W_K, W_R) = 0$. Solving for the level of dry-season water availability that satisfies this condition yields the frontier

$$r_R^*(r_K) = \frac{\bar{F}}{a} - \frac{b}{a(r_K + \varepsilon)}. \tag{A10}$$

This equation characterises the combinations of seasonal rainfall (r_K, r_R) for which irrigation adoption yields zero net gain.

Interpretation The frontier partitions the (r_K, r_R) plane into two regions: (i) If $r_R > r_R^*(r_K)$, then $\Delta > 0$ and irrigation is adopted. (ii) If $r_R < r_R^*(r_K)$, irrigation is not adopted.

The slope of the frontier is

$$\frac{dr_R^*}{dr_K} = \frac{b}{a(r_K + \varepsilon)^2} > 0. \tag{A11}$$

Higher monsoon rainfall therefore raises the level of dry-season rainfall required for irrigation to be profitable. Intuitively, when Kharif rainfall is abundant, the substitution value of irrigation is small, and stronger gains from dry-season production are needed to justify the fixed cost.

The curvature of the frontier is given by

$$\frac{d^2 r_R^*}{dr_K^2} = -\frac{2b}{a(r_K + \varepsilon)^3} < 0. \tag{A12}$$

The frontier is therefore concave in r_K. This curvature reflects diminishing marginal substitution value in the monsoon season: as rainfall increases, the incremental buffering value of irrigation declines at a decreasing rate. Figure A12 illustrates the irrigation adoption frontier implied by the model and depicts how it shifts with the frontier's key parameters.

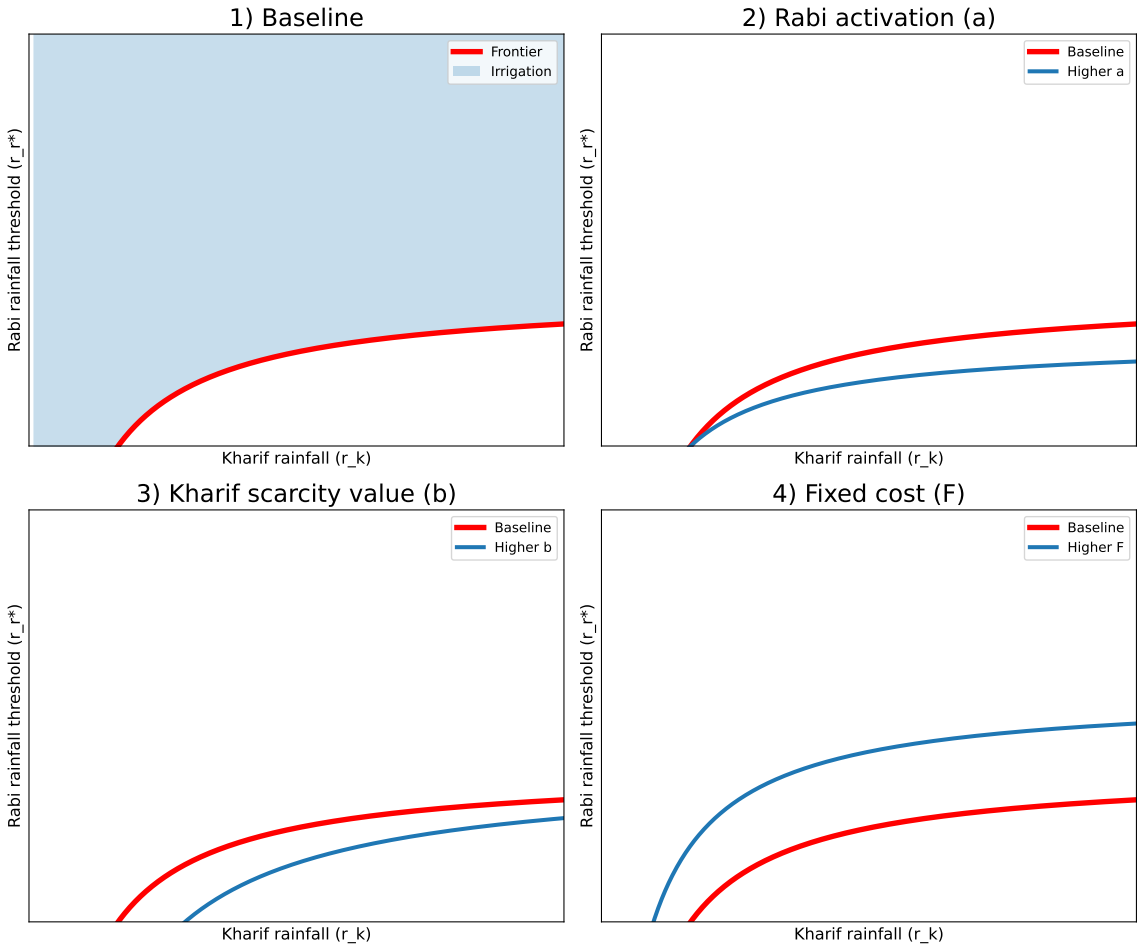


Figure A12: Irrigation Adoption Frontier and Comparative Statics

Notes: The figure illustrates the irrigation adoption frontier implied by the reduced-form representation of the model. The horizontal axis shows water availability during the monsoon (Kharif) season r_K, while the vertical axis shows the minimum level of dry-season (Rabi) water $r_R^*(r_K)$ required for irrigation adoption. Irrigation is adopted whenever the pair (r_K, r_R) lies above the frontier, i.e., in the blue shaded area in Panel (1). Panel (2) shows the effect of higher Rabi productivity (a), which lowers the threshold for adoption by increasing the profitability of dry-season cultivation. Panel (3) shows the effect of a higher Kharif scarcity value (b), which increases the substitution value of irrigation when monsoon rainfall is low. Panel (4) illustrates the effect of higher fixed costs (F), which shifts the adoption frontier upward and reduces irrigation adoption for all rainfall realisations.

C Additional Results

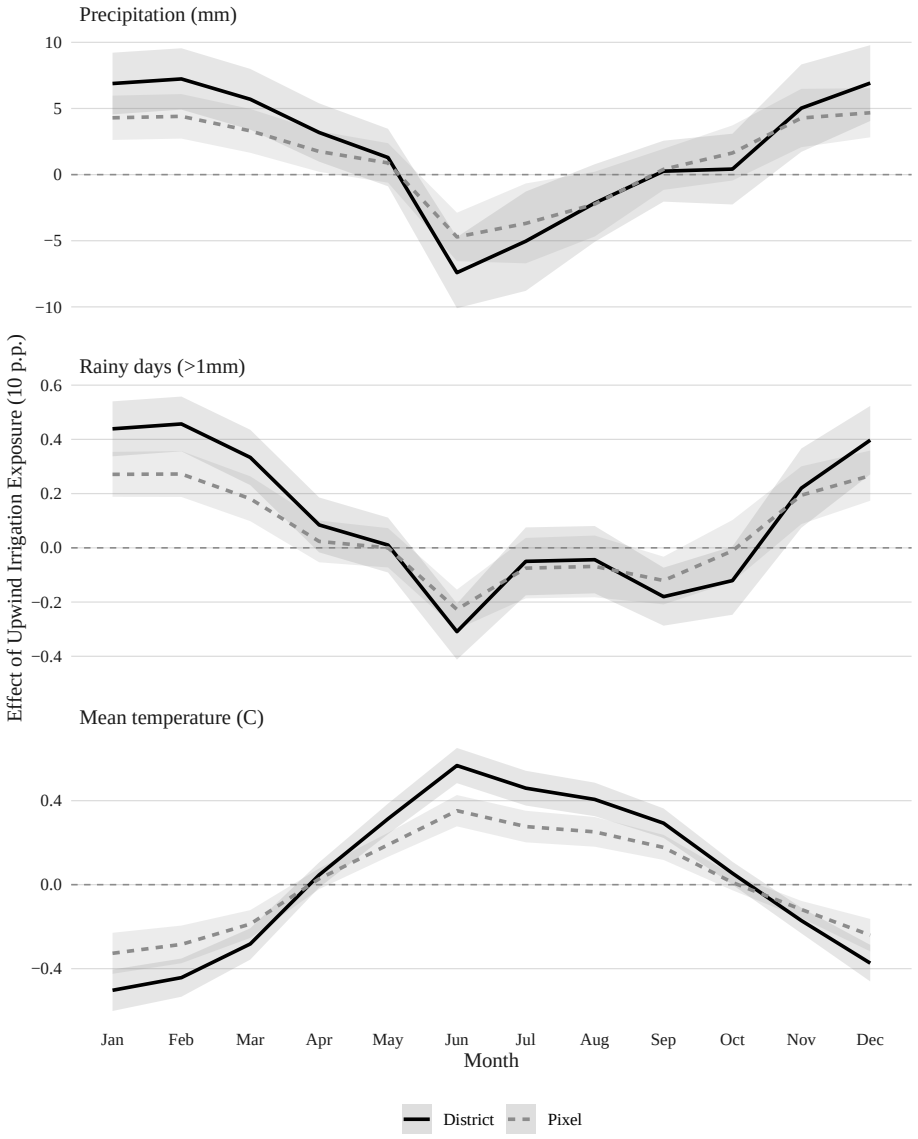


Figure A13: Seasonal Effect of Upwind Irrigation on Climate

Notes: Figure A13 reports the estimated coefficients from specification (4) on (a) monthly precipitation (in mm), (b) number of rainy days ($>$ 1mm) and (c) mean daily temperature (°C). Each estimated coefficient γ_m measures the *total* marginal effect of a 10 percentage point increase in upwind irrigation exposure in month m. Upwind irrigation is defined as the mean share of irrigated area in pixels located 50–150 km upwind of the focal pixel, weighted inversely by distance. Each panel carries the two levels of aggregation. The district regressions cover the 311 districts and include district, month and state-by-year fixed effects; the pixel regressions are on the 0.25° grid inside those districts and include pixel, month and district-by-year fixed effects. Standard errors are clustered at the district level in both. Shaded areas represent 90% confidence intervals.

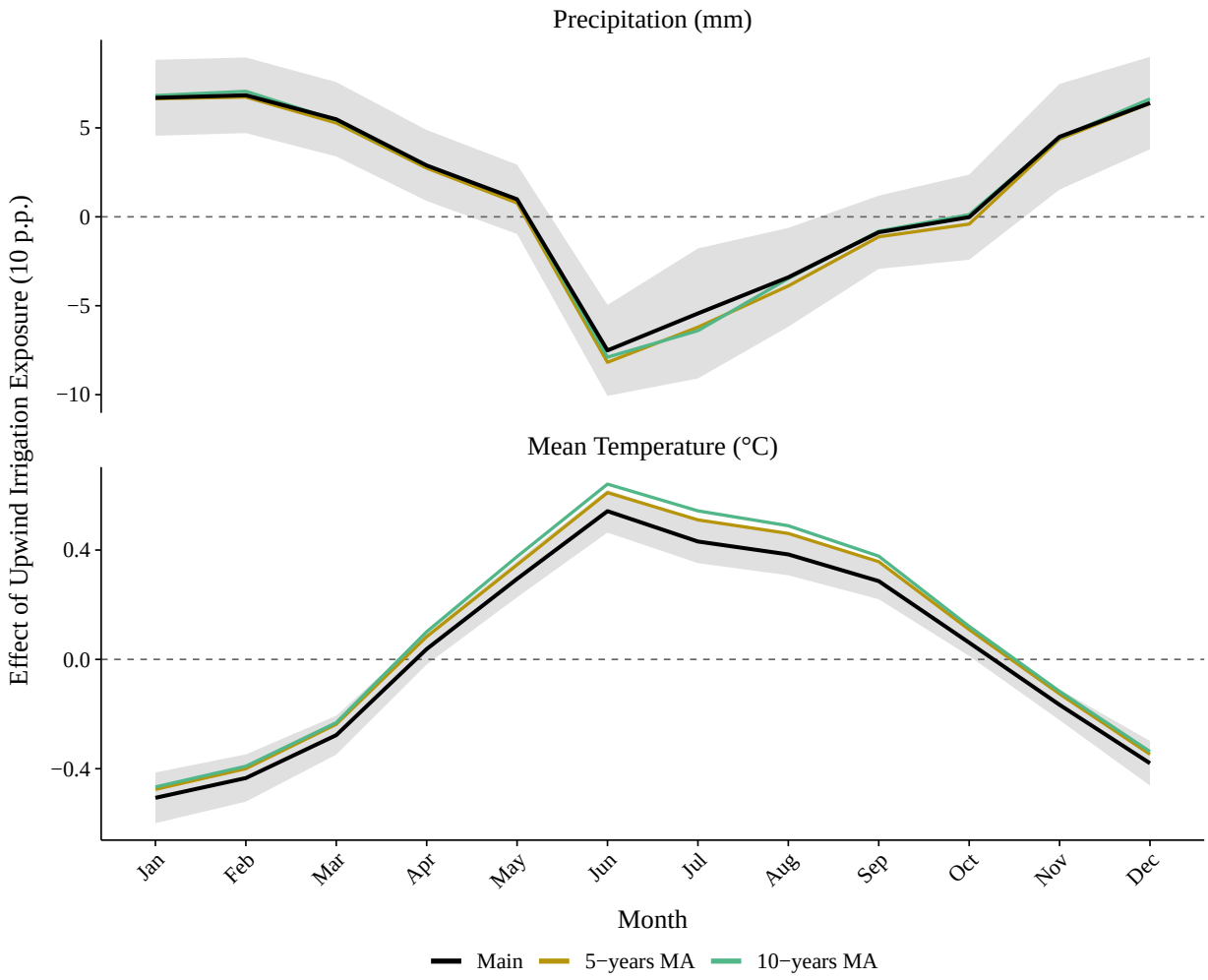


Figure A14: The monthly climate response under three estimation horizons

Notes: Figure A14 reports the estimated coefficients from specification (4) on monthly precipitation (mm) and mean daily temperature (°C), upwind arm alone, under four estimation horizons: the annual panel, five- and ten-year moving averages of each district-month cell, and a long difference between the two ends of the panel. Each estimated coefficient γ_m measures the *total* marginal effect of a 10 percentage point increase in upwind irrigation exposure in month m. Upwind irrigation is the mean share of irrigated area in pixels located 50–150 km upwind of the focal pixel, weighted inversely by distance, averaged over the district. The moving averages take five- and ten-year means of each district-month cell, with state-by-centre fixed effects; averaging is over years within a district-month cell and never across months. The long difference compares the 1966–1975 and 2011–2020 decade means of each district-month cell, with state and month fixed effects; a narrower window centred on the two ends of the panel produced noisy, wrongly-signed outliers and is not used. All four are estimated at the district level with standard errors clustered at the district level. Every line is solid; colour carries the horizon rather than significance.

C.1 Net Annual Impact of Irrigation on Climate

Specification. The analysis is conducted at the monthly level using observations available at the $0.25°$ degree grid and estimated as follows:

$$Y_{i,d,t,m} = \beta\, e_{i,d,t,m} + \mu_i + \lambda_{d,t,m} + \varepsilon_{i,d,t,m}, \tag{A13}$$

where $Y_{i,d,t,m}$ is the outcome of interest—climate variables—for pixel i in district d, year t, and month m. The key explanatory variable, *Upwind Irrigation* $e_{i,d,t,m}$, measures the share of upwind irrigated land affecting pixel i at time (t, m). Pixel fixed effects, μ_i, absorb time-invariant location characteristics, while district-by-year-by-month fixed effects, $\lambda_{d,t,m}$, capture local shocks and seasonal variation. Since $e_{i,d,t,m}$ is defined as the proportion of upwind area under irrigation (ranging from 0 to 1), the coefficient β can be interpreted as the change in climate associated with moving from rainfed to fully irrigated upwind; it is reported in the paper's own units, per 10 percentage points, in Table A8.

Results. Table A8 reports the net annual effect of upwind irrigation on downwind precipitation and temperature: a single coefficient with no month interaction, so it averages the opposing Rabi and Kharif responses documented in Section 6.1. The table is estimated twice, once on the pixel-month grid and once on the district-month panel, each clustered at its own level of observation. At pixel level a 10 percentage point increase in exposure raises monthly rainfall by 1.125 mm with a standard error of 0.367, adds 0.052 rainy days (0.017), raises mean daily temperature by 0.021°C (0.010) and removes 0.123 degree days above 29°C (0.060). Splitting the temperature distribution is informative: the whole of that mean warming sits in the cold tail. The coldest day of the month rises by 0.037°C (0.012), significant at one percent, while the hottest day moves by 0.008°C (0.008) and is indistinguishable from zero. The district panel reproduces the pattern, with a minimum-temperature coefficient of 0.083 (0.047) significant at ten percent and a maximum-temperature coefficient of 0.017 (0.030) that is not. Upwind irrigation therefore compresses the diurnal range

from below rather than adding heat at the top: it lifts night-time and cold-season minima, which is the signature of the added atmospheric moisture that suppresses radiative cooling, and it leaves the hot extreme, the margin that matters for crop damage, untouched. That is consistent with the negative coefficient on degree days above 29°C in column (4). The district panel returns point estimates of the same sign and larger magnitude, but none is distinguishable from zero. The two panels are not in conflict on the coefficients, only on their precision: clustering by district allows for the spatial correlation of upwind exposure across neighbouring pixels and roughly doubles every standard error, which is enough to remove significance. Read with that caveat, the net annual effect is small: a specification without a month interaction nets the Rabi gain against the Kharif loss and recovers little. It is reported here for completeness and is not used elsewhere in the paper.

Table A9 reports two further outcomes under the same equation, the start and duration of the rainy season, on their own specification. Onset and length are large-scale synoptic features rather than pixel-level ones, strongly correlated across a state in a given year; saturating the fixed effects with a state-by-year interaction, as in Table A8, absorbs almost all of that true regional variation and leaves β to identify off residual local noise. Replacing the interaction with a state-specific linear trend in year – which still controls for divergent long-run climate trends across states – raises ten percentage points of upwind irrigation to a 2.366-day contraction of the rainy season (0.460, $p < 0.01$), against 1.873 days under the fully saturated specification, and surfaces a 0.308-day delay in its onset (0.114, $p < 0.01$) that is null under every other fixed-effect structure tried. The length result is robust to this choice of specification; the onset result, while it survives excluding any one state at a time, is not, and is reported as suggestive rather than established.

This is also where the results depart from the closest reference. Grosset-Touba et al. (2024) study the 1930s Great Plains Shelterbelt and find that upwind forest cover raised precipitation and lowered temperature downwind for decades, over distances of up to 200 km, with downwind crop yields 11 to 22 percent higher. Their climate effect is a level shift: rainfall rises over the year, and the agricultural response follows from a uniformly more favourable growing season. The dry-

season estimates here have the same sign and a comparable spatial reach — Rabi rainfall rises and Rabi temperature falls, over an upwind band of 50 to 150 km — but they do not survive aggregation to the year, because the monsoon response has the opposite sign. Irrigation in India redistributes rainfall across the calendar rather than adding to it, which is also why the agricultural response documented here runs through cropping intensity and private irrigation rather than through yields.

Table A8: Effect of Upwind Irrigation on Climate: Net Annual Effect

	(1)	(2)	(3)	(4)
	Precipitation		Temperature	
	Sum (mm)	Rainy Days (Nb.)	Mean (°C)	29°C DD (Nb.)
Panel A: Pixel level				
Upwind irrigation (10 pp.)	1.125***	0.052***	0.021**	-0.123**
	(0.367)	(0.017)	(0.010)	(0.060)
Mean	88.14	6.37	24.63	19.99
Obs.	2,262,653	2,262,653	2,257,571	2,257,571
Nb. Pixel	4,275	4,275	4,260	4,260
Fixed Effects	Pixel, Month and District×Year			
Panel B: District level				
Upwind irrigation (10 pp.)	1.639	0.092	0.047	-0.078
	(1.398)	(0.062)	(0.035)	(0.157)
Mean	94.97	6.67	24.31	18.37
Obs.	167,857	167,857	167,857	167,857
Nb. District	311	311	311	311
Fixed Effects	District, Month and State×Year			

Notes: Each coefficient is the parameter β of equation (A13), estimated without a month interaction, so it is the net annual effect of a 10 percentage point increase in upwind exposure, averaging the opposing Rabi and Kharif responses of Figure 3. Precipitation outcomes are total monthly rainfall and the number of days above 1 mm; temperature is the monthly mean of daily temperature and degree days above 29°C. Panel A is the pixel-month panel on the 0.25° grid over 1966–2010; Panel B is the district-month panel over the same years. Estimated on upwind exposure without exclusion of the focal district's own pixels (pixel level) or with it (district level, the paper's own variable); standard errors are clustered at the level of observation of each panel – by pixel in Panel A, by district in Panel B. Standard errors are in parentheses. Significance: * $p < 0.10$, ** $p < 0.05$, *** $p < 0.01$.

Table A9: Effect of Upwind Irrigation on Monsoon Onset and Length: State-Trend Specification

	(1) Onset (days)	(2) Length (days)
Upwind Irrigation (10 pp.)	0.308***	-2.366***
	(0.114)	(0.460)
Mean	151.080	341.260
Std. Dev.	21.431	138.334
Obs.	9,018	9,018
Nb. District	311	311
Within R^2	0.0003	0.0027
Fixed Effects	District, Year and State-specific Linear Trend	

Notes: Onset and Length are the start and duration of the rainy season, in days from January 1 (Onset) and in days (Length), from the pentad (5-day period) rainy/dry season detection of Bombardi et al. (2019) applied to CHIRPS precipitation, multiplied by five. A higher Onset is a later start to the rainy season. Each project pixel is the mean of the source dataset's 0.05° cells within 0.16° of its centre, averaged to the district-year panel of Table A8's Panel B, over 1981–2009. Onset and length are large-scale synoptic features, correlated across a state in a given year: the state-by-year fixed effects of Table A8 would absorb most of their true variation, so this table replaces that interaction with a state-specific linear trend in year, which still controls for divergent long-run climate trends across states. Standard errors are clustered at the district level. The Length coefficient is robust across every fixed-effect structure tried, from the state-by-year interaction of Table A8 to no state control at all; the Onset result is significant only under the specification reported here and is read as suggestive. Season length should be read with caution outside the core monsoon belt, where the retreating (northeast) monsoon can chain onto the southwest monsoon in the pentad detection, spanning most of the year. Significance: * $p < 0.10$, ** $p < 0.05$, *** $p < 0.01$.

C.2 Non-linear Effect of Irrigation on Temperature

An important literature shows that agricultural output responds non-linearly to temperature, with yields increasing at moderate temperatures but declining sharply beyond crop-specific thresholds (Schlenker and Roberts, 2009). Therefore, I extend equation (5) to examine whether irrigation exposure affects the distribution of temperature exposure.

To this end, I adopt a binned Growing Degree Days (GDD) approach, which measures cumulative heat exposure relevant for crop growth by aggregating daily temperatures into predefined temperature bins over the growing season, following Schlenker and Roberts (2009). Specifically, the temperature distribution is partitioned into a set of 1-degree bins, and for each bin a separate GDD variable is constructed. Each GDD variable aggregates, over all days of the growing

season, the amount of heat received when daily temperatures fall within the corresponding temperature range. As a result, seasonal GDD captures cumulative thermal exposure in degree-days (°C×days), reflecting both the frequency and the intensity of heat within each temperature bin.[20]

As previously, this analysis is conducted separately for the two main agricultural seasons in India, the Rabi and Kharif seasons, which differ in crop composition and climatic conditions. I estimate the following specification:

$$\text{GDD}_{d,s,t,b} = \sum_{k \in \mathcal{B}} \beta_k \left(E_{d,t} \times \mathbf{1}\{b = k\} \right) + \mu_d + \lambda_{s,t} + \delta_b + \varepsilon_{d,s,t,b}. \tag{A14}$$

Here, $\text{GDD}_{d,s,t,b}$ denotes cumulative growing degree days accumulated in temperature bin b in district d, state s, and year t over an entire season, belonging to either the Rabi or the Kharif agricultural season. As in equation (5), $E_{d,t}$ corresponds to district-level upwind irrigation exposure, measured separately for the Rabi and Kharif seasons. The indicator $\mathbf{1}\{b = k\}$ allows irrigation exposure to have a fully flexible, non-linear effect across the temperature distribution.

The coefficients β_k capture the marginal effect of irrigation exposure on cumulative degree days in temperature bin k, that is, on the total amount of heat accumulated within that temperature range over the season. The specification includes district fixed effects μ_d, state-by-year fixed effects $\lambda_{s,t}$, and temperature-bin fixed effects δ_b, which absorb time-invariant district characteristics, common state-level shocks in a given year, and average differences across temperature bins common to all districts, respectively. Standard errors are clustered at the district level.

Figure A15 illustrates the non-linear relationship between upwind irrigation exposure and the distribution of temperature exposure across growing degree day bins. During the dry Rabi season, higher exposure to upwind irrigation reallocates thermal exposure away from higher temperature bins toward more moderate ones: cumulative degree days rise between 4 and 17°C and fall above 17°C, up to about 40°C. During the wet Kharif season the pattern is reversed. Cumulative degree

[20] To illustrate, consider a temperature bin spanning 34–35°C during a given growing season. If, over the season, temperatures reach 34.2°C on two days and 36°C on one day, the corresponding GDD in this bin would equal 0.2 + 0.2 + 1 = 1.4 degree-days. In contrast, a season with a single day at 34.1°C would generate only 0.1 degree-day in this bin. Thus, seasonal GDD summarises overall exposure to heat within a temperature range, rather than simply counting the number of hot days.

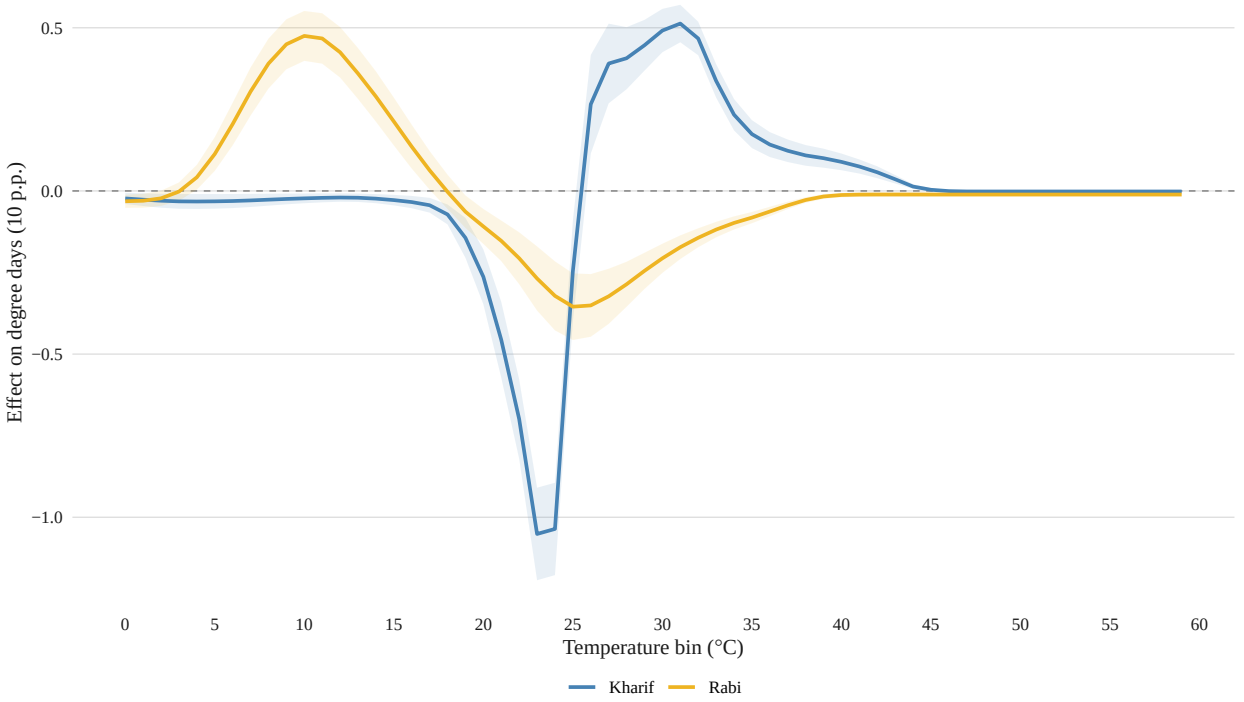


Figure A15: Non-linear Effect of Upwind Irrigation on Temperature Exposure by Season

Notes: Figure A15 plots the estimated coefficients $\hat{\beta}_b$ from equation (A14), which measure the marginal effect of upwind irrigation exposure on cumulative growing degree days in temperature bin b. Upwind irrigation exposure is defined as the mean share of irrigated area in pixels located 50–150 km upwind of the focal district, weighted inversely by distance. All regressions are estimated at the district level and include district fixed effects as well as state-by-year fixed effects. Standard errors are clustered at the district level. Shaded areas represent 95% confidence intervals. Estimates are reported separately for the Kharif (wet) season, shown in blue, and the Rabi (dry) season, shown in yellow.

days fall over the moderate range, most sharply between 20 and 25°C, and rise from 26°C upward. Irrigation therefore alters local thermal conditions in season-specific ways, mitigating extreme heat exposure during the dry season while amplifying high-temperature exposure during the monsoon.

Table A10: Effect of Upwind Irrigation on Climate Outcomes

	(1)	(2)	(3)	(4)	(5)	(6)
	Climate outcomes					
Season	Precipitation (mm/month)			Mean Temperature (°C)		
	Coef.	Mean(Y)	Effect (% Mean)	Coef.	Mean(Y)	Effect (% Mean)
Rabi	16.409***	29.09	56.41%	-0.276***	19.62	-1.40%
	(5.254)			(0.066)		
Zaid	4.178	50.49	8.27%	-0.024	27.71	-0.09%
	(3.303)			(0.099)		
Kharif	-7.226	215.14	-3.36%	0.073	25.83	0.28%
	(4.740)			(0.076)		
Obs.	768,938			766,932		
Fixed Effects	Pixel, and District × Season × Year					

Notes: Each coefficient is the season-specific marginal effect of upwind irrigation exposure moving from 0 (non-irrigated) to 1 (fully irrigated), estimated in one regression per outcome with a season-specific slope on exposure, and pixel and district-by-season-year fixed effects. The outcome is the average monthly value within the season. Seasons are *Kharif* = June–September, *Zaid* = April–May, and *Rabi* = the six remaining months, October through March. Standard errors, clustered at the district level, are in parentheses; the same estimates appear as the last rung of Figure A16. Significance: * $p < 0.10$, ** $p < 0.05$, *** $p < 0.01$.

C.3 Land composition and field wages

Table A11: Effect of Upwind Irrigation on Land Composition

	(1)	(2)	(3)	(4)	(5)	(6)	(7)	(8)
	Dep. Var.: Share of total geographic area							
	Non-agri.	Perm. past.	Net crop. area	Cult. waste	Cur. fallow	Oth. fallow	Barren	Forest
Upwind irrigation (10 pp.)	0.0014**	-0.0001	-0.0027**	-0.0005	0.0016*	0.0005	-0.0007	0.0006
	(0.0007)	(0.0002)	(0.0012)	(0.0007)	(0.0010)	(0.0004)	(0.0005)	(0.0011)
Mean	0.081	0.041	0.528	0.037	0.043	0.028	0.055	0.163
Std. Dev.	0.059	0.066	0.205	0.058	0.046	0.032	0.071	0.170
Obs.	13,357	13,356	13,325	13,357	13,356	13,354	13,357	13,354
Nb. District	311	311	311	311	311	311	311	311
Adj. R^2	0.908	0.928	0.962	0.907	0.771	0.841	0.893	0.956
Fixed Effects	District and State×Year							

Notes: Each coefficient is β of equation (5), the effect of a 10 percentage point increase in upwind irrigation exposure. Upwind irrigation is the average share of irrigated land in pixels 50–150 km upwind of the district, weighted by the inverse of distance and excluding the district's own area. Each outcome is a land-use category as a share of total geographic area; the eight categories together cover 99.4 percent of that area at the median, so the table is close to a complete decomposition. All columns include district and state-by-year fixed effects, and no baseline controls: neither log population nor high-yielding variety area enters any column. Standard errors are clustered at the district level in parentheses. Significance: * $p < 0.10$, ** $p < 0.05$, *** $p < 0.01$.

Table A12: Effect of Upwind Irrigation on Field Labour Wages

	(1)	(2)
	Daily wage – in log()	
	Male wage	Female wage
Upwind irrigation (10 pp.)	0.0043	-0.0195*
	(0.0077)	(0.0108)
Mean (log)	2.446	2.399
Std. Dev. (log)	1.239	1.229
Obs.	9,363	6,148
Nb. District	308	271
Adj. R^2	0.978	0.969
Fixed Effects	District and State×Year	

Notes: Each coefficient is β of equation (5), the effect of a 10 percentage point increase in upwind irrigation exposure. The dependent variables are the logarithm of the daily field labour wage for men and for women, available over 1966–2009. Both columns include district and state-by-year fixed effects, and no baseline controls, with standard errors clustered at the district level in parentheses. The female sample is markedly smaller than the male one, 271 districts against 308, because female field wages are reported less often. Significance: * $p < 0.10$, ** $p < 0.05$, *** $p < 0.01$.

D Robustness

D.1 Sensitivity to the fixed-effect structure

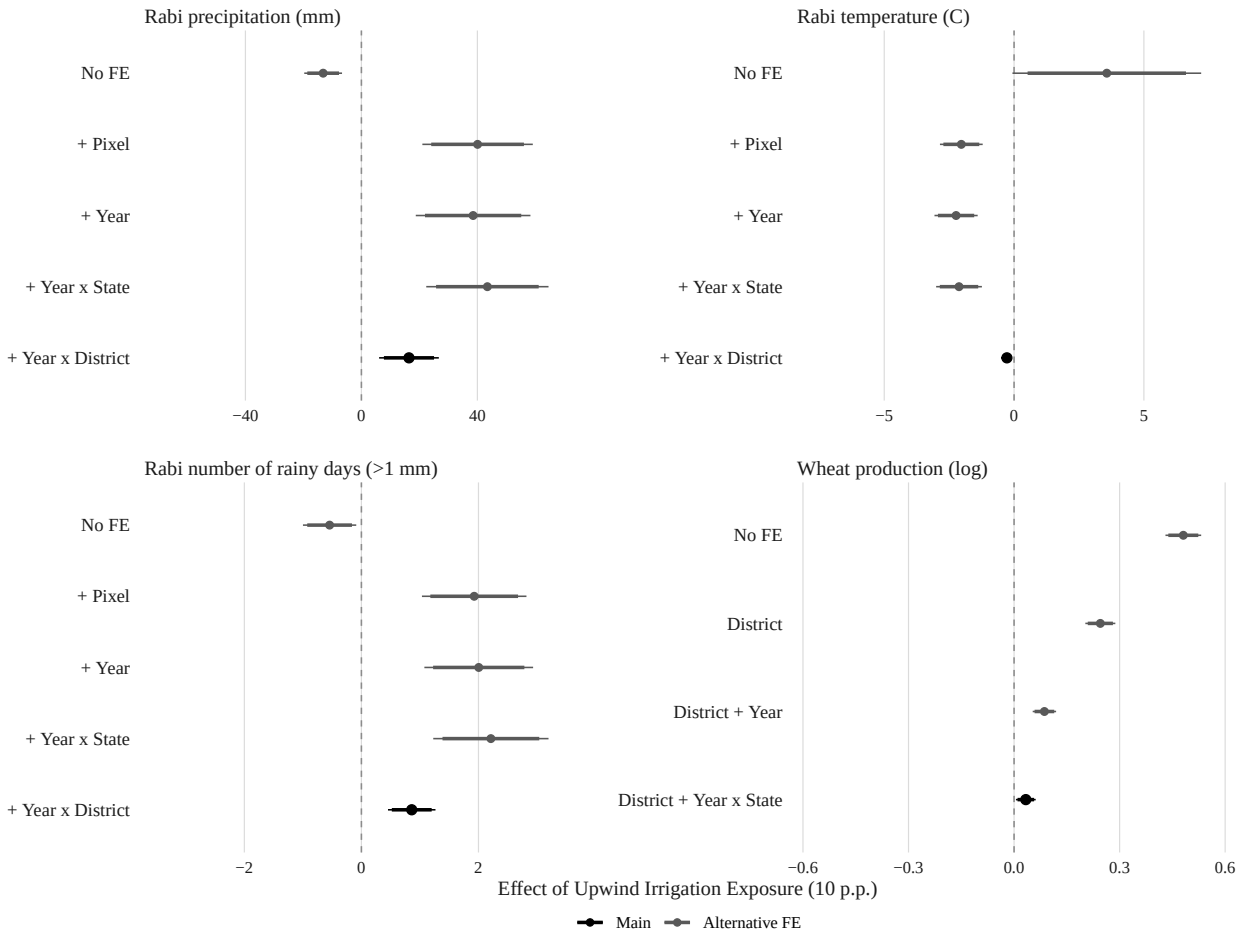


Figure A16: Sensitivity of the main results to the fixed-effect structure: a ladder

Notes: Each panel re-estimates the same regression, adding one fixed effect at a time, from none to the structure of the paper's own tables. The climate estimates are pooled across seasons with a season-specific slope on exposure and a season fixed effect at every rung, becoming district-by-season-by-year at the last rung; the agricultural estimates use the annual district panel. Upwind irrigation is the average share of irrigated land in pixels located 50–150 km upwind of the focal pixel, weighted inversely by distance. Standard errors are clustered at the district level. Error bars denote 90 and 95 percent confidence intervals. The last climate rung is the specification of Table A10 and reports the same coefficients for precipitation and temperature. The number of rainy days is only available for 1966–2010.

D.2 The definition of exposure

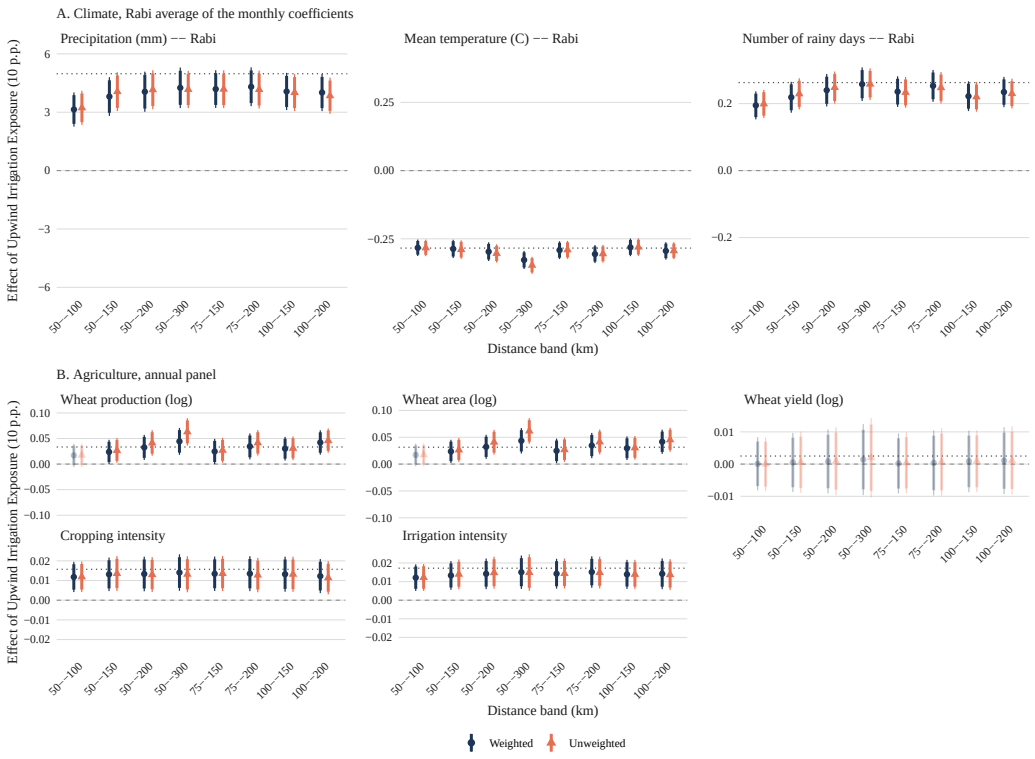


Figure A17: Different Definitions of Upwind Irrigation

Notes: Figure A17 re-estimates the main results under sixteen alternative definitions of upwind exposure, varying the distance band (horizontal axis) and the weighting: circles weight by inverse distance, as the paper does, triangles weight equally. Panel A reports the seasonal coefficient of specification (4); Panel B reports β of equation (5). District and state-by-year fixed effects; standard errors clustered at the district level. Thick bars are 90% and thin bars 95% confidence intervals; the dotted line is the published coefficient.

D.3 Geographic confounders

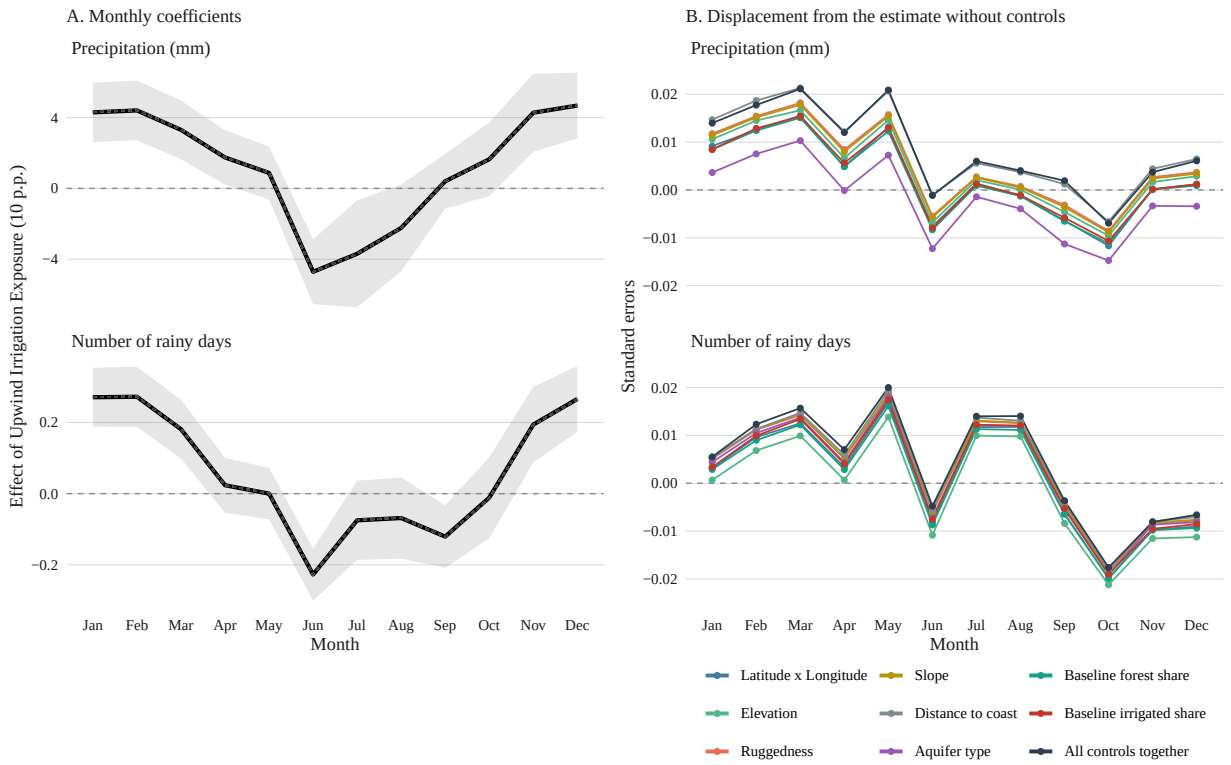


Figure A18: Monthly climate coefficients at pixel level, under every geographic control

Notes: Figure A18 reports the monthly coefficient of a 10 percentage point increase in upwind irrigation exposure on precipitation (mm) and mean temperature (°C), estimated at the pixel level. The black line is the paper's specification, with no geographic control; each coloured line adds one time-invariant geographic characteristic interacted with year, and the last adds all of them together. Pixel, month and district-by-year fixed effects; standard errors clustered at the district level.

Uttar Pradesh and the crop results. Uttar Pradesh contributes 54 of the 311 sample districts, 35 percent of wheat production and 60 percent of the within-district variation in upwind exposure: it is both where the wheat is grown and where the specification is identified. Dropping it removes the wheat result in logs and produces a rice result that was not there before, which looks like a single state carrying the crop effects. It is not; it is the logarithm. Outside Uttar Pradesh 16.9 percent of district-year wheat observations are true zeros, against 3.3 percent inside, and $\log y$ discards every one of them, so the log specification is silent precisely where wheat is grown

Table A13: Balance Table: District Characteristics on Upwind Irrigation Exposure

			No controls		State FE		State FE + other X	
	Mean	S.D.	$\hat{\beta}$	p	$\hat{\beta}$	p	$\hat{\beta}$	p
	(1)	(2)	(3)	(4)	(5)	(6)	(7)	(8)
Panel A: exposure in levels (mean 1966–2010)								
Latitude (°)	22.73	5	0.516***	0.000	0.062*	0.053	-0.059**	0.012
Longitude (°)	78.91	4.349	-0.010	0.830	-0.075*	0.091	-0.152***	0.001
Elevation (m)	297	212.8	-0.322***	0.000	-0.346***	0.001	-0.133**	0.023
Ruggedness (TRI)	12.74	15.55	-0.352***	0.000	-0.406***	0.003	0.007	0.238
Elevation s.d. (m)	88.34	95.58	-0.362***	0.000	-0.500***	0.000	-0.136***	0.009
Slope (°)	0.7728	0.9602	-0.346***	0.000	-0.418***	0.003	-0.005	0.404
Distance to coast (km)	440.7	307	0.667***	0.000	0.153***	0.001	0.150***	0.000
District area (km^2)	965.8	598.1	-0.381***	0.000	-0.179**	0.013	-0.088	0.335
Alluvial aquifer share	0.4289	0.4279	0.646***	0.000	0.336***	0.000	0.138**	0.017
Hard-rock aquifer share	0.1173	0.2107	-0.251***	0.000	-0.213**	0.012	0.048	0.595
Forest share, 1966–75	0.1514	0.1633	-0.351***	0.000	-0.332***	0.001	0.068	0.306
Irrigated share, 1966–75	0.2419	0.2109	0.673***	0.000	0.517***	0.000	-0.047*	0.088
Length of growing period (days)	188.7	48.21	-0.003	0.961	-0.122	0.150	0.021	0.805
Normal annual rainfall (mm)	1078	486.5	-0.179***	0.000	-0.191***	0.009	-0.051	0.122
Potential evapotranspiration	1567	184	-0.251***	0.000	0.034	0.616	-0.060	0.359
Moisture availability index	0.5661	0.3322	-0.124***	0.004	-0.203***	0.007	0.044	0.129
Rainfall 1968–72 (mm)	998	523	-0.230***	0.000	-0.185***	0.004	-0.062	0.223
Cropping intensity, 1968–72	1.19	0.1537	0.582***	0.000	0.246***	0.006	0.076	0.399
Irrigation intensity, 1968–72	0.2344	0.2038	0.695***	0.000	0.534***	0.000	0.070**	0.011
Imbalanced at 10%			17 / 19		17 / 19		8 / 19	
Joint F (geography → exposure)			38.57		5.82			
R^2			0.777		0.364 (within)			
Panel B: exposure in changes (1998–2002 minus 1968–1972)								
Latitude (°)	22.73	5	0.240***	0.000	0.010	0.626	-0.021*	0.051
Longitude (°)	78.91	4.349	0.263***	0.000	0.053*	0.055	0.018	0.540
Elevation (m)	297	212.8	-0.330***	0.000	-0.193***	0.000	-0.117***	0.000
Ruggedness (TRI)	12.74	15.55	-0.245***	0.000	-0.156***	0.005	0.004	0.111
Elevation s.d. (m)	88.34	95.58	-0.266***	0.000	-0.177***	0.002	-0.020	0.123
Slope (°)	0.7728	0.9602	-0.244***	0.000	-0.160***	0.005	-0.003	0.200
Distance to coast (km)	440.7	307	0.232***	0.000	0.037	0.220	0.027	0.180
District area (km^2)	965.8	598.1	-0.232***	0.000	-0.113***	0.006	-0.086**	0.047
Alluvial aquifer share	0.4289	0.4279	0.387***	0.000	0.166***	0.001	0.082***	0.004
Hard-rock aquifer share	0.1173	0.2107	-0.162***	0.000	-0.040	0.287	0.057	0.199
Forest share, 1966–75	0.1514	0.1633	-0.221***	0.000	-0.169***	0.001	-0.048	0.120
Irrigated share, 1966–75	0.2419	0.2109	0.087*	0.055	-0.020	0.668	-0.004	0.672
Length of growing period (days)	188.7	48.21	0.228***	0.000	0.025	0.491	0.064*	0.062
Normal annual rainfall (mm)	1078	486.5	-0.019	0.651	-0.095**	0.011	-0.028**	0.024
Potential evapotranspiration	1567	184	-0.193***	0.000	0.014	0.708	-0.032	0.294
Moisture availability index	0.5661	0.3322	0.014	0.746	-0.099**	0.015	0.016	0.182
Rainfall 1968–72 (mm)	998	523	-0.014	0.717	-0.090**	0.012	-0.033	0.240
Cropping intensity, 1968–72	1.19	0.1537	0.206***	0.000	0.008	0.899	-0.031	0.537
Irrigation intensity, 1968–72	0.2344	0.2038	0.034	0.443	-0.022	0.610	-0.001	0.926
Imbalanced at 10%			15 / 19		11 / 19		6 / 19	
Joint F (geography → exposure)			4.06		2.95			
R^2			0.335		0.184 (within)			

Notes: Cross-sectional balance on 272 districts in 13 states, one observation per district. Each row is a separate regression of the characteristic on upwind irrigation exposure; both are standardised, so $\hat{\beta}$ is the standard-deviation change in the characteristic per standard-deviation of exposure. Columns (3)–(4) have no controls, (5)–(6) add state fixed effects, (7)–(8) add every other characteristic in the table. Standard errors are heteroskedasticity-robust. The joint F tests all characteristics together in a regression of exposure on the full vector.

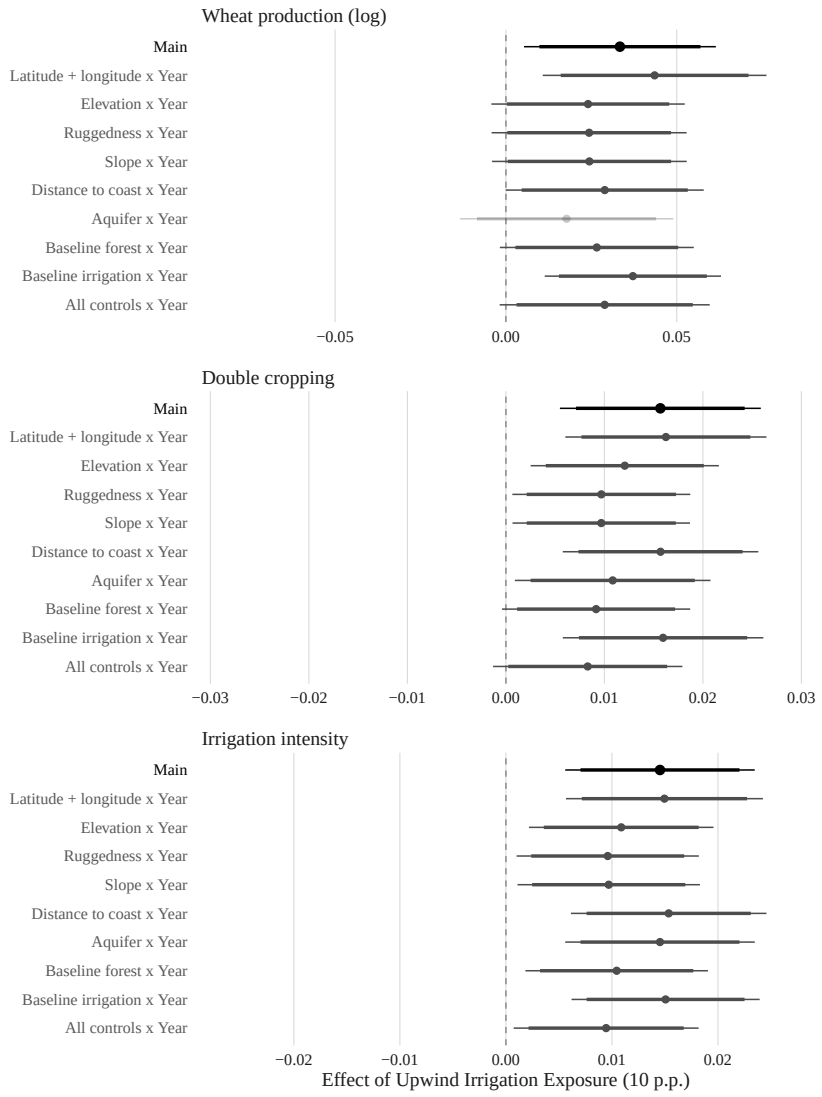


Figure A19: Agricultural outcomes under each geographic control

Notes: Figure A19 reports the estimated coefficients from $y_{d,t} = \beta E^{\uparrow}_{d,t} + \gamma(X_d \times \text{Year}_t) + \mu_d + \lambda_{s,t} + \varepsilon_{d,t}$ on four agricultural outcomes, adding one time-invariant geographic characteristic interacted with year (each row's label) and then all of them together. Each estimated coefficient β measures the marginal effect of a 10 percentage point increase in upwind irrigation exposure. Upwind irrigation is defined as the mean share of irrigated area in pixels located 50–150 km upwind of the focal pixel, weighted inversely by distance, averaged over the district. All regressions include district and state-by-year fixed effects and standard errors are clustered at the district level. Error bars denote 90% and 95% confidence intervals. The top row of each panel, in black, is the specification of the paper, without geographic controls; the rows below add one characteristic at a time and then all of them together. Wheat and rice production are in logs, as marked, and estimated on the positive observations; double cropping and irrigation intensity are bounded ratios and enter in levels, as in the main text.

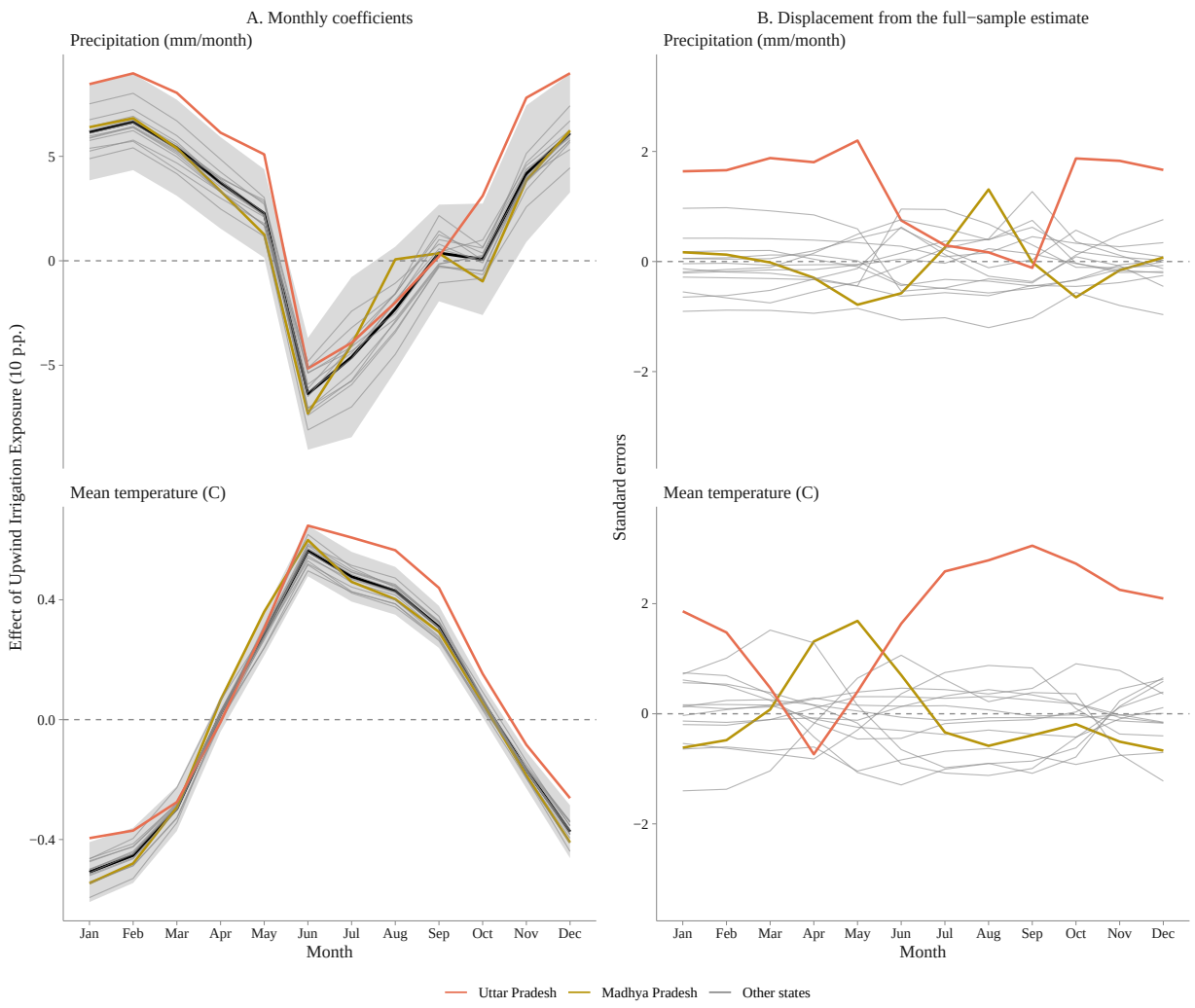


Figure A20: Leave-one-state-out: monthly climate response

Notes: Figure A20 reports the estimated coefficients from specification (4) on (i) monthly precipitation (mm) and (ii) mean daily temperature (°C), re-estimated fifteen times, each dropping one state from the sample. Each estimated coefficient γ_m measures the *total* marginal effect of a 10 percentage point increase in upwind irrigation exposure in month m. Upwind irrigation is defined as the mean share of irrigated area in pixels located 50–150 km upwind of the focal pixel, weighted inversely by distance, averaged over the district. All regressions are estimated at the district level and include district, month and state-by-year fixed effects. Standard errors are clustered at the district level. The black line is the full sample and the shaded area its 90% confidence interval. Each grey line is one leave-one-out sample, that is, the estimate obtained when one of the fifteen states is removed; the two whose removal displaces the coefficients furthest are drawn in colour and named in the legend. Panel B reports that displacement, in full-sample standard errors. Because the state-by-year fixed effects are separable, dropping a state does not alter how the others are identified.

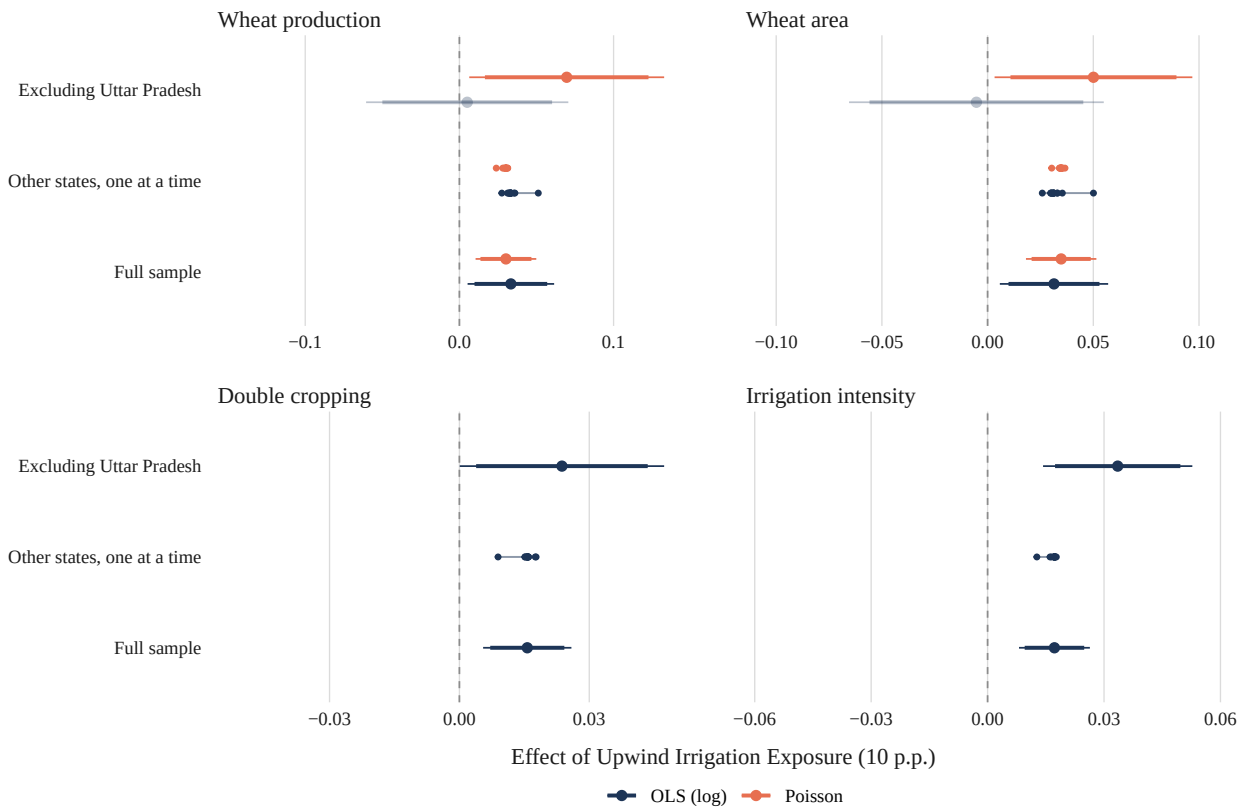


Figure A21: Leave-one-state-out: agricultural outcomes

Notes: Figure A21 reports the estimated coefficient on upwind exposure from $y_{d,t} = \beta E^{\uparrow}_{d,t} + \mu_d + \lambda_{s,t} + \varepsilon_{d,t}$, re-estimated sixteen times, once on the full sample and once dropping each of the fifteen sample states. Each coefficient is the effect of a 10 percentage point increase in upwind irrigation exposure. All specifications include district and state-by-year fixed effects and no baseline controls, with standard errors clustered at the district level, so the top row reproduces Tables 1 to 2 exactly. Both estimators are drawn: OLS on $\log y$, on the positive observations, and Poisson pseudo-maximum likelihood on every observation; the two bounded ratios are least squares in levels under either heading and are drawn once. The top row is the full sample, the second isolates Uttar Pradesh with its own 90 and 95 percent intervals, and the bottom row is one point per remaining state with a segment spanning their range.

intermittently. Poisson pseudo-maximum likelihood, which keeps the zeros, reverses the conclusion (Figure A21): dropping Uttar Pradesh *raises* the wheat coefficients rather than removing them, with wheat production at 0.070 ($p = 0.03$) outside against 0.030 ($p < 0.01$) on the full sample, and wheat area at 0.050 against 0.035. The rice response outside Uttar Pradesh, finally, is on area and not on yield — rice area 0.039 under Poisson and 0.092 in logs, against 0.015 and 0.014 on the full sample — which is acreage expansion under irrigation, the adaptation margin the paper describes, and not a direct effect of the monsoon rainfall that the estimates report as declining.

D.4 Functional form

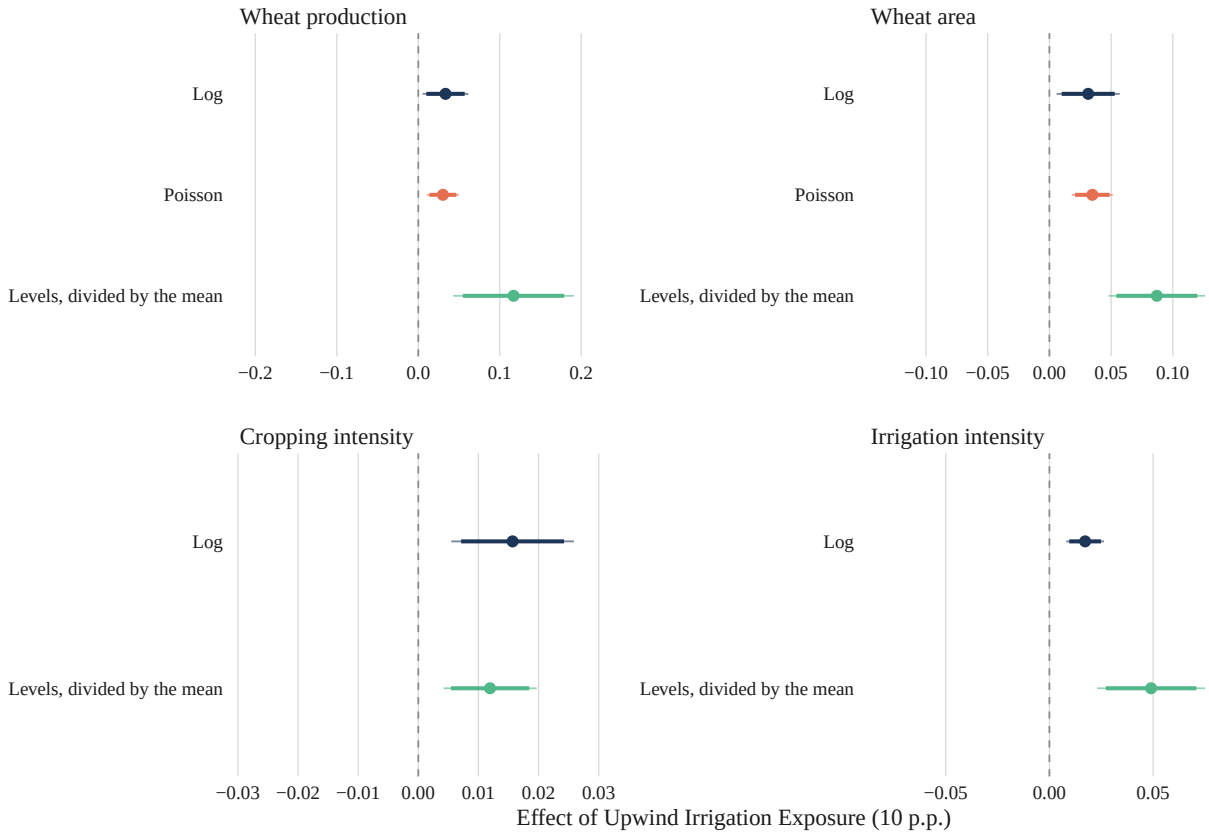


Figure A22: The main agricultural results under three functional forms

Notes: Figure A22 reports the estimated coefficient on upwind exposure from $y_{d,t} = \beta E^{\uparrow}_{d,t} + \mu_d + \lambda_{s,t} + \varepsilon_{d,t}$ under three functional forms: *log* (the main text's specification), *Poisson*, and *levels* divided by the outcome's mean. District and state-by-year fixed effects; standard errors clustered at the district level. Thick bars are 90% and thin bars 95% confidence intervals; estimates not significant at 10 percent are drawn at reduced opacity.

D.5 The Green Revolution

Table A14: Effect of Upwind Irrigation on Green Revolution Confounders

	(1)	(2)
	Effect	(s.e.)
Forest share of district land	-0.5%	(3.1)
Barren share of district land	-1.4%	(2.3)
NPK fertiliser per ha (NCA)	4.9%	(7.4)
HYV share of gross cropped area	14.5%	(9.2)
Log population	6.8%	(5.5)
Fixed Effects	District and State×Year	

Notes: Each row regresses a candidate confounder, measured at the focal district, on upwind exposure under the paper's own fixed effects. The test asks whether the treatment predicts the confounder at the receiving district. None does, at any conventional significance level. Coefficients are expressed as a percentage of the outcome's residual standard deviation for a 10 percentage point increase in exposure, since a coefficient is only small relative to the dispersion it is meant to explain. Standard errors are clustered at the district level. The same logic is applied to $PM_{2.5}$ in Appendix D.6 and to varietal adoption and fertiliser use in Appendix D.5.

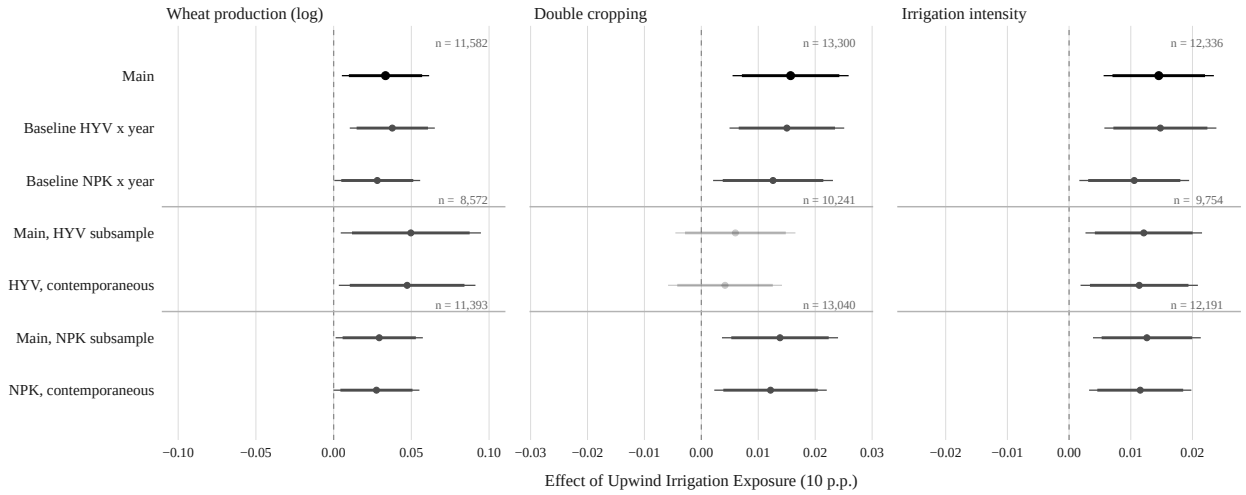


Figure A23: Agricultural results under Green Revolution controls

Notes: Figure A23 reports the estimated coefficient β from $y_{d,t} = \beta E^{\uparrow}_{d,t} + \mu_d + \lambda_{s,t} + \varepsilon_{d,t}$ on four agricultural outcomes, with the stated Green Revolution control added. Upwind irrigation is the mean share of irrigated area in pixels located 50–150 km upwind of the focal pixel, weighted inversely by distance, averaged over the district. The two markers are the share of gross cropped area under high-yielding varieties (HYV) and NPK fertiliser use. The panel is in three groups, separated by a grey rule, because each rests on a different sample: the top three rows — the paper's own specification and the two predetermined baseline controls, each the marker's 1966–1970 district mean interacted with year — use the full sample; the next two restrict to the district-years where HYV is observed, the paper's specification on that subsample and then with contemporaneous HYV added; the last two do the same for NPK. Each point carries its own observation count, since the three groups differ in N; comparisons should be read within a group, not across groups. Wheat and rice production are in logs, on the positive observations; double cropping and irrigation intensity are bounded ratios and enter in levels, as in the main text. Standard errors are clustered at the district level; error bars denote 90% and 95% confidence intervals.

D.6 Air pollution and crop-residue burning

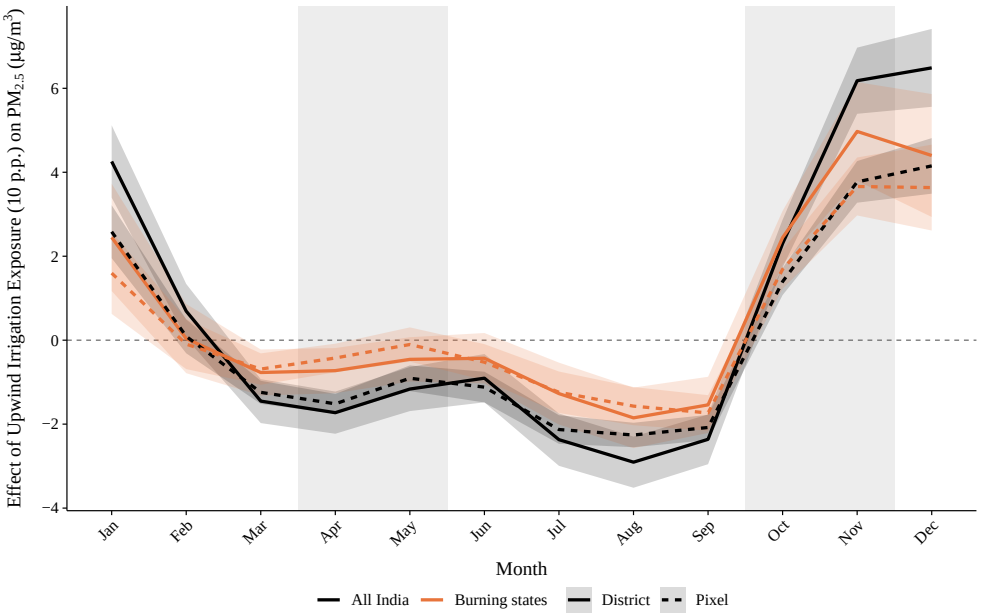


Figure A24: Upwind irrigation exposure and $PM_{2.5}$

Notes: Figure A24 reports the estimated coefficients from specification (4) with $PM_{2.5}$ as the dependent variable, 2000–2020. Each coefficient γ_m measures the *total* marginal effect of a 10 percentage point increase in upwind irrigation exposure in month m, in micrograms per cubic metre. Upwind irrigation is the mean share of irrigated area in pixels located 50–150 km upwind of the focal pixel, weighted inversely by distance. $PM_{2.5}$ is the ACAG satellite product, extracted monthly on the paper's own 0.25° grid. The district series is solid, with district, month and state-by-year fixed effects; the pixel series is dashed, with pixel, month and district-by-year fixed effects. Standard errors are clustered at the district level in both, since pollution is correlated far beyond a single 0.25° pixel. Black is all of India; orange restricts to the 89 districts of Punjab, Haryana, Uttar Pradesh and Bihar, where crop-residue burning is concentrated. The shaded columns are the two burning windows, April–May after the wheat harvest and October–November after the rice harvest. Shaded areas are 90% confidence intervals.

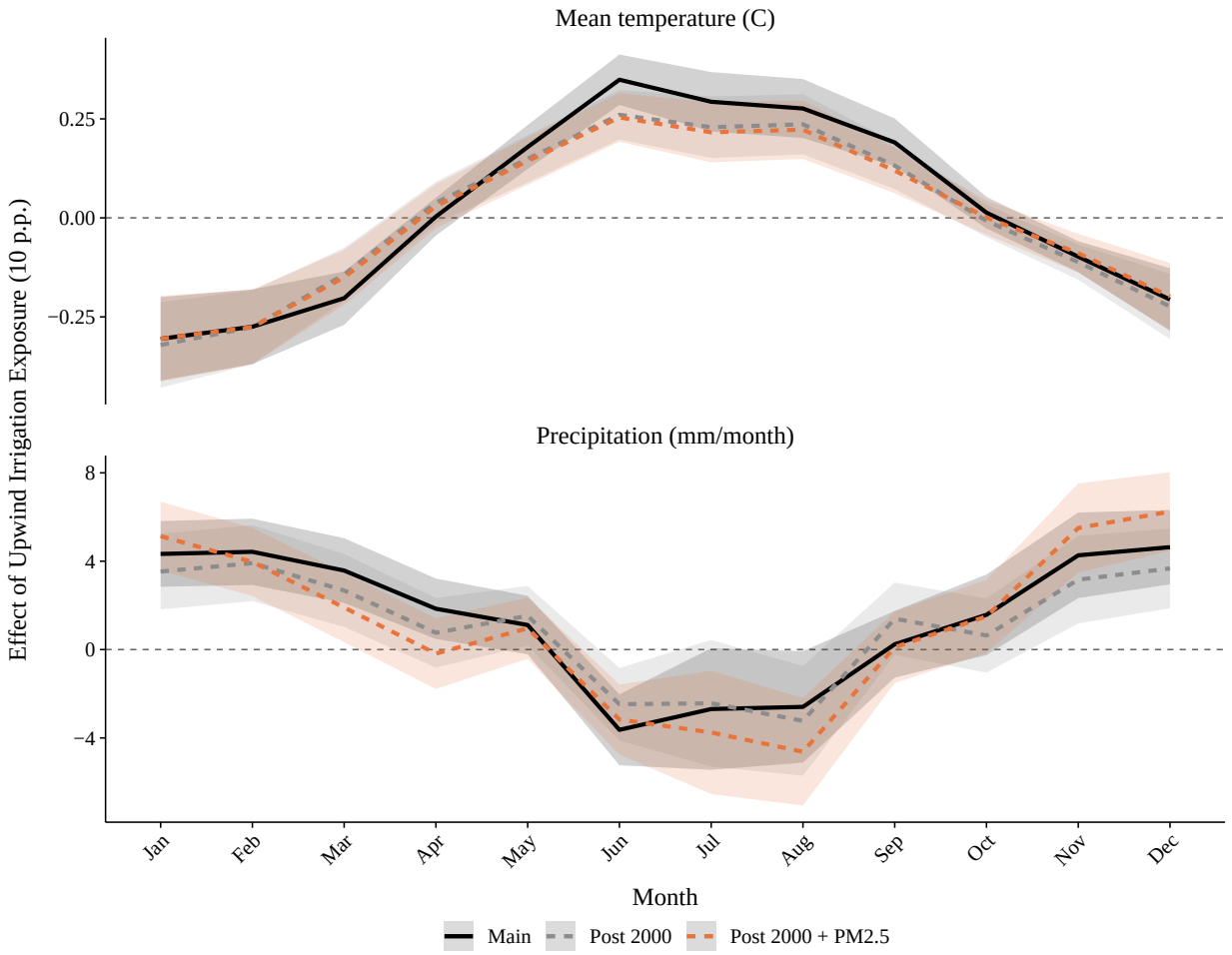


Figure A25: Climate Results controlling for PM 2.5

Notes: Estimated at the pixel level, with pixel, month and district-by-year fixed effects, clustered by district. Figure A25 reports the estimated coefficients from specification (4) on (i) monthly precipitation (mm) and (ii) mean daily temperature (°C). *Main* is the paper's specification on the full 1966–2020 panel. *Post 2000* restricts it to the years $PM_{2.5}$ is observed, and *Post 2000 + PM2.5* adds the contemporaneous, continuous, pixel-level measure directly. Only the contemporaneous control is reported: a predetermined control, each pixel's mean $PM_{2.5}$ interacted with year, is constant within a pixel-year and can therefore only translate the twelve monthly coefficients as a block, never deform the seasonal profile the paper reads. Shaded areas are 90% confidence intervals.

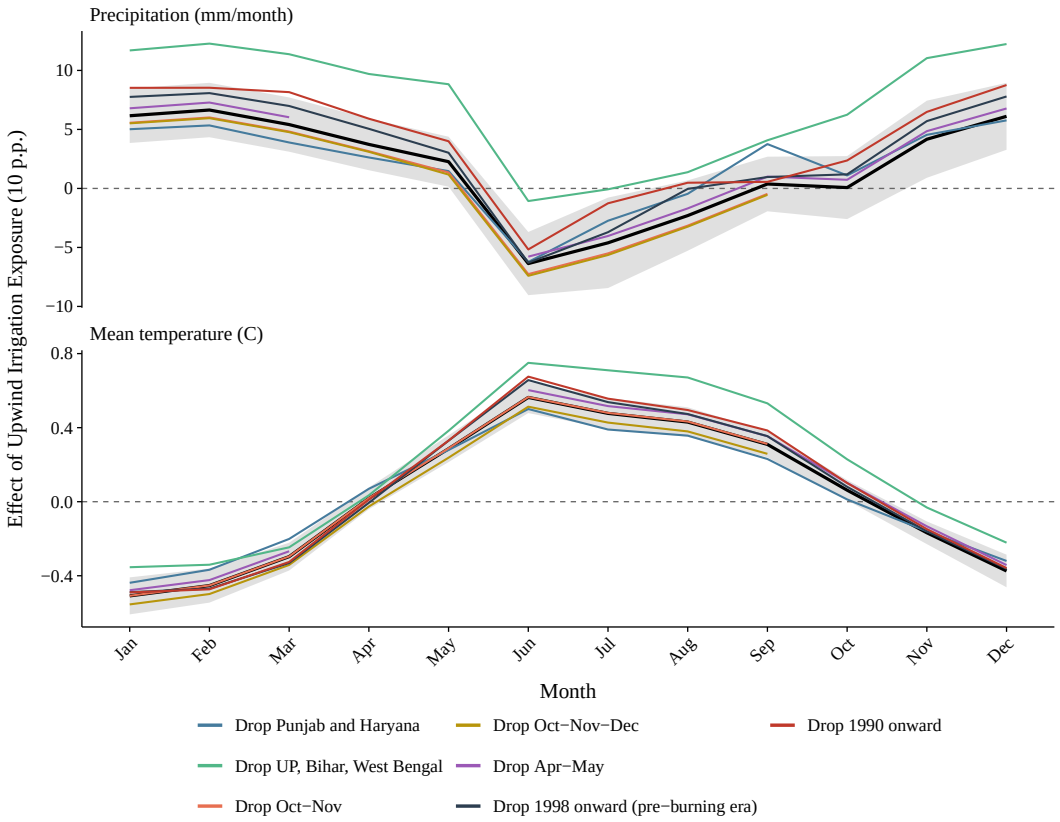


Figure A26: Climate Results dropping the burning regions and months

Notes: Figure A26 reports the estimated coefficients from specification (4) on (i) monthly precipitation (mm) and (ii) mean daily temperature (°C), re-estimated after removing the residue-burning regions, the burning months and the burning era. Each coefficient γ_m measures the *total* marginal effect of a 10 percentage point increase in upwind irrigation exposure in month m. Upwind irrigation is the mean share of irrigated area in pixels located 50–150 km upwind of the focal pixel, weighted inversely by distance, averaged over the district. All regressions are estimated at the district level with district, month and state-by-year fixed effects and standard errors clustered at the district level. *Main* is the full sample, drawn in black with its 90% confidence band; each coloured line drops the stated regions, months or years, and breaks over the months it no longer estimates.

Table A15: Effect of Upwind Irrigation on Agricultural Outcomes: Exclusions and Additional Controls

	(1) Wheat prod. (log)	(2) Double cropping	(3) Irrigation int.
Main	0.033**	0.016***	0.017***
	(0.014)	(0.005)	(0.005)
Panel A. Burning months removed from the exposure measure			
All months (rebuilt)	0.033**	0.015***	0.014***
	(0.014)	(0.005)	(0.004)
Excl. Oct–Nov (rice residue)	0.033**	0.015***	0.014***
	(0.014)	(0.005)	(0.004)
Excl. Apr–May (wheat residue)	0.034**	0.015***	0.014***
	(0.014)	(0.005)	(0.004)
Panel B. Controlling for other Wind-Borne Confounders			
No control (panel B sample)	0.035**	0.015***	0.014***
	(0.014)	(0.005)	(0.005)
+ forest share	0.033**	0.016***	0.014***
	(0.014)	(0.005)	(0.005)
+ fertiliser (NPK) per ha	0.029**	0.012**	0.012***
	(0.014)	(0.005)	(0.004)
+ forest and fertiliser	0.029**	0.012**	0.011***
	(0.014)	(0.005)	(0.004)
Baseline forest $\times$ year	0.027*	0.009*	0.010**
	(0.014)	(0.005)	(0.004)
Baseline fertiliser $\times$ year	0.025*	0.013**	0.010**
	(0.014)	(0.005)	(0.005)
Fixed Effects	District and State$\times$Year		

Notes: Each cell is the parameter β of equation (5) for a 10 percentage point increase in upwind irrigation exposure. **Main** is the specification of the main text, with district and state-by-year fixed effects and no additional control, and reproduces Tables 1 and 2. Each of the two panels below has its own sample and therefore its own uncontrolled reference row, against which the rows under it should be read. Wheat production is in logs and estimated on the positive observations; double cropping and irrigation intensity are bounded ratios in levels. Panel A rebuilds annual exposure from the monthly panel with the residue-burning months removed from the treatment, since dropping a month from an annual outcome would not be meaningful; the rebuilt all-months series correlates 0.998 with the published one. Panel B adds forest share of district area and fertiliser per hectare of net cropped area, contemporaneously and then as 1966–1970 baselines interacted with year. Standard errors, clustered at the district level, are in parentheses. Significance: * $p < 0.10$, ** $p < 0.05$, *** $p < 0.01$.

D.7 Spatial correlation of standard errors

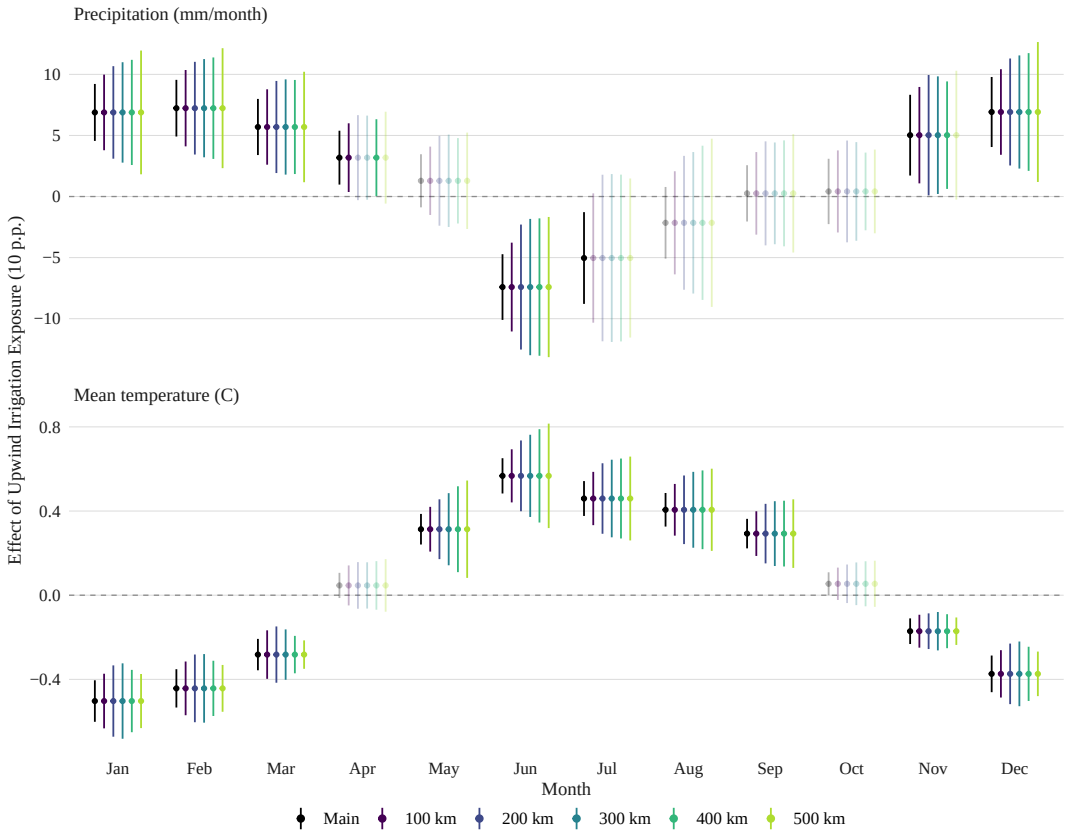


Figure A27: Conley spatial standard errors over a grid of cutoffs

Notes: Figure A27 reports the estimated coefficients from specification (4) on monthly precipitation (mm) and mean daily temperature (°C), upwind arm alone, with the standard error computed in five ways. Each estimated coefficient γ_m measures the *total* marginal effect of a 10 percentage point increase in upwind irrigation exposure in month m. Upwind irrigation is the mean share of irrigated area in pixels located 50–150 km upwind of the focal pixel, weighted inversely by distance, averaged over the district. Regressions are estimated at the district level and include district, month and state-by-year fixed effects, as in Figure 3. *Main* clusters by district; the four remaining series are Conley (1999) standard errors with a Bartlett taper in space, at the stated cutoff, and a three-year taper in time. The average district covers 8,900 km^2, an equivalent diameter of 102 km, so a cutoff below 100 km is shorter than the unit of observation and the grid begins there. The point estimate is identical across all five, so only the intervals differ. Error bars denote 90% confidence intervals.

D.8 Randomisation inference

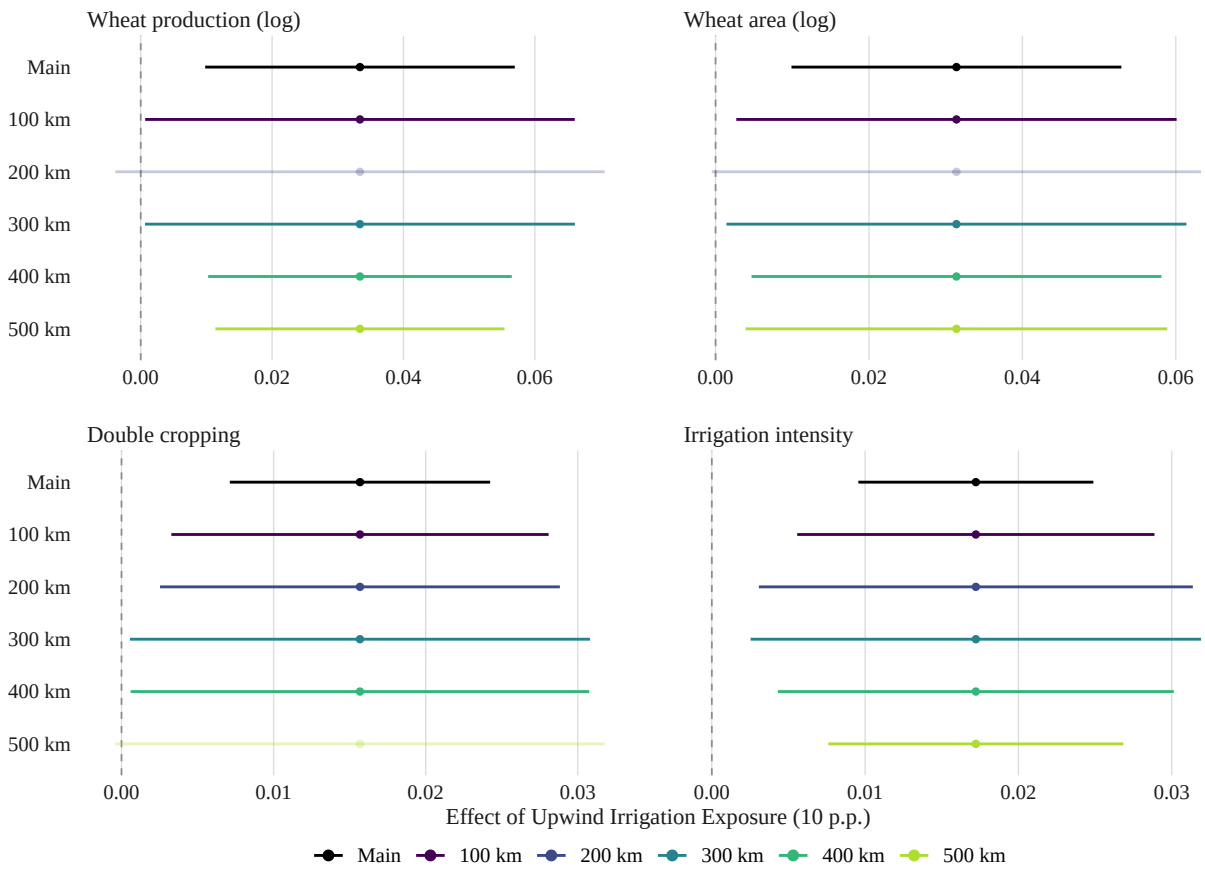


Figure A28: Conley spatial standard errors, agricultural outcomes

Notes: Figure A28 is the agricultural counterpart of Figure A27. It reports the estimated coefficient on upwind exposure from $y_{d,t} = \beta E^{\uparrow}_{d,t} + \mu_d + \lambda_{s,t} + \varepsilon_{d,t}$ at district level, with district and state-by-year fixed effects, in the functional form of the main text: log for the four crop outcomes, estimated on the positive observations, and levels for the two bounded ratios. The point estimates are therefore exactly those of Tables 1 to 2. *Main* clusters by district, the paper's own choice; the five remaining series are Conley (1999) standard errors with a Bartlett taper in space at the stated cut-off. The point estimate is identical across all six, so only the intervals differ; estimates not significant at 10 percent are drawn at reduced opacity. Error bars denote 90% confidence intervals.

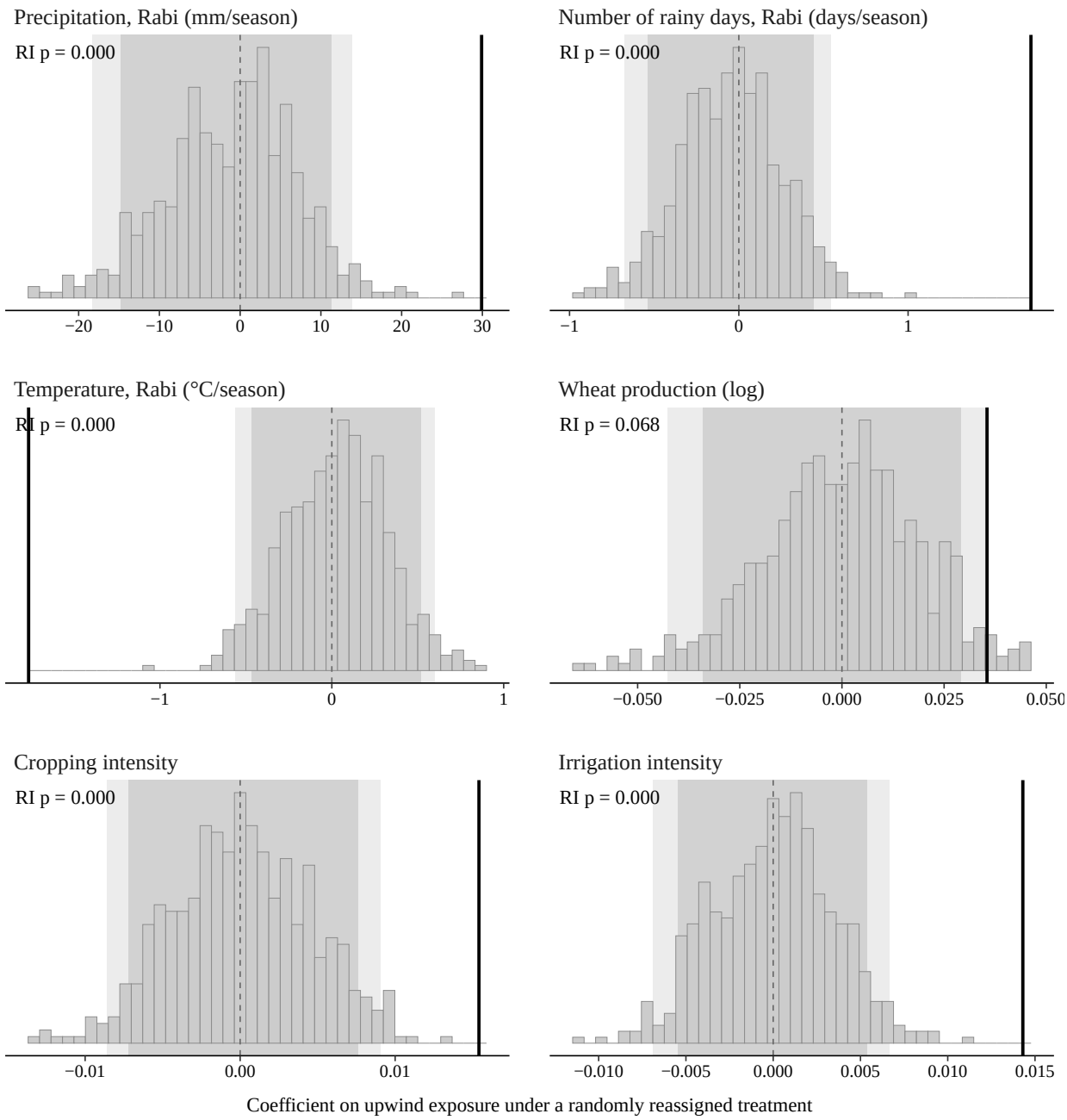


Figure A29: Randomisation inference: the treatment reassigned 500 times

Notes: Figure A29 reports the distribution of the coefficient on upwind exposure when the treatment is randomly reassigned 500 times. Each district's *entire* exposure series moves to another district, so the placebo keeps the real treatment's level, trend and serial correlation, and only the match between district and treatment is broken; every draw is then put through the paper's own specifications, equation (4) for precipitation, temperature and the number of rainy days, summed over the Rabi months, and equation (5) for wheat production, cropping intensity and irrigation intensity, in the functional form the main text reports. The grey histogram is the permutation distribution and the shaded bands its central 90 and 95 percent; the red line is the coefficient actually estimated, and the randomisation p-value is the share of permutations whose absolute coefficient is at least as large.

E Placebo

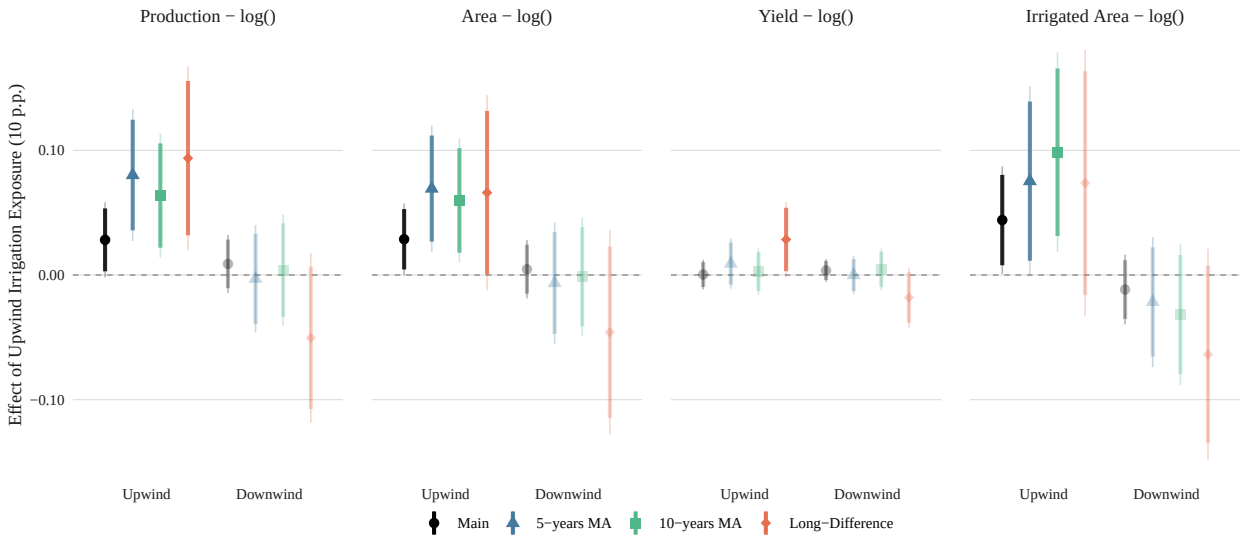


Figure A30: Directional placebo: wheat production, area, yield and irrigated area

Notes: Each panel reports the coefficient on upwind exposure beside the coefficient on downwind exposure, the two entered jointly in the same regression, so the upwind coefficient differs slightly from the tables of the main text, where it enters alone. Upwind irrigation is the average share of irrigated land in pixels located 50–150 km upwind of the focal pixel, weighted inversely by distance; the downwind arm reverses the wind. All four outcomes are in logarithm. The vertical scale is free across panels but symmetric about zero in each, so the dashed zero line sits at the same height throughout. *Main* is equation (5) on the annual panel. *5-years MA* and *10-years MA* average each district over windows of two and five years around anchor years 1970 to 2000, with district and state-by-anchor-year fixed effects. *Long-Difference* compares 1968–1972 with 1998–2002, with state fixed effects. No baseline control enters any specification. Standard errors are clustered at the district level; bars are 90 and 95 percent confidence intervals, and estimates not significant at 10 percent are drawn at reduced opacity.

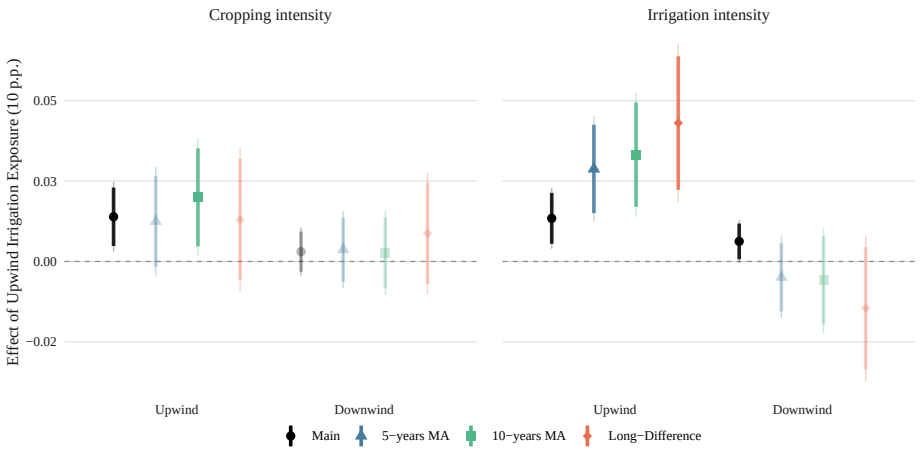


Figure A31: Directional placebo: cropping and irrigation intensity

Notes: Each panel reports the coefficient on upwind exposure beside the coefficient on downwind exposure, the two entered jointly in the same regression, so the upwind coefficient differs slightly from the tables of the main text, where it enters alone. Upwind irrigation is the average share of irrigated land in pixels located 50–150 km upwind of the focal pixel, weighted inversely by distance; the downwind arm reverses the wind. *Main* is equation (5) on the annual panel. *5-years MA* and *10-years MA* average each district over windows of two and five years around anchor years 1970 to 2000, with district and state-by-anchor-year fixed effects. *Long-Difference* compares 1968–1972 with 1998–2002, with state fixed effects. No baseline control enters any specification. Standard errors are clustered at the district level; bars are 90 and 95 percent confidence intervals, and estimates not significant at 10 percent are drawn at reduced opacity. Both outcomes are bounded ratios and enter in levels.

F Counterfactual exercise

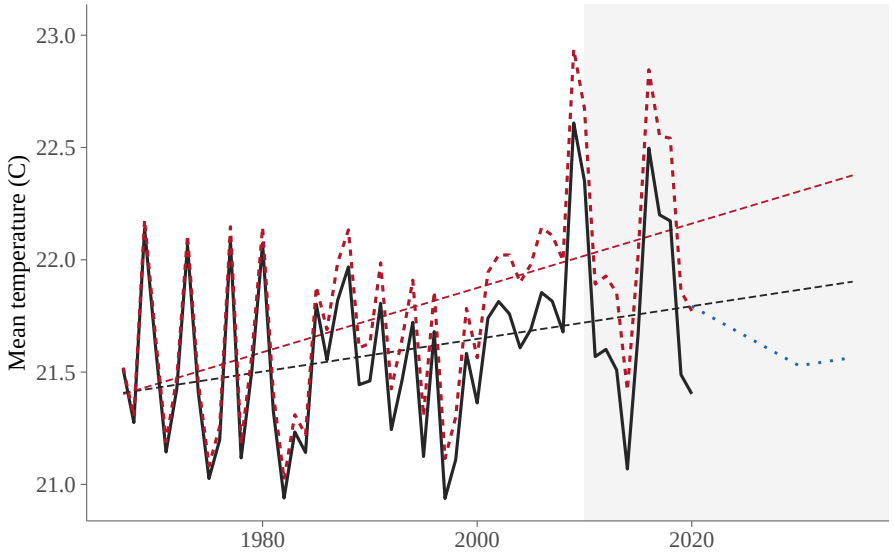
Table A16: Counterfactual exercise

	(1) Point estimate	(2) 95% interval
Panel A: Canals constructed by 2010		
Climate		
Dry-season rainfall (km^3/year)	37	[18, 55]
mm per season	13	[6, 19]
as % of dry-season rainfall	8.9	[4.2, 13.0]
Dry-season number of rainy days (days per season)	0.9	[0.6, 1.2]
as % of dry-season rainy days	7.1	[4.9, 9.0]
Dry-season temperature (°C)	-0.30	[-0.34, -0.26]
Agriculture		
Wheat production (Mt/year)	4.9	[1.4, 7.8]
Rice production (Mt/year)	8.4	[-6.6, 19.3]
Irrigation intensity (pp)	1.71	[0.55, 2.92]
gross irrigated area (Mha)	3.2	[1.0, 5.4]
Cropping intensity (pp)	1.69	[0.68, 2.65]
Value of the wheat, at current price		
Gross value (bn USD/year)	1.0	
Per hectare of command area (USD/year)	19	
Panel B: Canals under construction		
Dry-season rainfall (km^3/year)	48	[22, 70]
as % of dry-season rainfall	8.4	[3.9, 12.2]
Wheat production (Mt/year)	3.63	[0.94, 6.37]
Value of the wheat, at current price		
Gross value (bn USD/year)	0.76	
Per hectare of new command area (USD/year)	24	

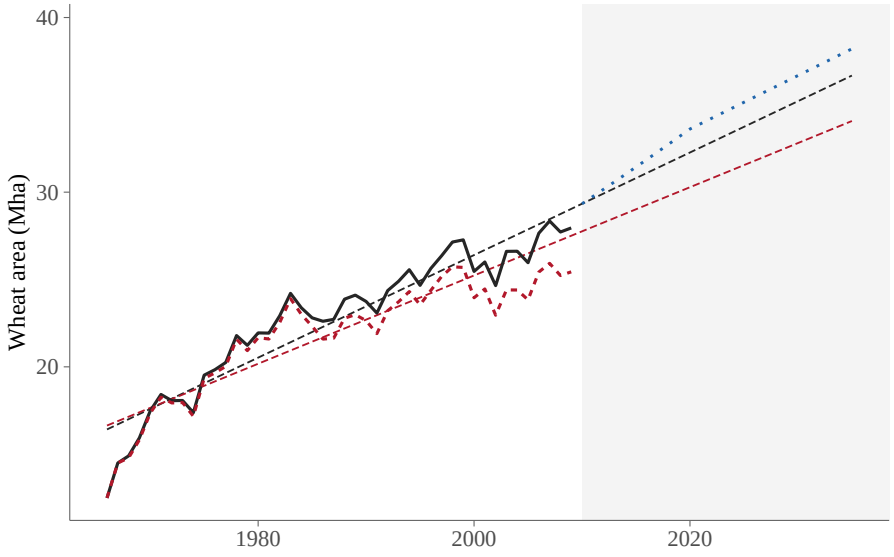
Notes: National totals, evaluated over 2006–2010. Panel A sets upwind exposure to zero for the completed network, including the 5.3 million hectares with no recorded completion year. Panel B is the increment from the 32.3 million hectares under construction or completed after 2010, and reports only the two margins inside the range identifying $\hat{\beta}$. Climate uses the level-identified monthly coefficients (district-year mean exposure), October to March for the dry season; the number of rainy days is estimated on 1966–2010 only. Agriculture uses equation (5). Intervals are the 2.5th and 97.5th percentiles of 300 district cluster bootstrap replications, the uncertainty in $\hat{\beta}$. Both panels value wheat at $210/tonne, the mean 2007–2010 support price. Rice is not significant and is reported for completeness only.

Weather response versus adaptation. To separate the plant's direct response to weather from what farmers did about it, I chain three stages – the effect of upwind exposure on dry-season weather, a weather-response function for wheat yield estimated with no exposure term of its own and re-estimated on Indian wheat in the tradition of Schlenker and Roberts (2009), and the induced weather pushed through that function. This agronomic channel accounts for 28–44 percent of the 3.8 percent reduced-form effect on wheat production; the remainder is consistent with the adaptation margins of Section 6.2.[21]

[21] Braun and Schlenker (2023) find a comparable split for corn and soybeans: the downwind, cooling-induced share of the yield effect is on average 27 percent of the direct on-farm irrigation effect, the same order of magnitude as the agronomic share found here.



(a) Mean temperature, Rabi



(b) Wheat area

Observed Without Irrigation Ongoing Construction

Figure A32: Historical trajectories with and without upwind irrigation, extended to 2035: temperature and wheat area

Notes: As the national historical-trajectory figure of Section 8.

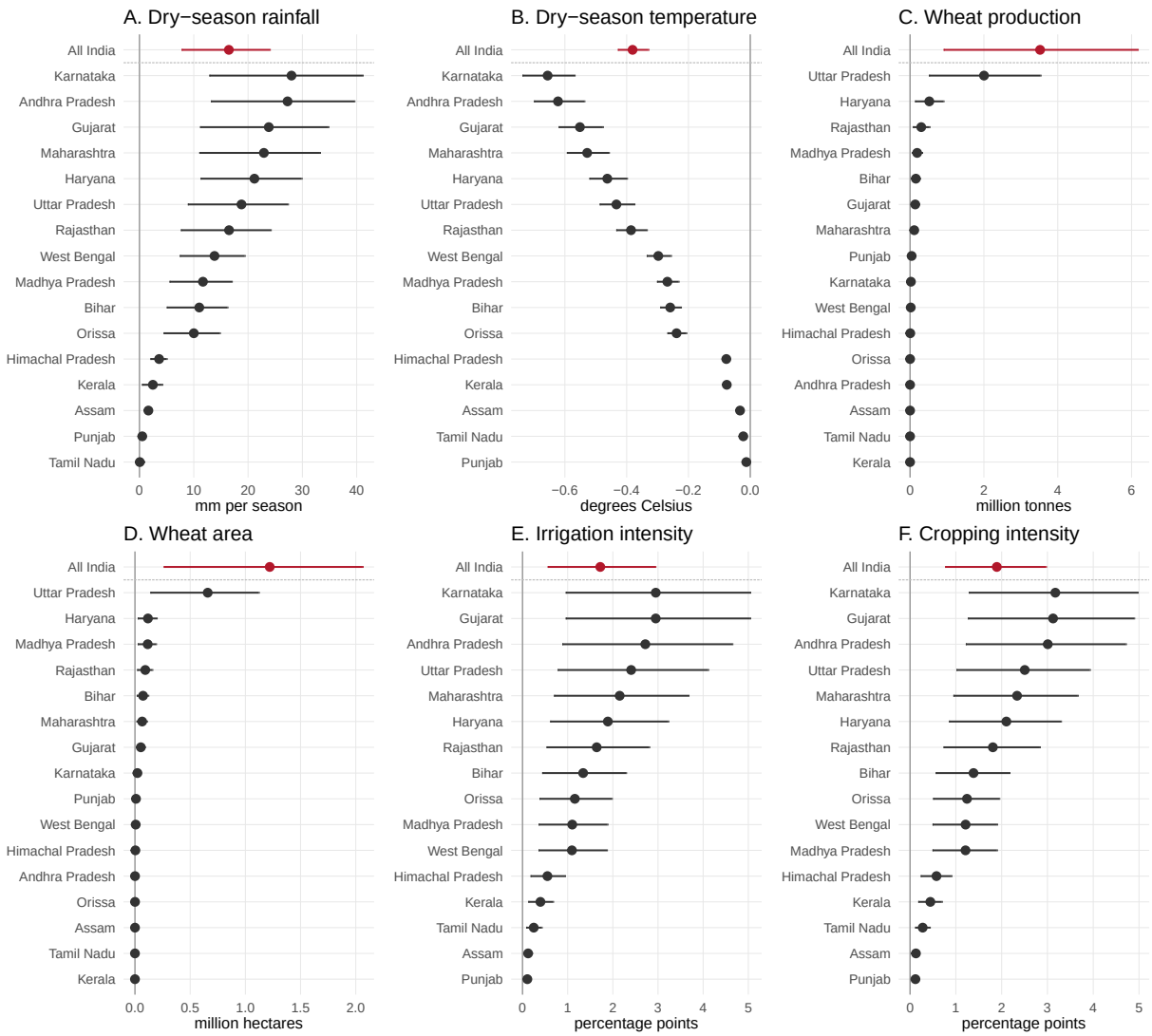


Figure A33: What the projects that came after 2010 would deliver, state by state

Notes: Points are the increment each state would receive; bars are 95 percent district cluster bootstrap intervals over 300 draws. **All India** in red.

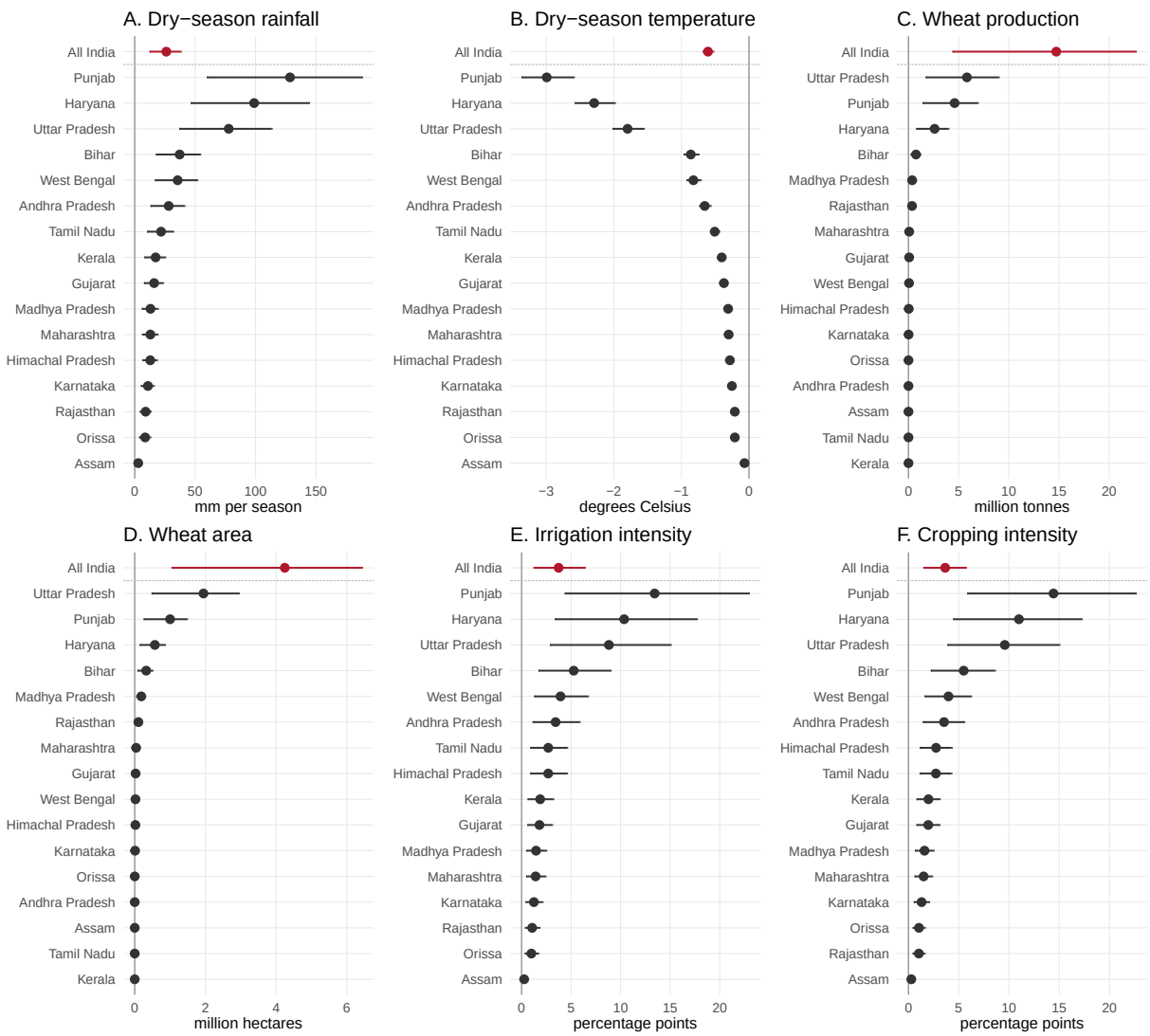


Figure A34: What the standing canal network delivers to each state today

Notes: As Figure A33, for the network already standing, averaged over 2006–2010.

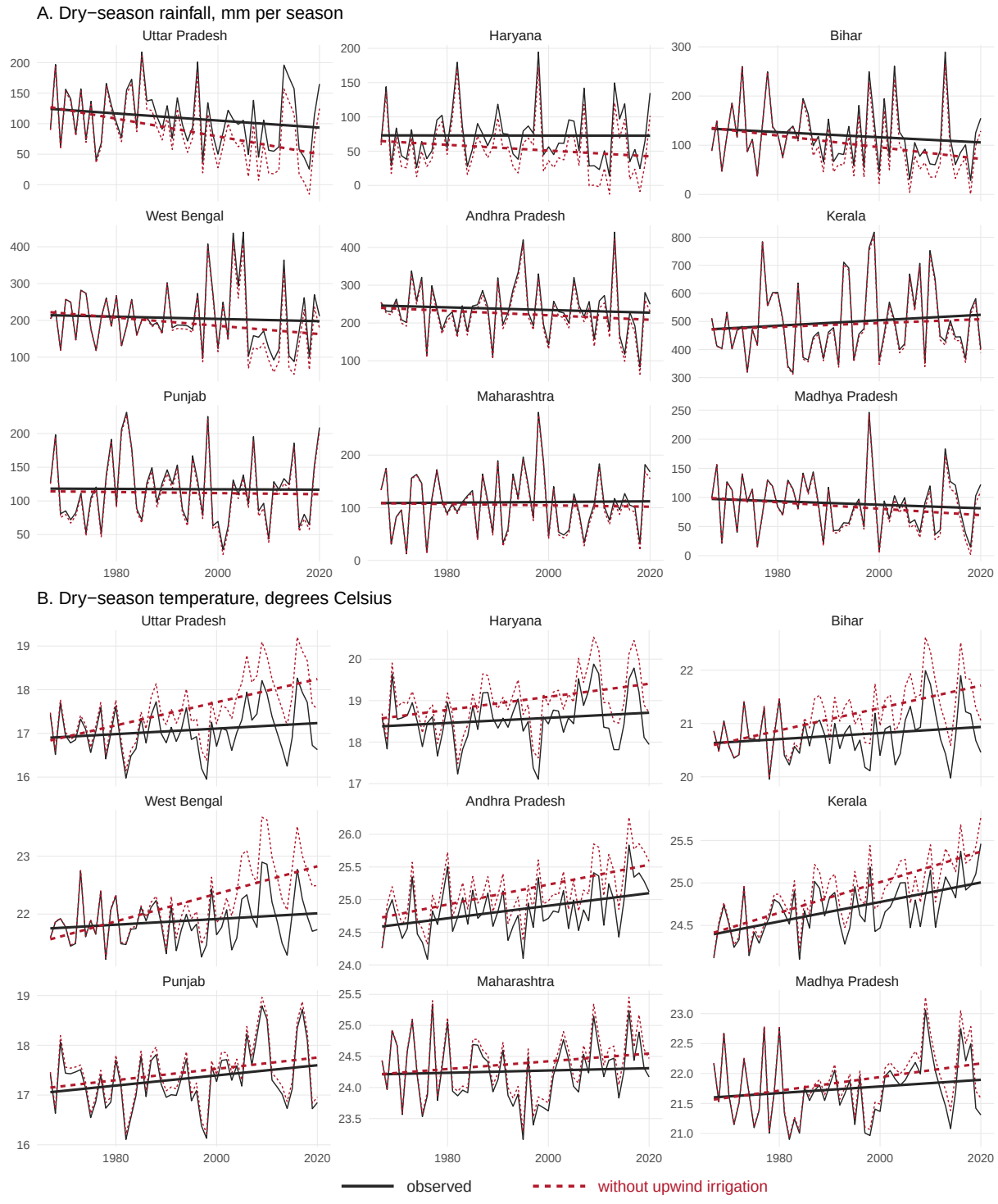


Figure A35: India with and without upwind irrigation, state by state

Notes: As the national historical-trajectory figure of Section 8, for the nine states with the largest effect. About 0 percent of Punjab's district-months and 7 percent of Haryana's have a negative counterfactual.